

STRUCTURE AND METAMORPHIC PETROLOGY OF THE FORTH METAMORPHIC COMPLEX

ROB LEWIS

A research thesis submitted in partial fulfilment of the degree
Bachelor of Science with Honours.

Geology department.
University of Tasmania



1991

ABSTRACT

The Forth Metamorphics outcrop in the lower reaches of the Forth River, Northern Tasmania and comprise a banded garnetiferous schist and quartzite, interlayered with sub-ordinate orthoamphibolites of tholeiitic MORB-type affinity. Geochemical and sedimentological constraints are consistent with a passive continental depositional environment and the sequence has been regionally metamorphosed during a two-phase tectono-metamorphic event.

An early isoclinal fold phase (D1) produced a penetrative muscovite foliation but is largely overprinted by the dominant S2 schistosity. High temperature, relatively low strain quartz mylonites developed in narrow zones during west-directed D2 transport and are separated by domains of west vergent isoclinal F2 folds.

Microprobe analyses of stable pelitic and metabasite assemblages have been used in conjunction with traditional/dataset thermobarometric methods and phase equilibrium constraints to estimate P-T conditions during D2.

Peak conditions of 700°C \pm 50° C and 13 kb \pm 2 kb for kyanite-garnet-biotite schists in the Forth Valley are matched by independent estimates for garnet amphibole plagioclase assemblages and the latter preserve an early garnet-clinopyroxene-albite assemblage indicating conditions of 660° C and 11 kb during core growth. These results are supported by semi-quantitative P-T modelling of local calcite-altered garnet clinopyroxene zoisite interbands, which formed in a locally H₂O-poor environment during compression/heating from 675° C 9-11 kb to peak conditions of 740° C and 13-15 kb.

Significant P-T zonation is indicated by the spatial distribution of pelitic assemblages and peak temperatures some 100° C lower are inferred for staurolite-chloritoid bearing schists in the western half of the area. Paragonite and chloritoid textures in these units are consistent with breakdown of glaucophane, and may indicate an early high P-low T history.

Late sphene and possibly albite developed during decompression but the preservation of substantially unretrogressed high grade assemblages indicates rapid late-D2 uplift and cooling. In the Forth Valley, garnet amphibolite assemblages preserve geochemical and textural evidence of late-D2 K-metasomatism. The alteration is confined to a 300m wide local high strain zone along the contact with adjacent pelitic schists and thermometry results indicate post-peak conditions of around 600° C.

The P-T history of the Forth Metamorphics is similar to that of the Collingwood River eclogites and may have developed during Precambrian partial subduction of a passive continental margin.

Serpentine bodies, enclosed within the metamorphics have minor structures consistent with early west-directed emplacement. The structural setting and geometry of these bodies has been modified by an east-directed thrust event of probable Devonian age, which produced a spatially restricted crenulation cleavage and minor folds in the metamorphics.

ACKNOWLEDGMENTS

I would like to thank Dr. Ron Berry for suggesting this topic and guiding it to a satisfactory conclusion. Special thanks also to Michael Roach who donated much of his time to help with data compilation, formatting and drafting using the GIS software system and to Mr P. Robinson and Mr W. Jablonski for their expertise in analytical techniques.

The year was made tolerable by a great group of honours students and I would like to thank Dave B., Stewart, Rob and Rob, Ben, Dave J., Fiona, Dean , Nigel, Brendan and Justin for their comeraderie and useful feedback.

Many thanks also to my fiance Amelia for her continued support and understanding (once again), particularly during the final stages of writing.

CONTENTS

	Page
Title page	i
Abstract.....	ii
Acknowledgements	iii
Table of contents	iv
List of figures.....	vii
List of tables	viii
 CHAPTER 1 - INTRODUCTION	 1
 CHAPTER 2 - FIELD RELATIONSHIPS	 3
2.1 Regional setting	5
2.2 Lithologies.....	6
2.2.1 Forth Schists.....	6
2.2.2 Quartzites	9
2.2.3 Metabasites.....	9
2.2.4 Serpentine	11
2.2.5 Minor rock-types.....	11
 CHAPTER 3 - GEOCHEMISTRY	 13
3.1 Pre-metamorphic affinities	13
3.1.1 Sedimentary vs, igneous origin.....	13
3.1.2 Petrologic/Tectonic affinities	17
3.2 Correlation	18
 CHAPTER 4 - STRUCTURE	 22
4.1 Syn-metamorphic structure	23
4.1.1 Mesostructure	23
4.1.1.1 Compositional banding	23
4.1.1.2 D1 structures	23
4.1.1.3 D2 structures	24
Fold-related structures	24
Mylonites	27
4.1.2 Macrostructure/correlation	33
4.2 Post-metamorphic structure	34
4.2.1 Dominant post-S2 deformation (D3)	35
4.2.1.1 Folding and cleavage development.....	35
4.2.1.2 S3 microstructure	35
4.2.1.3 Serpentine	37
Fabric	37
Contacts	37
4.2.1.4 Faulting	41

4.2.1.5 Correlation	43
4.2.2 Minor deformations	44
4.2.2.1 Group A	44
4.2.2.2 Group B - ?Cambrian	45
4.2.2.3 Post-S3 faulting	46
4.2.2.4 Post-Permian extensional faults	46
4.3 Structural summary	46
CHAPTER 5 - METAMORPHIC PETROLOGY	48
5.1 Petrography/mineral chemistry	48
5.1.1 Metapelites	48
5.1.1.1 Descriptive petrography/mineral chemistry.....	48
5.1.1.2 Critical assemblages	54
Chloritoid schists	54
Kyanite schists	55
Garnet albite schist	58
5.1.2 Metabasites	60
5.1.2.1 Amphibolites	60
5.1.2.2 Garnet-clinopyroxene gneisses	65
5.1.2.3 Retrogressed amphibolites	72
5.1.2.4 Micaceous amphibolites	73
5.1.3 Serpentine	75
5.2 Thermobarometry	77
5.2.1 Introduction	77
5.2.1.1 Calibrations	77
5.2.1.2 Activity models	78
5.2.2 Thermometry	79
5.2.2.1 Garnet-biotite	80
5.2.2.2 Garnet-phengite	81
5.2.2.3 Garnet-clinopyroxene	82
5.2.2.4 Garnet-hornblende	84
5.2.2.5 Plagioclase-hornblende	85
5.2.3 Barometry	87
5.2.3.1 Metapelites	87
Garnet-aluminosilicate-plagioclase-quartz	87
Garnet-plagioclase-muscovite-biotite	88
Other empirical calibrations	88
5.2.3.2 Metabasites	89
Garnet-plagioclase-hornblende-quartz	89
Garnet-clinopyroxene-plagioclase-quartz	91
Jadeite	91
5.2.4 Database methods	1

- kyanite parageneses	98
- albite parageneses	99
5.3.2 Metabasites	102
5.3.2.1 Amphibolites	103
5.3.2.2 Garnet clinopyroxene gneisses	104
5.3.2.3 Micaceous amphibolites	105
CHAPTER 6 - CONCLUSIONS	108
6.1 P-T Summary	108
6.2 Tectonic implications	109
APPENDICES	111
A. Whole-rock analyses	111
B. Rock catalogue	115
REFERENCES CITED	118

LIST OF FIGURES

	<i>Page</i>
1.1 Locality Map	1
1.2 Physiography and access	3
2.1 Regional geology - Northern Tasmania	5
2.2 Lithological distribution - Forth Metamorphics	8
3.1 Ortho- vs. Para-amphibolite discriminant diagrams.....	15
3.2 CaO vs. Al ₂ O ₃ - garnet clinopyroxene gneisses and garnet amphibolites	16
3.3 Petrologic discriminant diagrams	19
3.4 Tectonic discriminant diagrams	20
3.5 Tasmanian high grade metabasites and hornblende mylonites	21
4.1 Structural zones - Forth Metamorphics	22
4.2 'Porcupine Hill' style intersection lineations	28
4.3 'Goldie Creek' style stretching lineations	29
4.4 P-T orientation of deformation lamellae	31
4.5 Late brittle-style structural elements	36
4.6 Serpentine structures	38
4.7 Geology of the Lower Claytons Rivulet	39
4.8 Thrust zone at DQ331409	40
4.9 Fault-related structures	41
4.10 Fault striation analysis - best fit stress tensors	42
4.11 Structural profile across the north-western (coastal) part of the Forth block	43
4.12 Interpretive composition section across the Forth Metamorphics	44
5.1 Phengite compositions - FeO* vs. Al ₂ O ₃ , Na/(Na+K) vs. Si	50
5.2 Biotites - K vs. Mg#	51
5.3 Pelitic garnets - CFM diagram	52
5.4 White mica compositions - 75602	55
5.5 Garnet zonation - 75641	58
5.6 Garnet, amphibole and clinopyroxene compositions - amphibolites	60
5.7 Amphiboles - Al _{iv} vs. (Na + K) _A	63
5.8 Garnet, amphibole and clinopyroxene compositions - gneisses	65
5.9 Clinopyroxene compositions	70
5.10 Amphibole zonation - 75627	71
5.11 Amphibole compositions: (v) _A -Al _{iv} -Al _{vi} , Al _{iv} vs. Al _{vi}	86
5.12 GEOCALC PTX results - 75641	93
5.13 Chloritoid parageneses	97
5.14 AFM projection - 75602	98

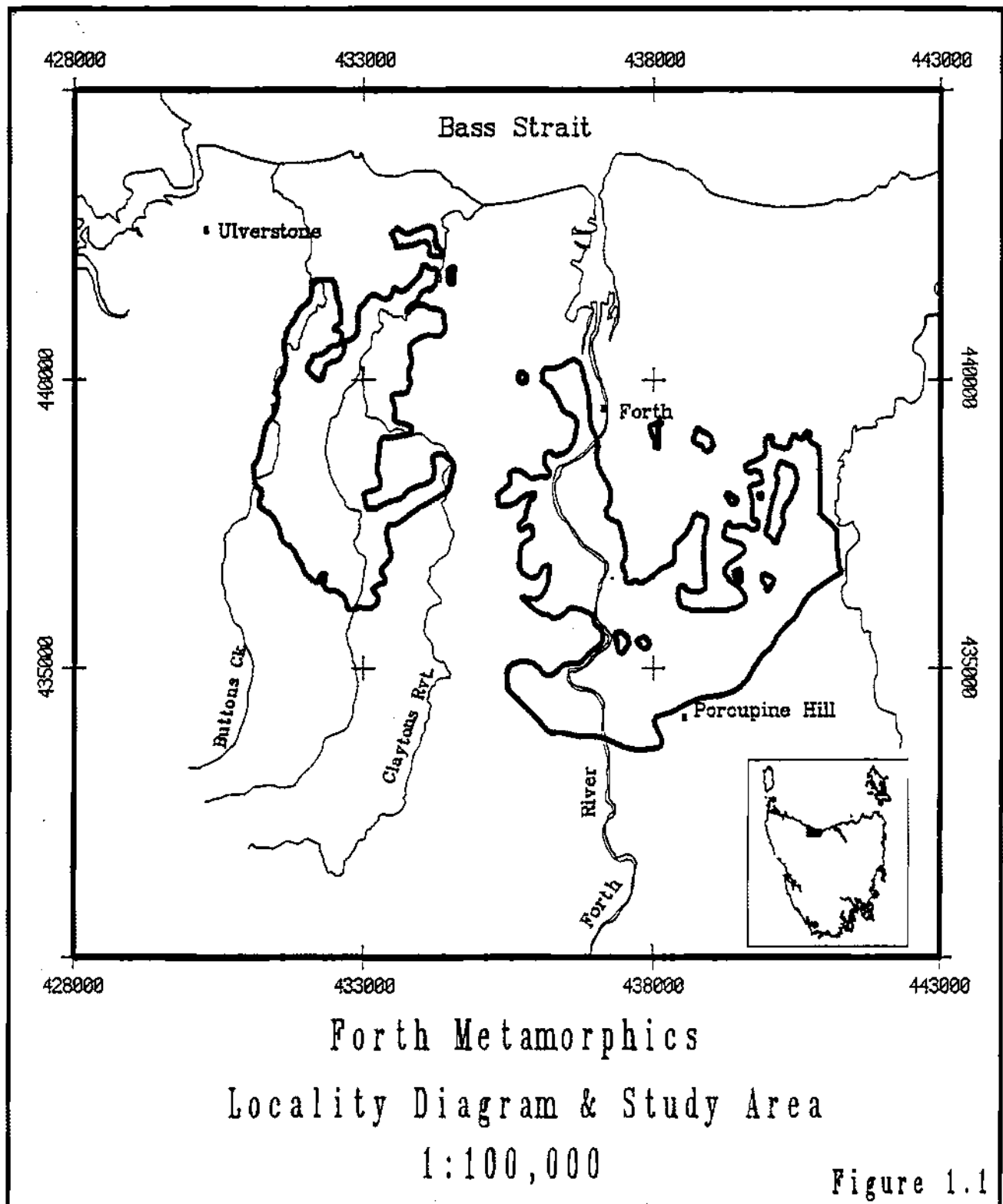
5.15 AFM projection - 75641	99
5.16 Albite parageneses	100
5.17 GEOCALC PTX results - 75637	101
5.18 GEOCALC P-X _{CO2} results - 75662	106
5.19 GEOCALC PTX results 75662	107

LIST OF TABLES

	<i>Page</i>
3.1 Selected whole-rock analyses	14
4.1 Results of fault striation analysis	42
4.2 Structural sequence in the Forth Metamorphics	47
5.1 Whole-rock and mineral compositions - 75602	56
5.2 Whole-rock and mineral compositions - 75641	57
5.3 Mineral compositions - 75637	59
5.4 Mineral compositions - 75628	61
5.5 Mineral compositions - 75617	62
5.6 Mineral compositions - 75627	66
5.7 Mineral compositions - 75662	68
5.8 Mineral compositions - 75619	69
5.9 Mineral compositions - 75605	72
5.10 Mineral compositions - 75669	74
5.11 Mineral compositions - 75636	76
5.12 Garnet-biotite thermometry	81
5.13 Garnet-phengite thermometry	82
5.14 Garnet-clinopyroxene thermometry	83
5.15 Garnet-hornblende thermometry	84
5.16 Plagioclase-hornblende thermometry	85
5.17 GASP calibrations	88
5.18 Empirical pelitic barometers	89
5.19 Garnet-hornblende-plagioclase-quartz barometry	90
5.20 Garnet-clinopyroxene -plagioclase-quartz barometry	91
5.21 Jadeite barometry	92
5.22 Mineral chronology - Forth schists	94
5.23 Mineral chronology - Forth metabasites	102

CHAPTER 1 - INTRODUCTION

Burns (1963) defined the Forth Metamorphics as the quartzite, garnet schist and amphibolite which outcrop in the valley of the Forth River, between the township of Forth (DQ367397) and a reef of Ordovician conglomerate on Porcupine Hill (DQ385342). The metamorphics underlie an area of approximately 60 km² and together with the Ulverstone Metamorphics to the west, form zoned complex known as the Forth Region (Burrett & Martin 1989). In addition, the study area includes a number of ultramafic bodies and is shown in figure 1.1.



AIMS.

The principal aims of this study are as follows:

- (i) To determine the metamorphic pressure-temperature-time (PTt) conditions that affected the rocks in the study area.
- (ii) To establish the geochemical affinities of the amphibolites.
- (iii) To document and re-evaluate the syn-metamorphic structural history.
- (iv) To assess the tectonic significance of ultramafic bodies and post-metamorphic deformation in the context of current models for Northern Tasmania.

PHYSIOGRAPHY/ACCESS.

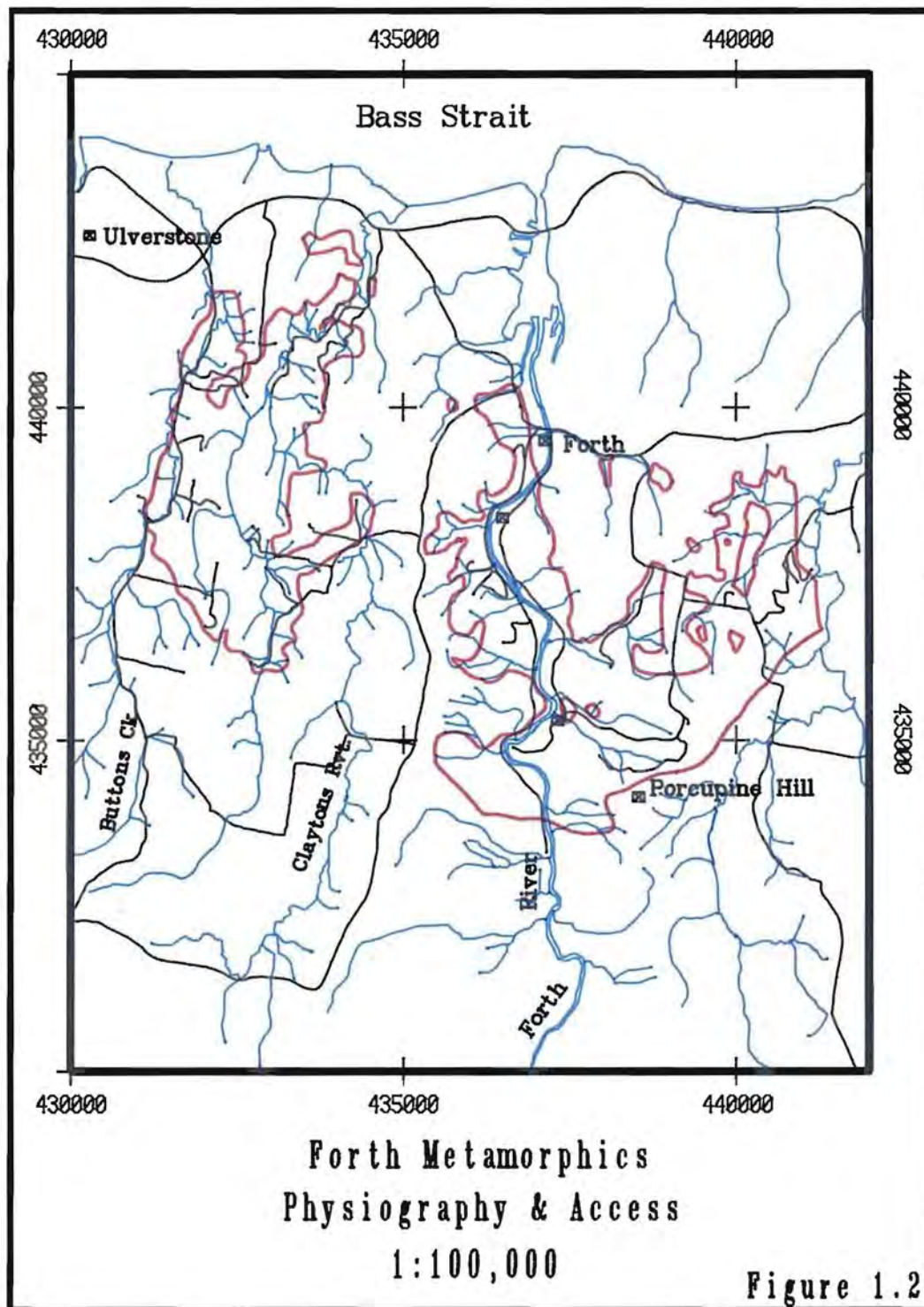
The area comprises a low coastal plain backed by an undulating plateau which rises to approximately 300m on Porcupine Hill (fig.1.2).

The plateau is underlain by a discontinuous cover of Tertiary basalt and dissected by a northward trending drainage system, which includes the catchments of Buttons Creek, Claytons Rivulet and tributaries of the Lower Forth River.

The temperate sub-humid climate supports intensive cultivation on the rich plateau soils and the metamorphics are largely restricted to lower valley slopes, on which steep terrane and generally poor soils support uncleared open to closed sclerophyll forest.

Physical access is aided by a dense network of roads and vehicular tracks (figure 1.2), although natural exposure of the metamorphics is restricted to creeks, which are only accessible on foot. The area is extensively sub-divided and, despite the relatively easy physical access, legal access is complicated by the large degree of private ownership.

Natural outcrop is poor, but the metamorphics are well-exposed in scattered quarries, gravel pits and road-cuttings. Smaller gullies are often filled with Cainozoic gravels or overgrown with blackberries and have limited exposure. Outcrop along the Forth River, depends on water flow which is controlled by H.E.C operations upstream.



PREVIOUS WORK.

The Forth Metamorphics were first described by Gould (1867) during reconnaissance mapping of northern Tasmania. Petterd (1893, 1896, 1910) reported kyanite-bearing schists from the Claytons River, collected by Gould in 1873. Twelvetrees (1906b, 1909b) described the amphibolites as "hornblende gneiss" and selected whole rock analyses are presented in Spry (1962). Spry (1962) assigned the Forth Metamorphics to a lower division of the Precambrian, deformed and regionally metamorphosed during the Frenchmans orogeny (800Ma).

Regional mapping by Burns (1963, 1964) outlined a complex polyphase deformation sequence and correlated post-metamorphic brittle-style deformation with Tabberraberran structures in the surrounding Lower Paleozoic sediments.

The ultramafic bodies were recorded by Gould (1867) and Twelvetrees (1906b, 1909b) described the original rock as an olivine-enstatite peridotite or harzburgite. An intrusive relationship with the metamorphics was suggested by Blake (1928c) and supported by Taylor (1955) who postulated a discontinuous series of 4 or 5 sub-concordant sill-like bodies. Burns (1963, 1964) correlated the serpentinite with other ?Cambrian ultramafic bodies in Tasmania and reported large aligned xenoliths of lineated amphibolite from near the western margin of the Claytons Rivulet body.

The following report is organised into 4 main sections. Field relationships - which define critical structural and metamorphic problems - are outlined in chapter 2. Geochemical features of the metabasites are presented in chapter 3. Syn-metamorphic and later brittle-style deformation are considered in detail in Chapter 4. Chapter 5 discusses the metamorphic petrology and P-T conditions inferred from traditional and database thermobarometric methods.

The tectono-metamorphic evolution of the Forth Metamorphics, as constrained by the geochemical, structural and petrological conclusions, is summarised in chapter 6.

CHAPTER 2 - FIELD RELATIONSHIPS

2.1 REGIONAL SETTING:

The geology of Northern Tasmania is complex and not well understood, despite over thirty years of work (Woodward *et al* - *in review*). The regional setting of the Forth Metamorphics is shown in figure 2.1 and summarised below, based on mapping by Burns (1963, 1964) and the recent compilation of Burrett & Martin (1989).

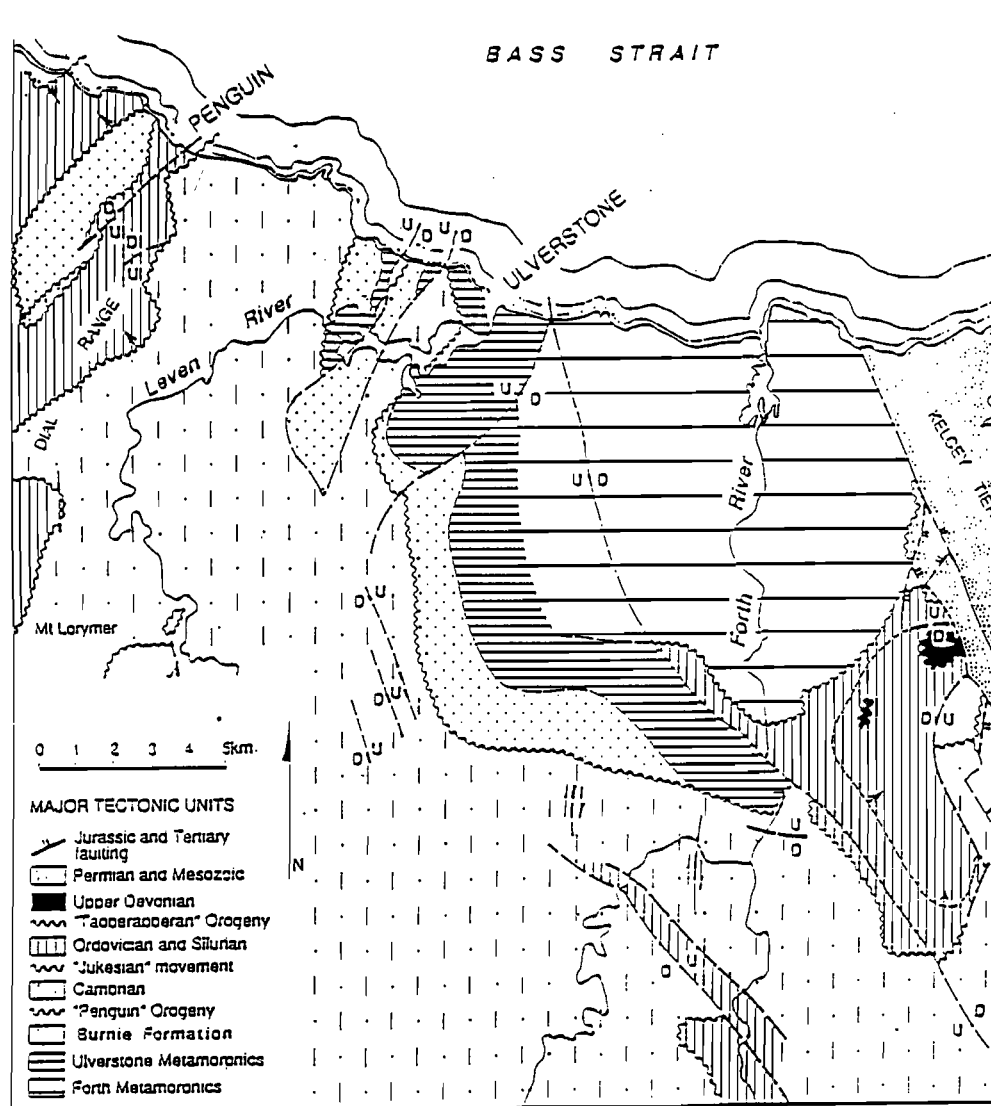


Figure 2.1: Geology of the Forth Region (modified from Burns 1963).

The Forth Metamorphics form the eastern half of the Forth Region ("Forth Block or Nucleus" of Carey (1953)) - a zoned metamorphic complex which includes the lower greenschist facies Ulverstone Metamorphics (Burns 1964). The boundary between the two assemblages was arbitrarily defined by Burns (1964) at the first appearance of garnet in the Forth Metamorphics - which corresponds approximately to the eastern-most limit of metaconglomerate (Spalford Conglomerate) in the Ulverstone Metamorphics. Mapping and sample collection for the present study is confined to the Forth assemblage, as defined above and delineated on the Devonport Sheet (Burns 1965).

Burns (1964) considered the two complexes to be structurally concordant as the dominant syn-metamorphic foliation (S2) is of similar style and orientation along the margin, although this may largely reflect post-metamorphic deformation (Chapter 4).

To the east, the Forth Region is in faulted contact with sub-horizontal Permian sediments and is unconformably overlain to the south-east by deformed but un-metamorphosed quartzose clastics of the Ordovician Dial Subgroup (Burns 1964, Woodward *et al* - *in review*).

Although poorly exposed, the Ulverstone Metamorphics appear to be faulted along their western margin against relatively unmetamorphosed turbidites of the Burnie Formation which are in turn unconformably overlain to the south-west by Late Middle to Late Cambrian volcanics and volcanoclastics. The latter occupy a bifurcating N-S and E-W trending belt - the Dial Range or 'Fossey Mountain' Trough - generally considered to be a northern extension of the Mount Read Volcanic Arc (Williams *et al* 1989). The southern margin of the Forth Region is obscured by Tertiary cover and generally poor outcrop. The Forth Metamorphics are overlain to the north by unconsolidated Pleistocene/Holocene marine and fluvial sediments and are not exposed along the coast.

2.2 LITHOLOGIES:

The present study follows the grouping of Burns (1964) and mapping units are defined in terms of four major lithologies: schist, quartzite, amphibolite and serpentinite. Major lithological units outcrop as elongate, roughly N-S striking belts 100-700m wide, with lithological layering, on all scales, generally sub-parallel to the dominant tectonic foliation (S2) (fig. 2.2).

2.2.1 FORTH SCHISTS:

The pelitic lithologies are well-foliated rocks with a 1-30 cm lithological banding defined by alternation of garnet mica and quartz mica schist and will be collectively referred to as the Forth

schists. The rocks outcrop poorly, are often deeply weathered and generally unsuitable for petrological work.

The schists show a significant variation in structural and metamorphic style across the Claytons Valley. Along the western margin, the metapelites are pale or dark grey, fine to medium-grained foliated or penciled rocks with small (<1mm), often weathered, porphyroblasts of garnet and rare < 0.5mm albite. The early deformation style in this area is relatively open and garnet-free lithologies are phyllitic rather than schistose, in field appearance.

In the Claytons Valley, similar units with larger (>1mm) and more abundant garnet enclose discrete pods of coarse chloritoid + paragonite +/- staurolite-bearing lithologies.

In contrast, east of the Claytons Valley, the dominant pelitic lithology is a brown to pale grey, medium to coarse-grained schist with equant 1.5-2mm porphyroblasts of garnet in an anastomosing foliated matrix of muscovite with minor biotite, quartz and usually chlorite. Garnetiferous units are interbanded with pale quartz muscovite schists which grade into bands of coarse micaceous quartzite. In the Forth Valley (DQ368361), garnet mica schist bands interlayered with mylonitic quartzite, contain kyanite as tabular 1-1.5mm porphyroblasts mantled by clots of coarse muscovite. Kyanite has also been reported from the Claytons rivulet (Petterd 1893), but this was not found during the present study.

Bands of highly feldspathic, garnet-free schists occur, generally east of the Forth River, as discrete zones interlayered with both schist and quartzite. These contain strongly weathered 0.3 - 2.0 mm feldspar porphyroblasts wrapped around by a foliated matrix of muscovite and quartz, which is locally mylonitic. In places, abundant asymmetric augen reach up to 8mm across, suggesting an arkosic or tuffaceous protolith or possibly a pegmatitic phase owing to the coarse grain size of the blasts. The coarse feldspathic bands are laterally discontinuous but apparently concordant with compositional banding.

In general, the metapelites show little field evidence of retrogression, but are locally interlayered with concordant zones of a dark strongly weathered foliated rock, containing 1.5mm asymmetrical lenses of chlorite (after ?garnet) in a cataclastic matrix of fractured muscovite.

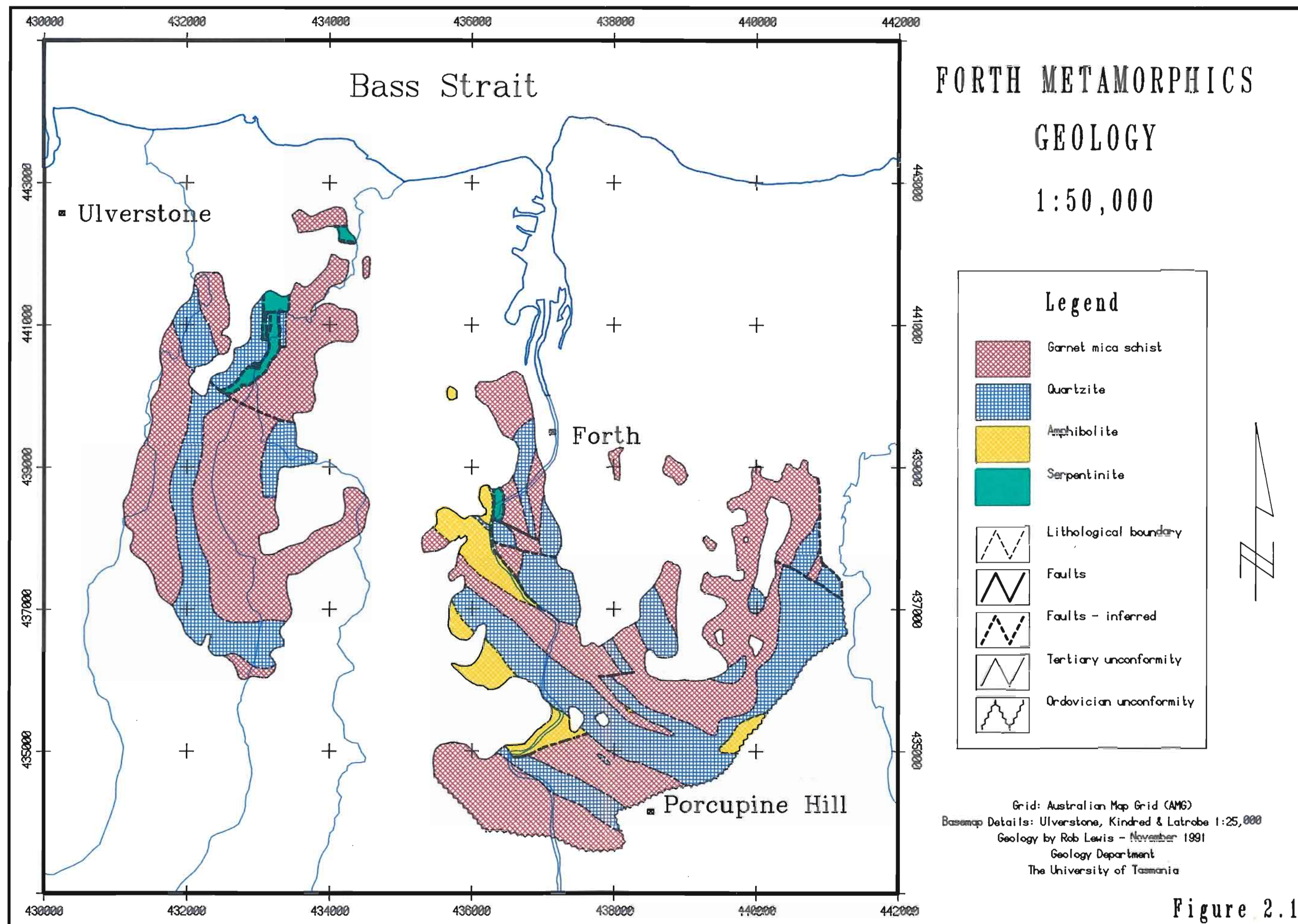


Figure 2.1

2.2.2 QUARTZITES:

Quartzites are well exposed in a number of large gravel pits (e.g. Porcupine Hill) and quarries along N-S trending strike ridges which form topographic highs between the major catchments.

The majority of quartzites are coarse-grained rocks with a spaced muscovite foliation sub-parallel to interbands of quartz mica schist. Rare garnet porphyroblasts, often weathered to limonite, occur as skeletal grains mantled by clots of chlorite. A coarse shallow plunging muscovite intersection lineation (L12) is the dominant structure in most outcrops and in places forms well-developed 5-10cm wide mullions on the margin of quartzite and mica schist bands.

Very pure, coarse vitreous quartzite occurs as a massive poorly foliated sequence up to 200m thick, near Forth Township, and also as discrete 1-5m thick bands interlayered with micaceous quartzite. The former is a distinctive marker horizon which can be traced for 4km along strike, and has been quarried for metallurgical flux at DQ385368, Sayers Hill (DQ365380) and at the Dunham quarry (DQ367394), where the rock contains over 99.9% silica (Burns 1963).

Quartz mylonites are common in the Forth Valley and occur in narrow zones associated with high grade pelitic interbands. The field appearance is a tough compact fine to medium-grained rock with a penetrative quartz muscovite foliation and closely spaced muscovite, quartz +/- tourmaline stretching lineation. This lineation differs in style and orientation from the more widely developed intersection lineation and is a useful field indicator of local mylonitic zones.

2.2.3 METABASITES:

Amphibolites, of variable textural and mineralogical style, occur in two 500m wide belts in the Forth Valley, as a small inlier NW of Forth township and as thin discontinuous bands along the western margin of the Claytons serpentinite. Burns (1964) mapped an area of amphibolite along the SE margin of the block, but this was not rediscovered during the present mapping.

The dominant lithology in the Forth Valley is a medium to coarse grained, massive or foliated rock with a variably developed down-dip LS fabric and locally, gneissic texture due to mineral segregation (Twelvetrees 1906b).

Typically, the amphibolites contain abundant 1-2mm porphyroblasts of pink garnet in a matrix of dark green prismatic hornblende, pale elongated zoisite, minor interstitial plagioclase and rare clinopyroxene (75628, 75622). In gneissic units, the garnet is segregated into 1-5cm bands interlayered with moderately foliated hornblende + zoisite domains. Plagioclase is a relatively minor

component, concentrated in medium-grained granoblastic garnet-free bands with quartz, hornblende and granular epidote (75617).

Bodies of garnet clinopyroxene zoisite quartz rock occur at DQ361382 and 1.2km south at DQ359370. The rocks resemble the Lyell Highway eclogite in hand specimen/thin section but despite the field appearance, the clinopyroxene is low in Na (i.e. not omphacite) and, on textural grounds, this rocktype will be referred to as garnet-clinopyroxene gneiss (gnt-cpx gneiss).

At DQ361382, the gneiss outcrops as locally continuous layers in a 1.5m thick zone enclosed within and sharply bounded by clinopyroxene-free garnet amphibolite. Individual layers are up to 30cm thick and contain thin bands of coarse granoblastic garnet + clinopyroxene (75627) interlayered with moderately foliated medium-grained zoisite-clinopyroxene-quartz domains (75625, 75662). The rock has a weakly developed LS fabric, concordant with a similar, but more strongly developed fabric, in the enclosing amphibolites. The gneiss at DQ359370 has a distinct colour banding due to 1-3mm wide strings of pink fine-granular garnet and bands of well foliated pale-green clinopyroxene + zoisite + quartz (75615) and occurs as surface float over an area of 100m².

Quartz and mica-rich garnet amphibolites occur in a narrow zone along the west bank of the Forth River (DQ361382) and where fresh, outcrop as tough compact, moderately well-foliated units with a variably developed down dip biotite + hornblende +/- muscovite lineation.

The micaceous sequence is at least 300m thick and inter-layered with 1-5m bands of massive garnet amphibolite. Micaceous bands locally wrap around and appear to be replacing 30cm x 10cm lenses of well-foliated mica-free garnet amphibolite which are oriented with their long axes parallel to the enclosing foliation. Both pods and the enclosing units have weakly developed but structurally concordant mylonitic textures and contain rare strongly deformed 3mm amphibole porphyroclasts.

The anomalous zone is close to the margin of mica-free garnet amphibolite and pelitic schist and continuous along strike with gnt-cpx gneiss-bearing amphibolites and mylonitic, kyanite-bearing quartzites. The field relationships suggest that micaceous bands formed at the expense of mica-free garnet amphibolite. This possibility is supported by geochemical, petrographic and structural evidence and is evaluated in a later section.

The range of lithologies in the Forth Metamorphics is similar to that of other metamorphic complexes in Tasmania and indicates derivation from a largely clastic pelite-psammite sequence (Spry 1962a, Boulter 1978, Turner 1989). The predominantly homogeneous field appearance of the amphibolites suggests they were originally massive lava flows, although local banding is not inconsistent with a sedimentary origin. The pre-metamorphic affinity of these rocks is evaluated in Chapter 3.

2.2.4 SERPENTINITE:

The metamorphics enclose bodies of serpentinite in the lower reaches of the Claytons Rivulet and in the vicinity of Forth Weir (Gould 1867, Twelvetees 1906b, 1909b, Blake 1928c, Taylor 1955, Burns 1963, 1964).

In the Lower Claytons Rivulet, strongly sheared but locally massive serpentinite forms a discontinuous west-dipping meridional belt approximately 1 x 4 km, interlayered with 2-20m thick slivers of quartzite, schist and minor amphibolite (fig.4.6) and structurally overlain to the west by massive quartzite.

An isolated body of well-foliated and lineated chlorite tremolite serpentine schist occurs 500m south of and along strike from a small serpentinite body at Forth Weir (DQ363383). The schist is enclosed by and structurally concordant with foliated garnet amphibolite but correlates with the ultramafics on geochemical and mineralogical grounds (Chapter 3).

Discontinuous layers of well-foliated and lineated, banded 'greenschist' are interlayered with quartzite along the western margin of the Claytons serpentinite body. The banding is defined by domains of coarse amphibole which are wrapped around and locally cut by zones of fine-grained amphibole + epidote + albite. Relict garnet porphyroblasts, now substantially altered to epidote, are present as discontinuous trails in some units, suggesting that at least some of the rocks were originally garnet amphibolites.

The structural characteristics and field appearance of these amphibolites are not dissimilar to basal hornblende mylonites, reported from the margins of other ultramafic bodies in Tasmania (Berry 1988, Berry & Crawford 1988) and this is discussed further in chapter 3 .

2.2.5 MINOR ROCKTYPES:

Discordant 1-3m pods and lenses of coarse, highly weathered quartzo-feldspathic rock occur on Porcupine Hill. The outcrop style is similar to the ?Cambrian Dove Granite, which intrudes Precambrian quartzites and schists on the northern margin of the Tyennan Region .

At DQ408374, pegmatitic quartz feldspar tourmaline veins cross-cut schist bands containing a medium-grained pink mica which may be lepidolite (?pseudomorphing muscovite). Feldspathic schist bands at DQ319386 contain 1mm cubic voids after ?pyrite and films of pale green malachite possibly after chalcopyrite. Apart from these scattered occurrences, there is no mineralisation in the study area.

Brittle fault zones in quartz-rich lithologies contain angular misoriented blocks of quartzite in a siliceous matrix of granulated quartz and well-foliated quartz muscovite cataclasite is locally developed in pelitic lithologies (DQ407385). Late faults are often bounded by smooth polished surfaces, which carry fibres and striation indicating the sense of shear.

CHAPTER 3

GEOCHEMISTRY

Whole-rock XRF analyses of representative compositions have been obtained, in order to address the following issues:

- 1) Were the metabasites originally igneous compositions and if so what were their petrologic and tectonic affinities?
- 2) Do mineralogical variations reflect differences in bulk geochemistry (or differences in metamorphic grade)?
- 3) Do the Forth Metabasites correlate with other high grade (Nye Bay Amphibolites and Lyell Highway Eclogites) and low grade (Rocky Cape Dykes) metabasites in Tasmania?
- 4) Do the amphibolites occurring near the Claytons Serpentinite resemble basal hornblende mylonites from other ultramafic complexes in Tasmania?

In addition to Sr, Rb, Zn and Cu, analyses include trace elements which are generally considered immobile during regional metamorphism - Zr, Nb, Y, V, Ni, Cr (Winchester & Floyd 1976) and have been grouped into 4 categories, based on mineralogy: garnet amphibolites, garnet-clinopyroxene gneisses, (retrogressed) epidote-albite amphibolites and micaceous amphibolites. Representative samples are given in table 3.1 and the entire dataset, including two 'wet' chemical analyses from Spry (1962) is reproduced in Appendix A.

3.1 PRE-METAMORPHIC AFFINITIES:

3.1.1 SEDIMENTARY VS. IGNEOUS ORIGIN:

The garnet amphibolites resemble igneous compositions of basaltic to andesitic affinity and are compositionally similar to apparently retrogressed lithologies from the Claytons Rivulet.

Metamorphic hornblende + plagioclase +/- garnet assemblages may be derived from igneous parents of basaltic affinity (ortho-amphibolites) are, more rarely, from calcareous or dolomitic shales (para-amphibolites) (Orville 1969). The latter often show well-developed compositional banding (Leake 1964), which is also a locally developed feature of the Forth amphibolites.

Leake (1964) documented a number of inter-element variation trends, which may be used to distinguish the two parageneses (fig. 3.1). The Forth amphibolites show a positive correlation between 'Niggli Mg' (a measure of Mg-enrichment generally and igneous fractionation in particular) and both Ni or Cr which is consistent with an igneous protolith. An igneous derivation is also supported by coupled variation in Niggli Mg and Niggli C and the amphibolites plot towards the evolved end of typical igneous fractionation trends (fig.3.1c).

	75606	75660	75663	75670	75636
SiO ₂	51.36	45.99	49.11	61.12	36.63
TiO ₂	0.88	0.84	1.44	1.51	0.22
Al ₂ O ₃	15.09	13.79	11.86	13.64	4.55
Fe ₂ O ₃	10.79	11.17	10.52	10.00	12.28
MnO	0.14	0.19	0.13	0.12	0.16
MgO	6.12	12.04	5.00	4.07	31.61
CaO	8.22	10.38	19.07	1.63	2.84
Na ₂ O	4.95	2.84	0.98	2.68	1.04
K ₂ O	0.60	0.47	0.06	2.38	0.06
P ₂ O ₅	0.09	0.10	0.25	0.22	0.02
LOI	1.52	1.60	1.56	2.12	10.66
TOTAL	99.76	99.41	99.98	99.49	100.07
Nb	8	8	20	41	2
Zr	56	50	175	365	10
Y	21	18	36	59	8
Sr	120	97	512	142	13
Rb	14	7	-	85	-
Ni	181	391	100	88	1794
Cr	678	730	254	143	3001
V	276	228	216	154	65
Zn	88	89	103	127	51
Cu	57	23	88	57	16

Table 3.1: Selected representative whole rock analyses. 75606 - retrogressed amphibolite (Claytons Rivulet - DQ331405). 75660 - garnet amphibolite (Forth Valley DQ357401). 75663 - garnet clinopyroxene gneiss (Forth Valley DQ361382). 75670 - micaceous amphibolite (Forth Valley DQ363375). 75636 - serpentinitic schist (Forth Valley DQ367371).

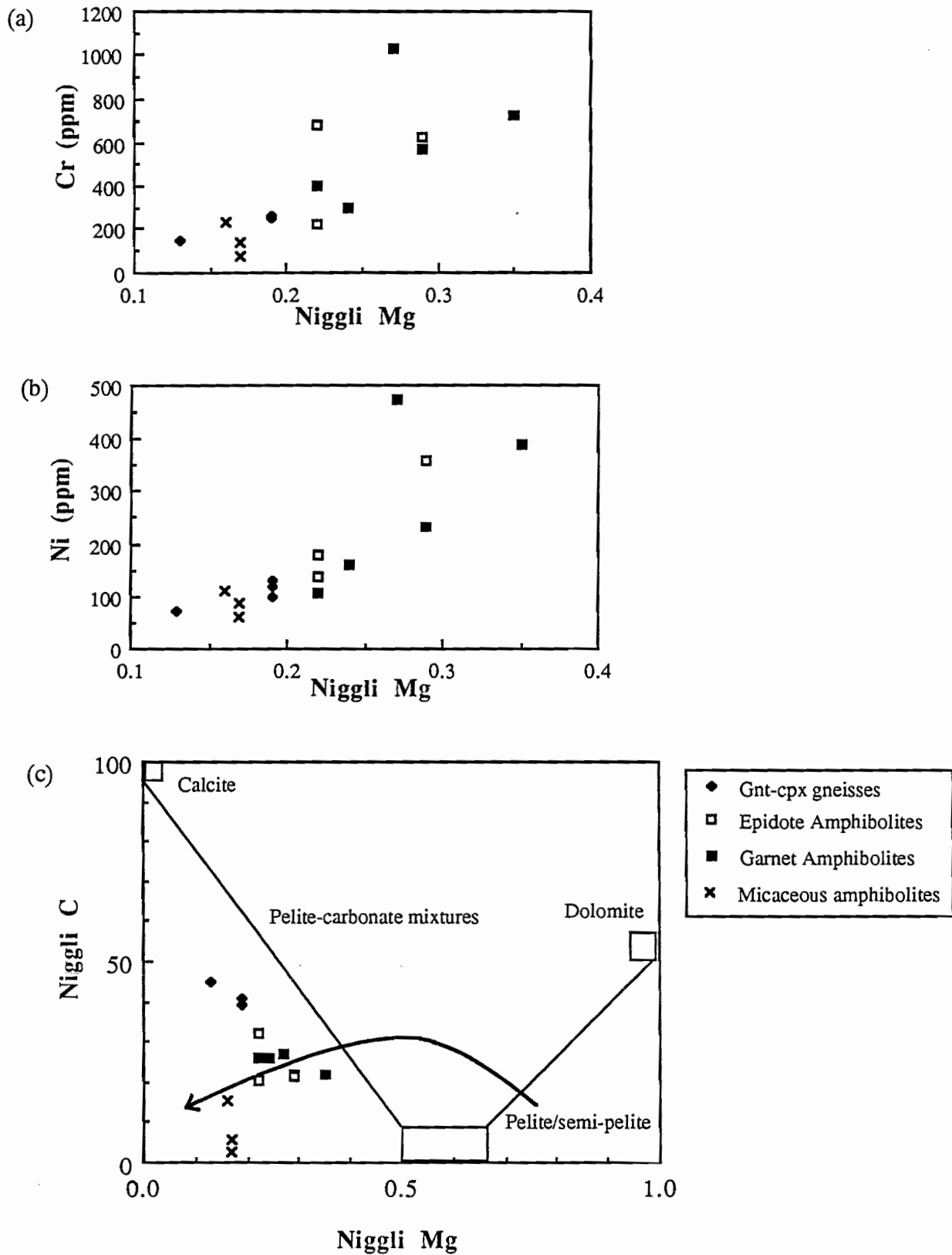


Figure 3.1: (a) Cr (ppm) vs. Niggli Mg. (b) Ni (ppm) vs. Niggli Mg ($\text{MgO}/(\text{FeO} + \text{MnO} + 2\text{Fe}_2\text{O}_3 + \text{MgO})$). (c) Niggli C ($100\text{CaO}/(\text{CaO} + \text{MgO} + \text{FeO} + \text{Fe}_2\text{O}_3 + \text{Al}_2\text{O}_3)$) vs. Niggli Mg - trend line of Karoo dolerites and pelite-carbonate mixtures after Leake (1964).

The garnet clinopyroxene gneisses are geochemically distinct from the amphibolites, having up to 20% CaO (cf. 12%) and are correspondingly depleted in MgO, Na₂O and K₂O. The high CaO content is unlike common magmatic liquid compositions (fig.3.1c) and three alternative explanations for the enrichment have been considered.

A cumulate origin is consistent with the interbanded morphology of the units, although the excess CaO is not matched by high MgO (clinopyroxene cumulate) or Al₂O₃ (plagioclase cumulate - see below) and therefore this model has been discarded.

In newly accreted oceanic crust, enrichment in CaO may result from local precipitation of hydrous calc-silicates (such as hydrogrossular, prehnite, pumpellyite or epidote) in a process known as rodingitisation (Honnorez & Kirst 1975, Ito & Anderson 1983). The Ca-rich fluids are derived from heated sea-water during amphibolitisation/albitisation of clinopyroxene/anorthitic plagioclase assemblages (Hardie 1983, Bideau et al 1991).

This possibility can be discounted, as CaO vs. Al₂O₃ variation between the gneisses and amphibolites, is unrelated to representative calc-silicate compositions (fig.3.2).

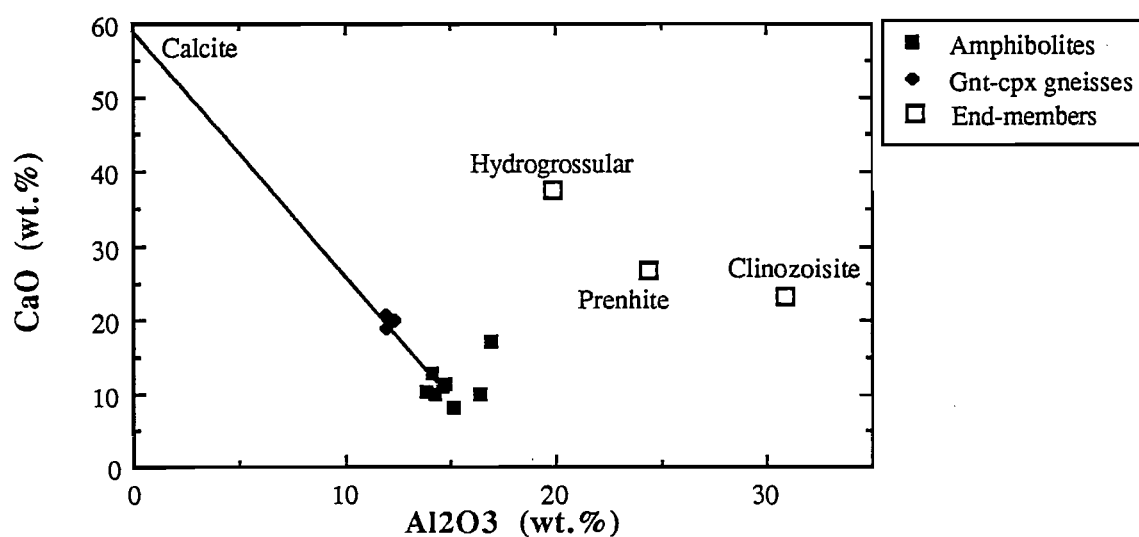


Figure 3.2: CaO (wt%) vs. Al₂O₃ (wt%) for garnet clinopyroxene gneisses and amphibolites. Compositions of calc-silicate phases from Deer *et al* (1967).

The gneisses are intermediate in composition between garnet amphibolites and an Al-free end-member with approximately 60% CaO. A similar trend is shown in figure 3.1c, where the gneisses lie on a mixing line between the garnet amphibolite cluster and a 100% CaO/ 0% MgO diluent. These considerations support calcite (60% CaO, Niggli C = 100) alteration, possibly as a result of local veining, as the cause of the CaO anomaly.

This is consistent with petrogenetic constraints (sect.5.3) suggesting significant H₂O-dilution by a CO₂-rich fluid during prograde metamorphism and, in this context, the mineralogical difference between the gneisses and amphibolites is largely a result of geochemical, rather than P-T variation.

As apparent from their mineralogy, the mica-rich garnet amphibolites are enriched in Si, K and Na and depleted in Ca and Mg in comparison with adjacent garnet amphibolites. The group forms isolated clusters or linear trends on most inter-element variation diagrams, and shows strong enrichment in Rb, Zr, Ti/V and Nb/Y. The enrichment in alkalis and incompatible elements is not modelled by typical igneous fractionation trends (fig.3.1c) and sub-horizontal variation of FeO*/MgO vs. Ti, Zr and FeO* (fig.3.5) also argue against a magmatic origin - for which coupled variation would be expected (Hall 1987).

The distinctive geochemical signature is, however consistent with textural evidence suggesting heterogeneous syn-post metamorphic development of alkali-rich phases and is considered to be metasomatic in origin.

3.1.2 PETROLOGIC/TECTONIC AFFINITIES:

Simple trace element discriminant diagrams, based on the petrological features of fresh igneous rocks, have been compiled by Floyd & Winchester (1975) and Winchester & Floyd (1976). Coupled variation of TiO₂, Zr and P₂O₅ indicate a broadly tholeiitic character for the Forth amphibolites (fig.3.3).

Zr-Y-Ti-V discriminant diagrams, based on the geochemistry of recent volcanics, may also be used to constrain the original tectonic setting of metamorphosed basaltic compositions (Pearce & Cann 1973).

The micaceous amphibolites and garnet clinopyroxene gneisses plot wholly within the calc-alkaline field but in view of their anomalous major element geochemistry, this is of doubtful significance. The unaltered amphibolites appear to have no within plate affinity and figure 3.4a suggests ocean-floor affinities. This is however complicated by ambiguous overlap with both ocean floor and island arc basalts fields and the associated, largely clastic sequence makes an ocean-floor (i.e. mid-ocean ridge) origin unlikely. Local sequences of extremely pure quartzite may be derived from deep-sea chert, but show no mineralogical evidence of the Fe or Mn enrichment, characteristic of these rocks.

Despite this conclusion, an island arc origin appears equally unlikely given the quartz-rich, potassic composition of the metasediments. These features are more characteristic of a passive continental rather than convergent margin setting, in which sediments are typically dominated by Ca-rich (plagioclase-derived) greywackes.

Continental rift tholeiites, approaching MORB compositions have been reported from continental provinces (Crawford & Berry 1991 - *in review*) and a passive margin setting with minor MORB-type volcanics appears to be the most plausible tectonic model for this sequence.

3.2 CORRELATION:

The petrologic features of the Forth metabasites are unlike the Rocky Cape Dyke suite which has well defined alkaline affinities (Brown 1989) and this correlation is not pursued further.

The garnet amphibolites are broadly similar in their major element geochemistry to other high grade Tasmanian metabasites - specifically the Lyell Highway eclogites (Kamperman 1984) and Nye Bay Amphibolites (McNeill 1985). Trace element variation between the groups is ambiguous and significant differences are evident in terms of Zr/Ti and Nb/Y variation. The co-genesis of these suites cannot be established on available data.

The Forth amphibolites have little affinity with basal hornblende mylonites associated with mafic-ultramafic complexes in Tasmania, which are significantly depleted in incompatible elements. Serpentinitic schist from the Forth Valley (75636) correlates with the ultramafics in terms of both major (low SiO₂ -36.63%, high MgO - 31.61%) and minor elements (low Ti, high Ni and Cr), and in most inter-element diagrams plots within hornblende mylonite fields. Of three epidote amphibolites from the western margin of the Claytons serpentinite, 75608 plots consistently within or on the margin of this group. Apart from the absence of a Ti-bearing phase, however, this unit is petrographically similar to other amphibolites in the area, and the significance of this correlation cannot be assessed.

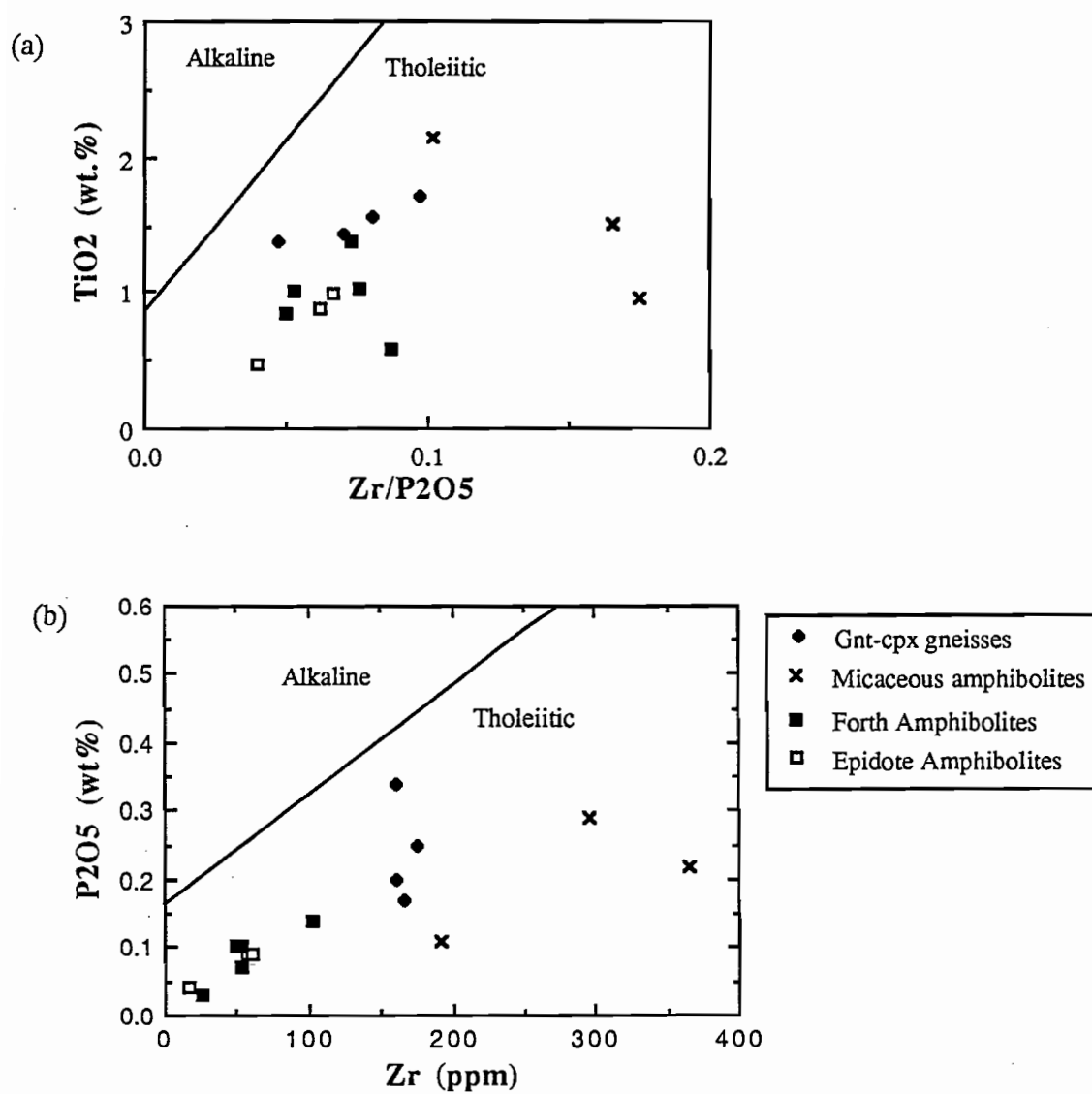


Figure 3.3: Forth amphibolites - petrologic discriminant diagrams. (a) TiO_2 (%) vs. $\text{Zr}/\text{P}_2\text{O}_5$. (b) P_2O_5 (%) vs. Zr (ppm). Fields from Floyd & Winchester (1975) and Winchester & Floyd (1976).

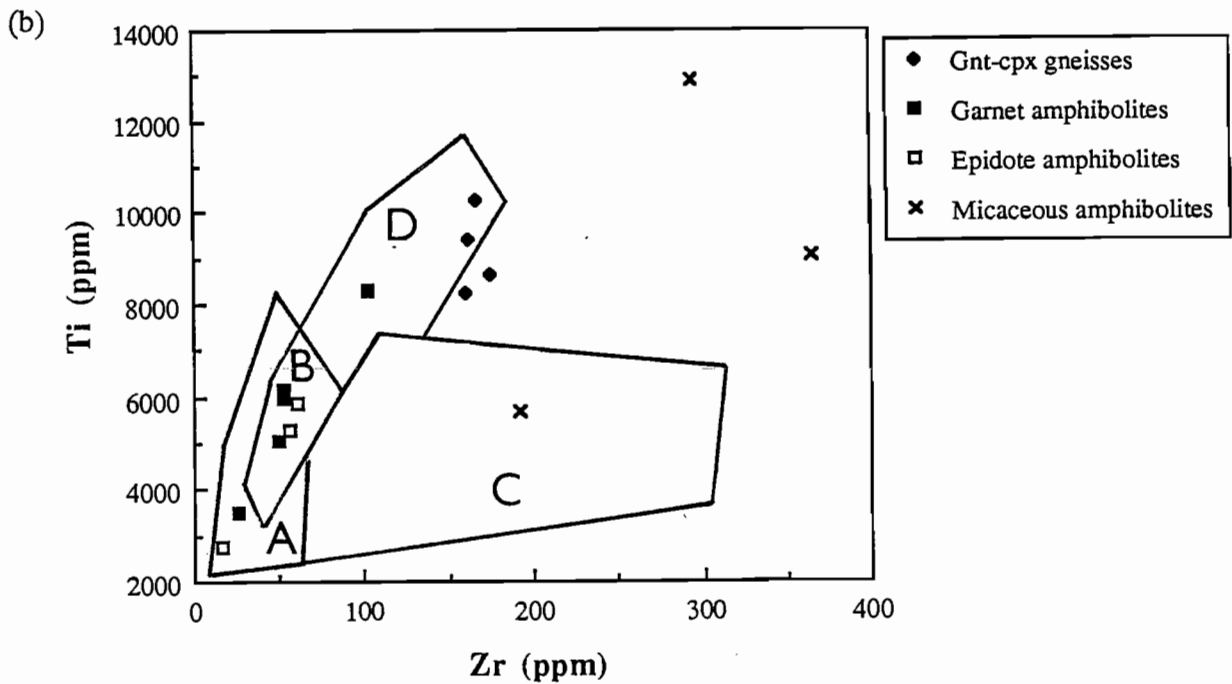
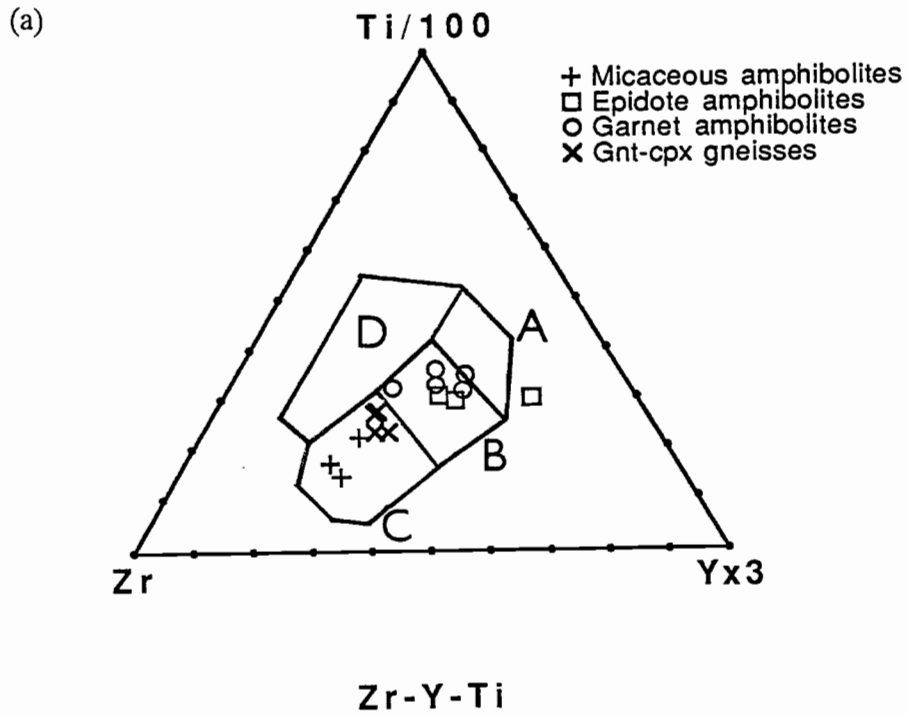


Figure 3.4: Forth amphibolites - tectonic discriminant diagrams. (a) Zr (ppm) - Y (ppm) $\times 3$ - Ti (ppm)/100. (b) Ti (ppm) vs. Zr (ppm). Within plate basalts = D, ocean floor basalts = B, low-K tholeiites = A&B, calc-alkali basalts = B&C (Pearce & Cann 1973).

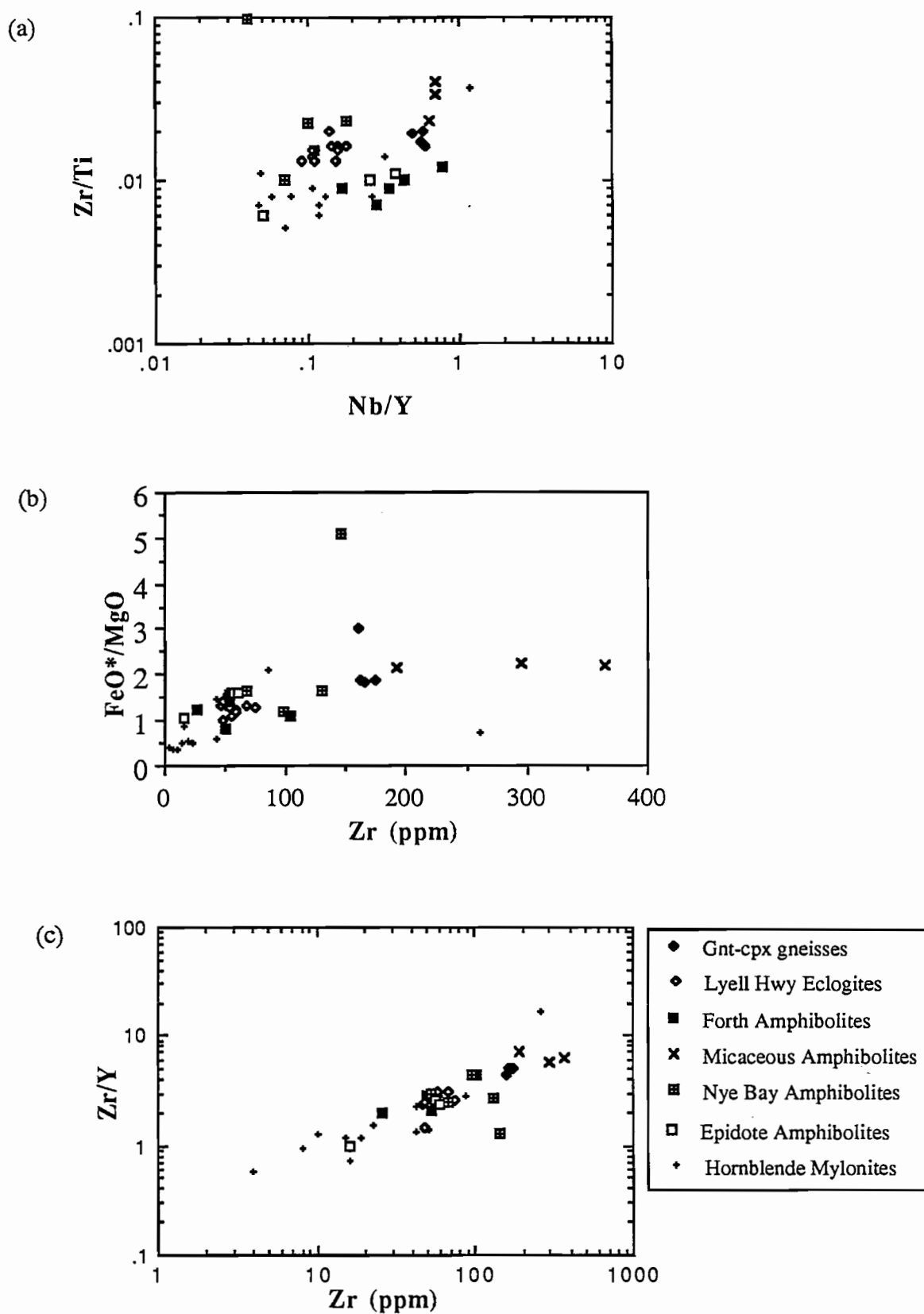


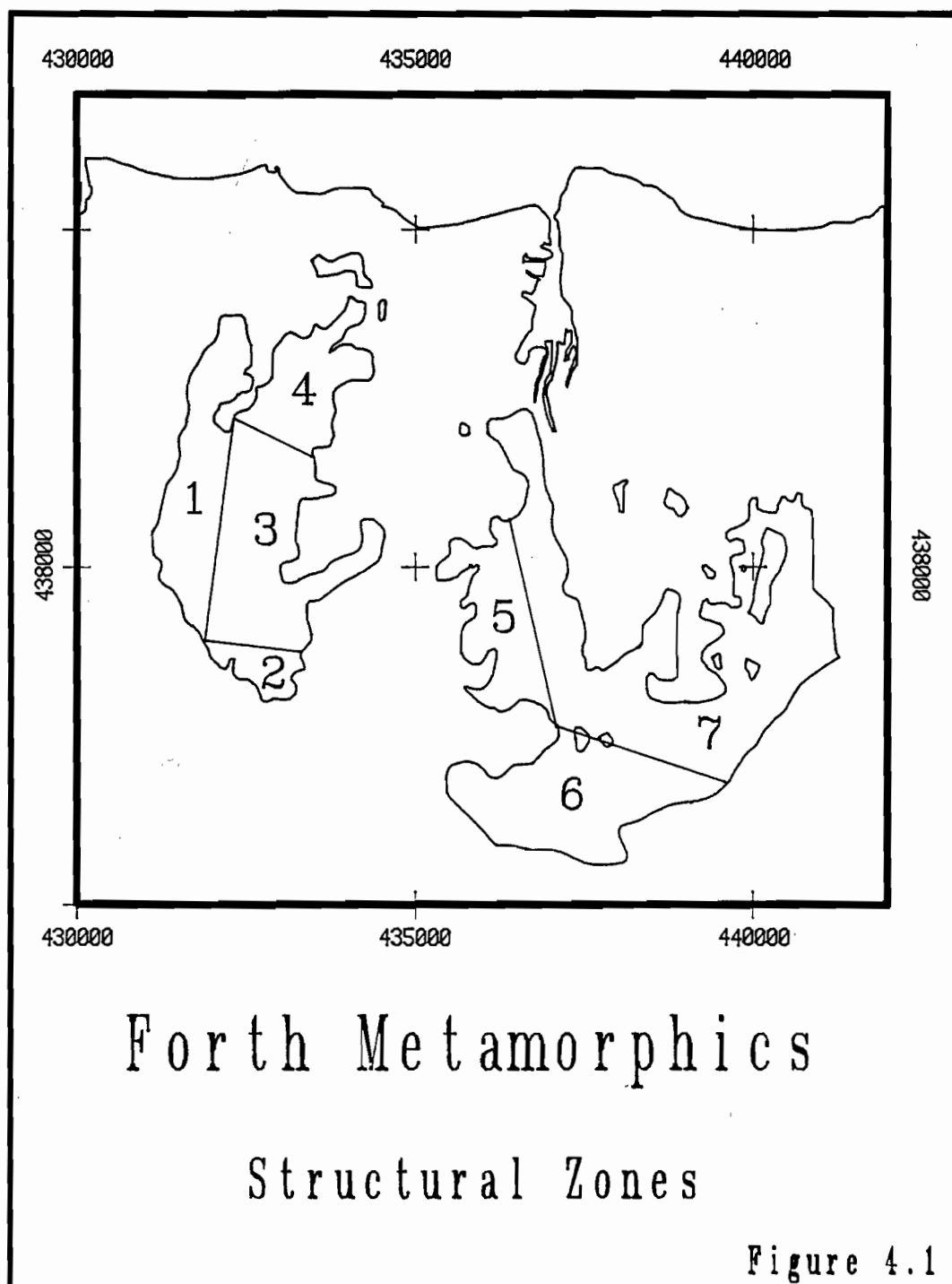
Figure 3.5: Inter-element variation of Tasmanian high grade metabasites and hornblende mylonites. (a) Zr/Ti vs. Nb/Y. (b) FeO*/MgO vs. Zr (FeO* = FeO + 0.9 x Fe₂O₃). (c) Zr/Y vs. Zr.

CHAPTER 4

STRUCTURE

Apart from scattered reconnaissance work (Gould 1867, Twelvetees 1906b, 1909b) and regional mapping by Burns (1963, 1964), little work has been done on the structure of the Forth Metamorphics. This early work proposed a broad division between early syn-metamorphic ductile strain and later more brittle-style deformation which is maintained in the following discussion.

Interpretation of the early structural history is complicated by later events and, for this reason, the area is sub-divided into a number of zones (fig.4.1).



4.1 SYN-METAMORPHIC STRUCTURE:

4.1.1 MESOSTRUCTURE:

4.1.1.1 COMPOSITIONAL BANDING:

The earliest recognisable structure in the metasediments is a well-developed compositional layering due to 1-10 cm alternation of quartzite and garnetiferous schist bands. In most cases this is a transpositional layering, parallel to the dominant tectonic surface (S2) and has no stratigraphic significance. Near Abbotsham, however, 1-2cm dark layering due to layers rich in iron oxides is folded by F1 and may represent original bedding (Burns 1964). No other sedimentary structures are preserved .

Compositional banding in the amphibolites/gneisses, due to alternating pale plagioclase/quartz and dark garnet or hornblende/clinopyroxene/zoisite domains, is always parallel to the dominant foliation and probably due to metamorphic segregation.

4.1.1.2 D1 STRUCTURES:

Mesoscopic F1 folds are only found in fine grained garnet mica schist along the western margin of the metamorphics. At DQ312384, 1-2cm quartzite bands are folded into a series of isoclinal 5cm wavelength rootless intrafolial folds with a muscovite foliation, S1 as axial plane.

Away from F1 hinge zones, S1 is parallel to compositional layering and moulds discontinuous lenses of quartzite and vein quartz. In pelitic layers, the foliation is a well developed penetrative dimensional preferred orientation of muscovite (Pl.4.1). In quartz-rich interbands, S1 is a statistical preferred orientation of fine-grained muscovite in a mosaic of equant undulose quartz with fine-grained disseminated ?hematite and scattered granular rutile. In quartzites, S1 is mesoscopically preserved in the hinge zone of F2 folds as a variably developed fine-grained muscovite foliation parallel to compositional layering.

East of the Claytons Rivulet, mesoscopic F1 folds are absent and S1 is only present as a microstructure. Relicts of S1 are preserved in micaceous units either as microlithons at a high angle to the dominant S2 foliation (Pl.4.1), as a statistical preferred orientation of muscovite in quartz-rich domains or as linear or curved quartz inclusion trails in coarse garnet porphyroblasts which are wrapped around by S2. In places, coarse S2 muscovite and quartz contain linear trails of very fine-grained ?hematite at a high angle to S2 which may represent S1 or compositional banding.

4.1.1.3 D2 STRUCTURES:

The morphological expression of the dominant D2 deformation varies between different lithologies and spatially from west to east across the Forth Metamorphics.

Fold related structures:

Fold Style:

F2 folds are only rarely found in pelitic lithologies. Near Abbotsham (DQ312384), S1 is parallel to a quartzite-schist compositional banding and folded in narrow bands of angular upright 2m wavelength close to tight symmetrical folds with a 1mm spaced crenulation cleavage (S2) as axial plane (Pl.4.1). Further east, tight to isoclinal intrafolial folds in quartzite interbands are the only evidence of F2 folding in schist, and S2 is a closely spaced domainal schistosity defined by coarse flakes of syntectonic muscovite and biotite.

F2 folds in quartzite are widespread but not abundant. Two kilometers south-east of Buttons Creek, the small gravel pit at DQ316373 exposes a sequence of south-west dipping, shallow north-west plunging tight to isoclinal folds in interlayered banded quartzite and quartz mica schist. The folds are defined by thin trails of opaque material, rotate an early penetrative layer-parallel mica foliation (S1) and have a weak axial plane cleavage (S2) due to spaced muscovite flakes and flattened quartz grains. In profile, the folds have rounded thickened hinge zones, attenuated planar limbs and are type 2 similar folds according to the dip isogon classification of Ramsey (1967). The fold hinges at this locality form a series of north-east facing synformal closures, of 2m wavelength, separated by small shear zones which have a streaky stretching lineation at approximately 90 ° to the fold axes. These features are consistent with local westward transport.

On Porcupine Hill, isolated small-scale F2 folds in interbanded quartzite and schist have variable morphology. Quartzite layers are preserved through the fold profile and have a weakly developed S2 cleavage which crenulates layer-parallel S1 on the limbs. Schist bands, in contrast, are markedly attenuated on the limbs and thickened in the hinge zones forming angular wedges with a strongly developed axial plane schistosity.

Where F2 folds are absent, S2 is sub-parallel to compositional banding but is locally deflected into discrete low angle slip planes which transect the mesoscopic layering, forming an asymmetrical tapered wedge known as foliation boudinage. This is a high strain feature, characteristically developed under extensional stress, on the limbs of isoclinal folds (Platt & Vissers 1982).

The amphibolites, in places, contain strings of disjunctively folded quartz veins with axial surfaces sub-parallel to a moderately developed amphibole-zoisite foliation but otherwise show little evidence of folding. Where present, the foliation is parallel to a hornblende-plagioclase compositional banding and sub-parallel to S2 in adjacent schists. Burns (1964) describes long-limbed isoclinal folds in compositional banding with the amphibole foliation as axial plane, but these were not rediscovered during the present study. During D2 the amphibolite bodies appear to have behaved as massive competent blocks or were folded on a long wavelength only. The dominant foliation may have formed during D1 and been passively rotated parallel to S2.

S2 Microstructure:

The petrographic expression of S2 varies with the mesoscopic F2 style. In the west, S2 is a medium-grained 1mm spaced crenulation cleavage in fine to medium-grained schists, defined by thin foliae of muscovite and chlorite which offset a layer parallel S1 fabric. The foliae separate domains of medium-grained non-undulose granoblastic quartz +/- plagioclase and wrap around 0.5mm garnet porphyroblasts.

Over most of the Forth Metamorphics, however, S2 is a coarse anastomosing domainal foliation, axial plane to rare isoclinal crenulations in recrystallised S1 muscovite. Phyllosilicate-rich (P-) domains enclose discontinuous ribbons or lenses of weakly undulose, medium to coarse granoblastic quartz (Q-domains) and wrap around porphyroblasts of garnet +/- deformed kyanite +/- chloritoid (Pl.4.1 & 5.1).

The dominant amphibolite foliation is expressed petrographically as a strong dimensional preferred orientation of non-undulose, sub-idioblastic 1-1.5mm hornblende +/- zoisite prisms which enclose granoblastic lenticular domains of medium-grained non-undulose plagioclase +/- undulose quartz. Equilibrium grain textures are indicated by curvilinear grain boundaries and predominantly three-phase intersections.

The gneiss at DQ361382 has granoblastic domains of equant 1.5mm garnet intergrown with plates of coarse xenoblastic clinopyroxene. These are interlayered with foliated bands of prismatic zoisite, elongate clinopyroxene and trails of 0.4mm garnets in a matrix of granoblastic quartz.

Plate 4.1: Pelitic microtextures. Scale bar 0.5mm.

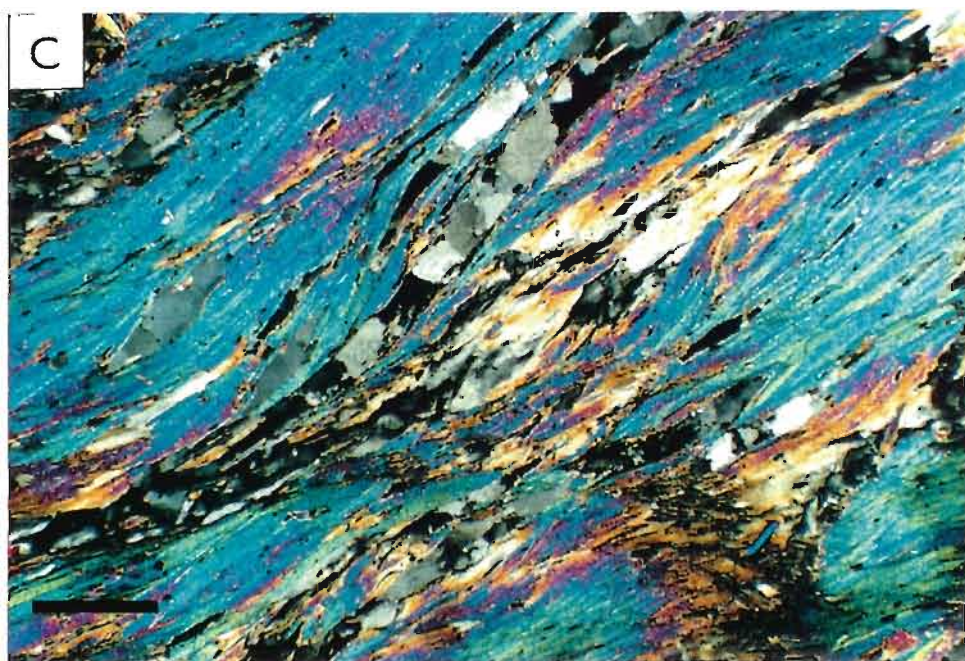
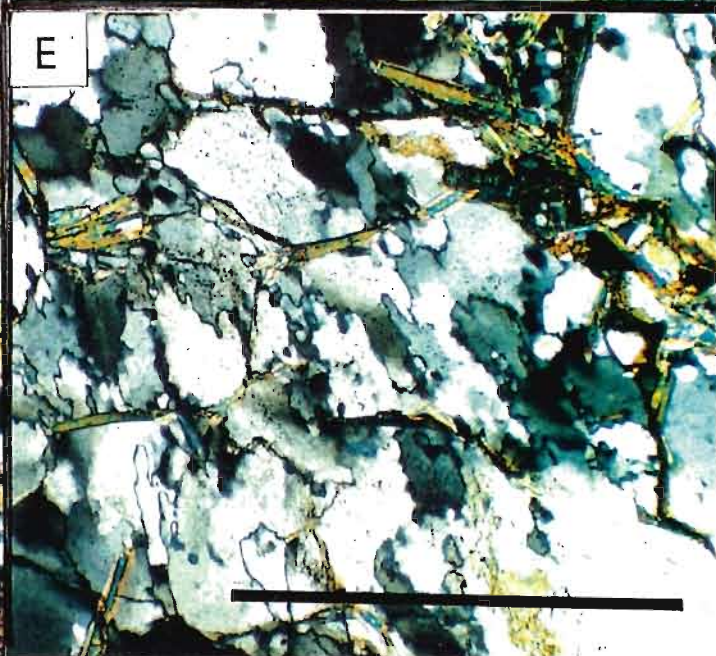
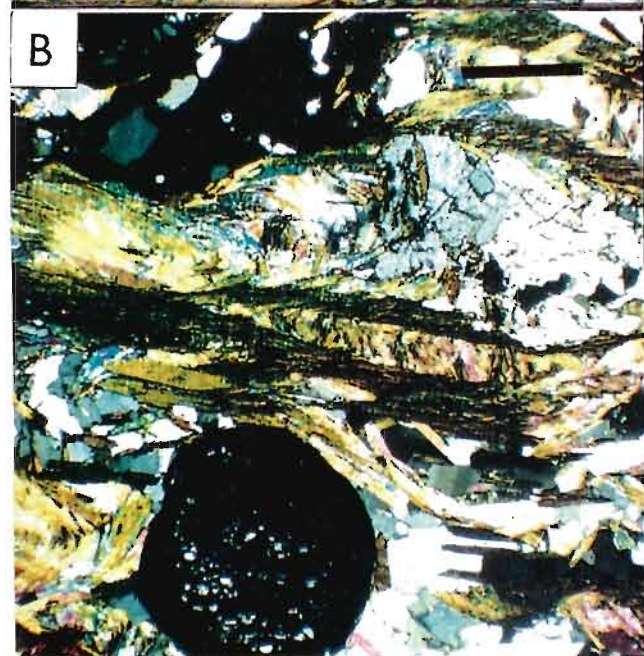
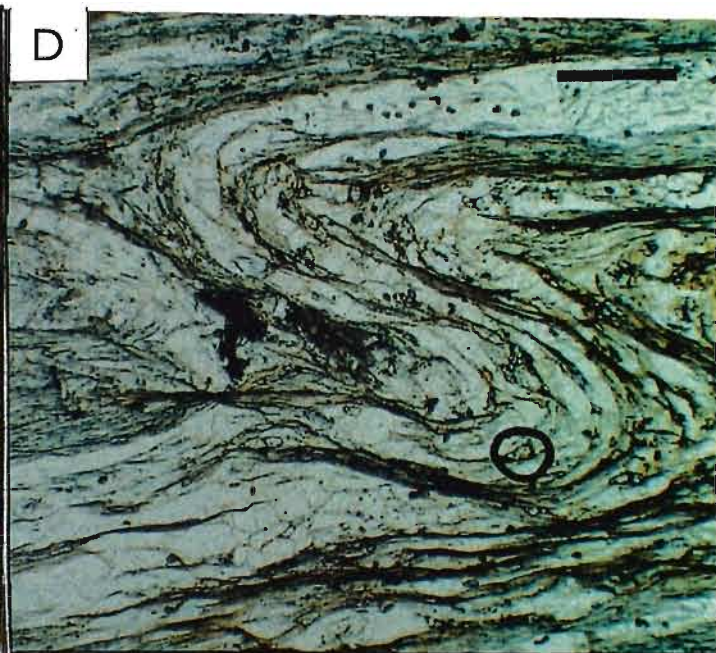
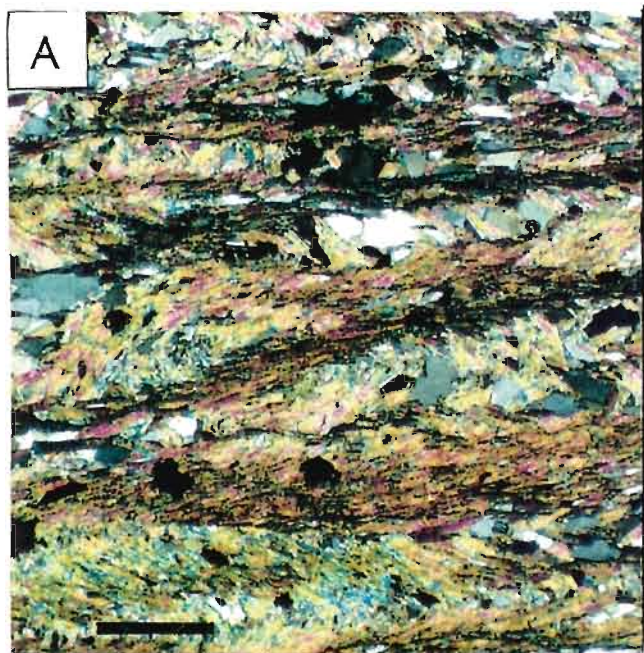
A. Buttons Creek. Penetrative S1 cleavage preserved between spaced foliae of S2 - Crossed Nicols (XN)(75598 - DQ315385).

B. Forth Valley. S1 microlithon between coarse anastomosing S2 in albite garnet schist - XN (75637 - DQ372366).

C. Forth Valley. Coarse domainal S2 schistosity - XN (75641 -DQ368361).

D. Claytons Rivulet. F3 microfold - Plane Polarised Light (PPL). Grains of apparent high relief (circled) are plagioclase mantled with a thin selvage of iron oxides (75600 - DQ322396).

E. S3 quartz sub-grain preferred orientation at a high angle to spaced S2 muscovite foliation in hinge zone of F3 microfold - XN (75600 - DQ322396).



Micaceous and quartz rich amphibolites have complex mineralogy and grain textures. S2 in these units is defined by irregular elongate domains of quartz + plagioclase and ragged prisms of subidioblastic amphibole. The amphibole is overgrown by interlayered biotite and muscovite which may be parallel or at a high angle to the foliation.

Lineations:

The quartzites have a coarse muscovite lineation due to the intersection of S1 and S2, which in places forms a characteristic mullion structure on the margin of quartzite and schist bands. Where S1 is well-developed, the lineation on S2 is a variable striping of medium to coarse grained muscovite depending on the local development of S1. Similar intersections are not found in schist, owing to the almost complete transposition of S1 parallel to S2.

The zonal orientation and geographical distribution of these lineations are shown in figure 4.2. In each of the structural zones, L12 is locally sub-parallel to F2 fold axes and has a characteristic uniformly shallow pitch on S2. The lithological distribution and consistent orientation define a distinctive morphology, which Burns (1964) named the Porcupine Hill Style. The shallow pitch is maintained despite the late brittle-style rotation of S2: this is a significant feature and is returned to in a later section (see 4.2.1.4).

Mylonites:

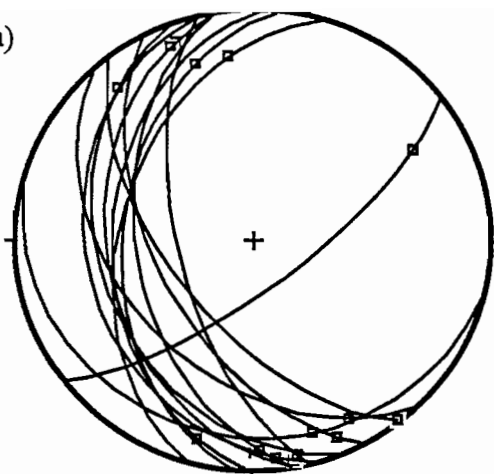
Field Relationships:

In addition to the shallow pitching axial structures of the Porcupine Hill Style, Burns (1963,1964) noted a second distinctive linear morphology on S2, well developed in schists (?) and amphibolites near the mouth of Goldie Creek.

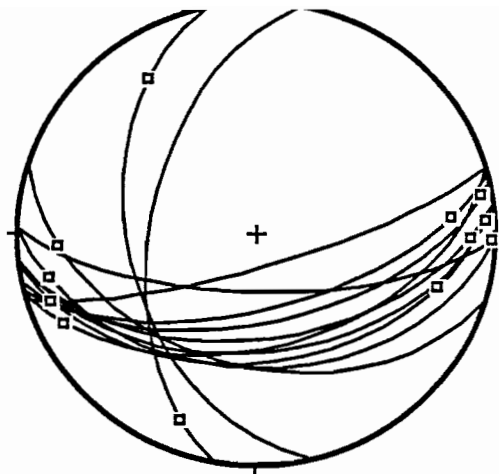
In amphibolites, the 'Goldie Creek Style' is a strong hornblende or zoisite lineation producing a well-developed mesoscopic LS fabric in hand-specimen. A similar but weakly developed clinopyroxene + zoisite lineation is also present in gneiss interbands at DQ361382. In quartzites, the style is a dimensional preferred orientation of quartz, fine-grained muscovite and prismatic tourmaline developed on S2 surfaces in compact, well-foliated rocks which lack the L12 intersection.

In contrast to the Porcupine Hill intersections, Goldie Creek Style lineations have a *steep* pitch on S2 and are only found east of the Claytons Rivulet (fig.4.3). They are best developed along the axis of the Forth Valley, where gnt-cpx gneisses and coarse kyanite-bearing schists are found. Despite suggestions by Burns (1964), lineations of this style and orientation were not found in pelitic units.

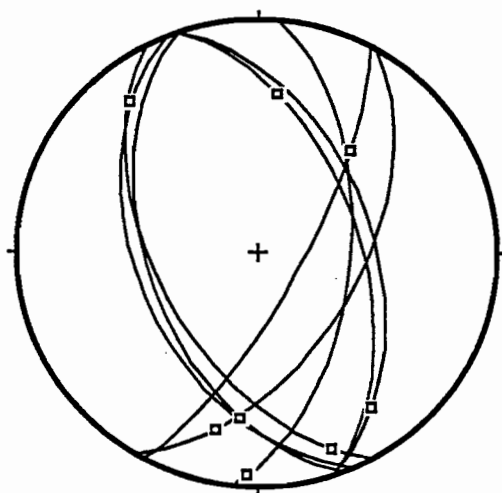
(a)



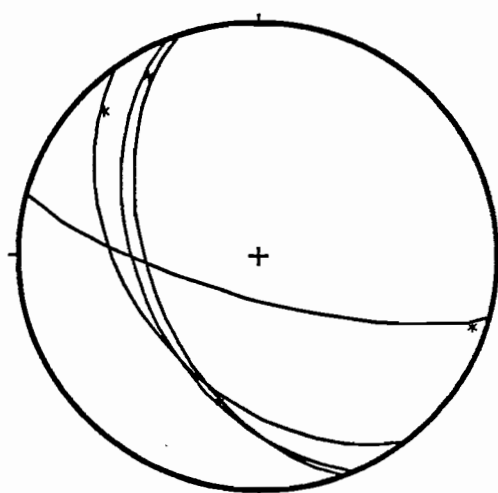
ZONE 3 - L12



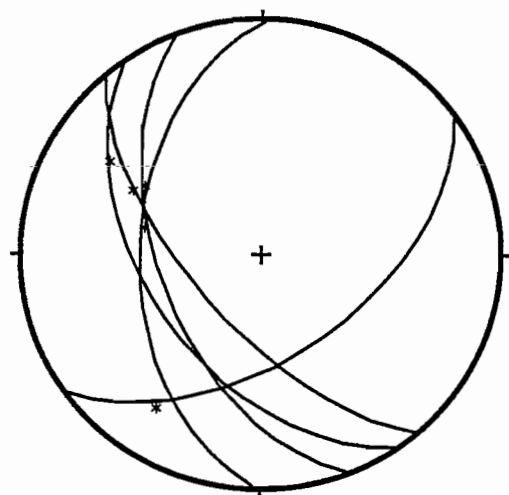
ZONE 6 - L12



ZONE 7 - L12



ZONE 7 - F2 HINGES



ZONE 1 - F2 HINGES

(b)

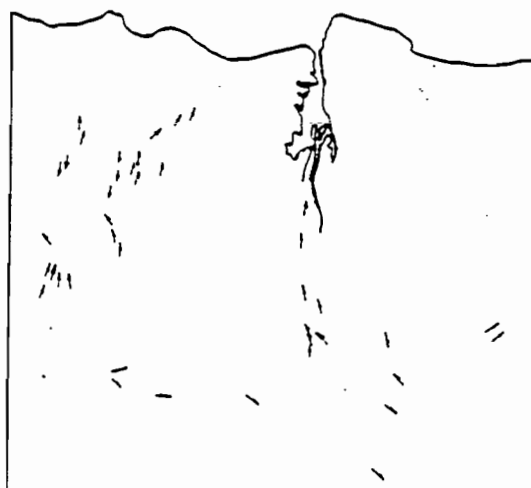
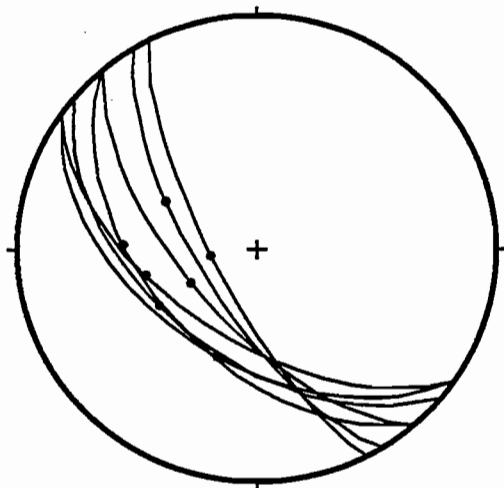
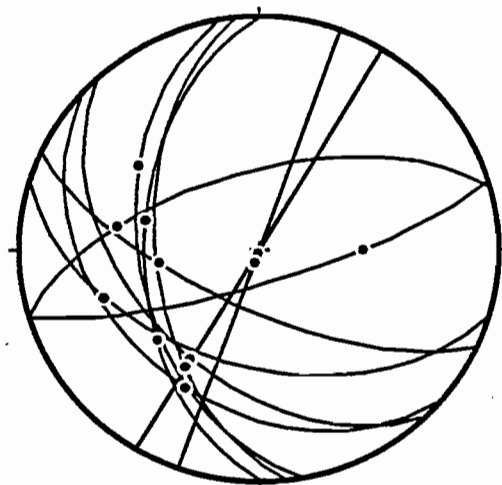


Figure 4.2: (a) Zonal orientation of L12 and F2 fold axes. (b) Geographical distribution of 'Porcupine Hill Style' lineations (*from* Burns 1964).

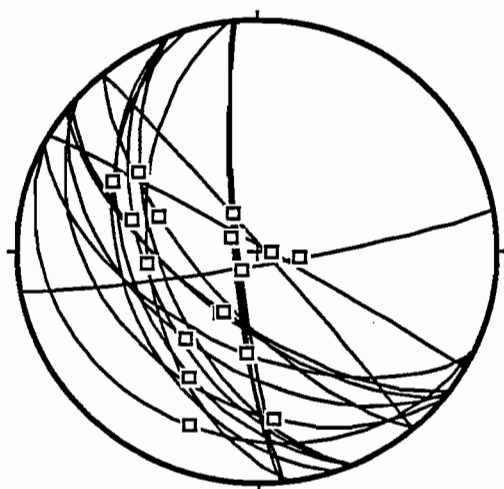
(a)



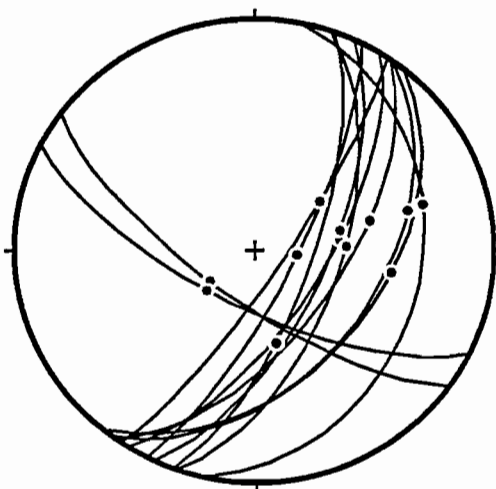
ZONE 5 - Lmus



ZONE 6 - Lmus



ZONE 5 - Lh



ZONE 7 - Lmus

(b)



Figure 4.3: (a) Zonal orientation of hornblende and muscovite stretching lineations. (b) Geographical distribution of 'Goldie Creek Style' lineations (*from* Burns 1964).

Burns (1964) noted strong quartz microfabrics in some units of the Forth Metamorphics, but gave no explanation for the bimodal distribution of lineation types. In the present study, down dip mineral lineations in quartzite and amphibolite are found to be associated with mylonitic grain fabrics. In this context, the Goldie Creek Style marks the location of ductile shear zones, which separate folded domains where axes and intersections of the Porcupine Hill style are developed.

Mylonitic micro-fabrics:

In thin section, the quartz mylonites have a medium-grained mosaic of elongate strongly undulose quartz with serrate or partially recrystallised grain boundaries. The mylonitic foliation is defined by a preferred orientation of quartz and strongly appressed muscovite +/- biotite flakes. The latter have an asymmetric 'fish' morphology, show evidence of (001) slip and wrap around rare 1.5mm tourmaline prisms which have spaced extensional microfractures. Individual quartz grains have sub-parallel 0.1mm deformation bands which dictate a strong optical preferred orientation (Pl.4.2). Deformation lamellae are common and appear as 0.05mm lenticular bands of slightly different refractive index from the host grains. The lamellae terminate within grain margins and are consistently oriented at 80-90 ° to deformation bands.

In quartz aggregates, experimentally deformed below about 700°, deformation bands characteristically result from basal <c> slip on (0001), although prism <a> slip mechanisms may operate at high temperatures (Nicolas & Poirier 1976) or under conditions of high fluid pressure (Garbutt & Teyssier 1991). Basal slip appears to be the dominant mechanism of plastic deformation in most natural quartz mylonites (Vernon 1976).

Experimental work by Ave Lallemant & Carter (1971) has shown the orientation of deformation lamellae to be dependant on the P-T conditions during deformation (fig.4.4). This model must be applied with caution, however, as TEM investigation of natural quartzites, has shown that microstructural features identified as deformation lamellae can result from a number of physical processes and may not necessarily define active slip planes (Christie & Ardell 1974). The model also requires the extrapolation of experimental conditions to natural strain rates.

In the majority of mylonites studied here, deformation lamellae are consistently oriented at 80-90° to deformation bands (Pl.4.2) and two interpretations are possible. According to figure 4.4, if the deformation bands resulted from basal slip, the prismatic lamellae orientation indicates temperatures at or above 800°C. Alternatively, the lamellae may have a non-prismatic orientation with respect to prism slip deformation bands. Without c-axis determination, it is not possible to specify the slip

mechanism, although relatively high temperature and low stress conditions are suggested by the relatively coarse grain size, lack of recrystallisation and limited retrogression of these mylonites (Nicolas & Poirier 1976).

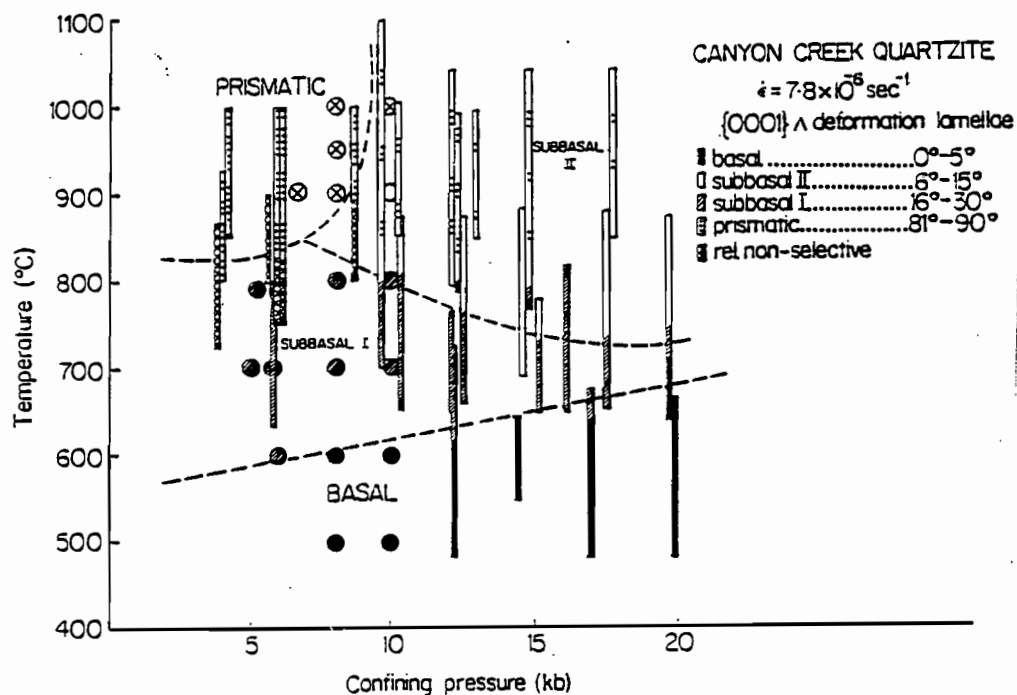


Figure 4.4: Orientation of deformation lamellae ($\{0001\}$ lamellae) with respect to temperature and confining pressure (from Ave Lallemant & Carter 1971).

Well-developed mylonitic textures are also found in albitic schists from the eastern margin of the metamorphics (DQ407386). In 75653, abundant 1mm porphyroblasts of asymmetrical elongate albite, containing sigmoidal opaque inclusion trails, are wrapped around by a fine-grained well-foliated matrix of asymmetrical 'fish-like' muscovite. The mylonitic foliation has a strong down dip lineation and is disrupted by abundant extensional shear bands. The mineralogy and grain texture of this unit resemble albitic schists from the Mary Group in central Tasmania, and indicate albite growth prior to mylonitisation.

Despite the strong mesoscopic LS fabric, mylonitic micro-textures are only weakly developed in the amphibolites and only in a restricted area. Along the west bank of the Forth River, rotational grain fabrics are preserved in pods of foliated mica-free garnet amphibolite enclosed within bands of muscovite and biotite-rich amphibolite. The pods have a strong mesoscopic LS fabric and contain asymmetric garnet porphyroblasts, weakly developed sinistral shear bands and spectacular 2mm long lensoid porphyroclasts of kinkbanded amphibole (Pl.4.2).

Plate 4.2: Mylonitic textures. Scale bar 0.5mm.

A. Quartz deformation lamellae - XN (75657 - DQ409373).

B. Quartz deformation bands/lamellae and mica 'fish'. Note sub-vertical deformation bands oblique to mica foliation and lamellae (fine sub-horizontal hatching) at approximately 90° to bands - XN (75657 - DQ409373).

C. Quartz microtexture - XN (75666 - DQ330364).

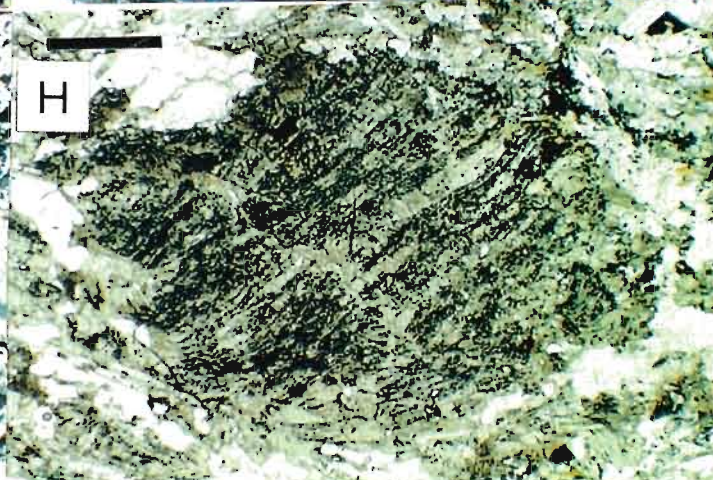
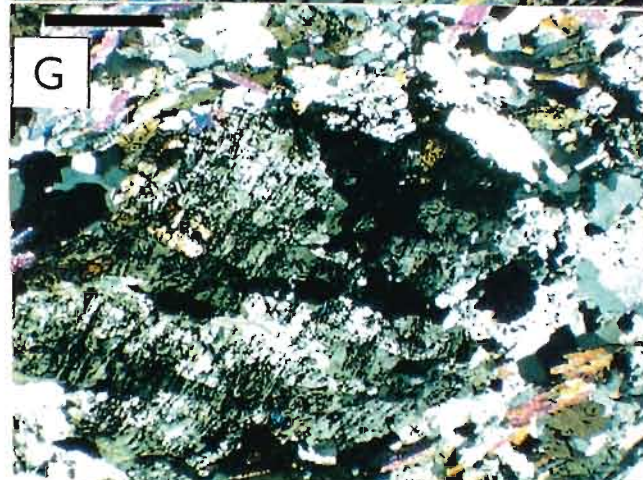
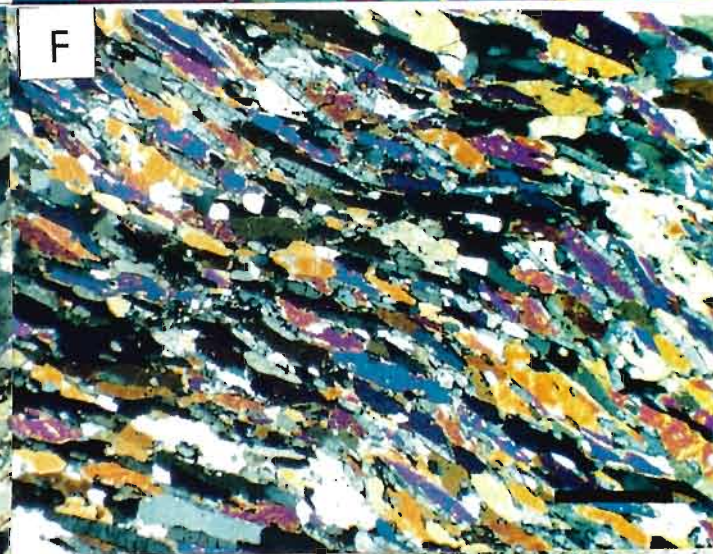
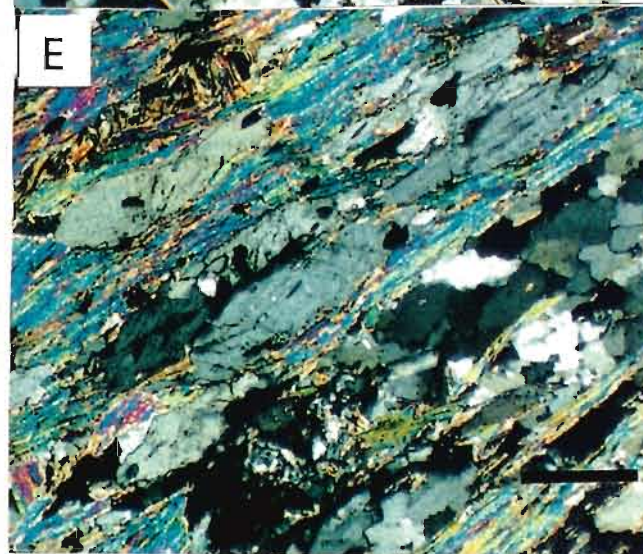
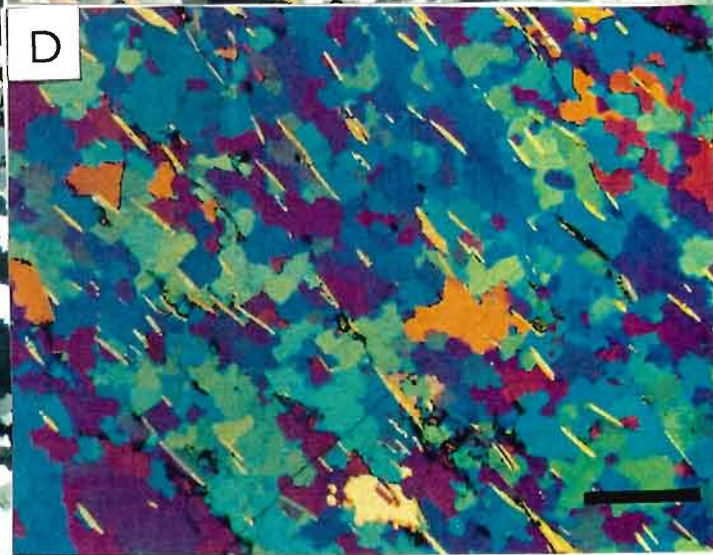
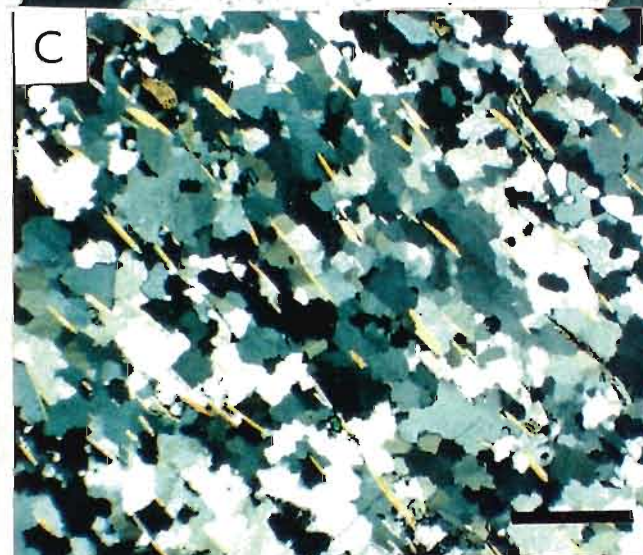
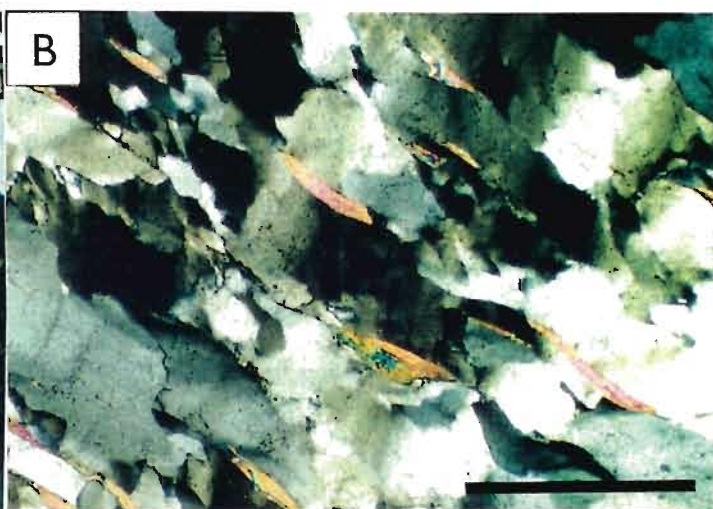
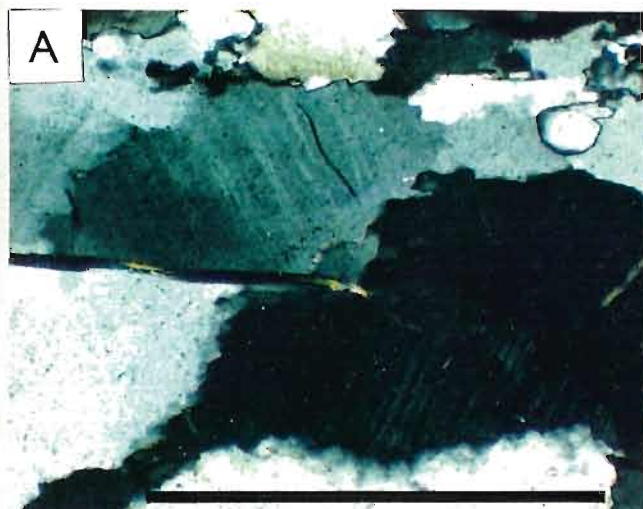
D. As above with gypsum plate showing strong quartz lattice preferred orientation.

E. Strongly appressed albite porphyroblasts - XN (75653 - DQ407386).

F. Shear band in well-foliated amphibole zoisite amphibolite - XN. Zoisite has low birefringence and spaced transverse fractures (756710 - DQ362375).

G. Recrystallisation in large amphibole porphyroblast - XN (75669 - DQ361375).

H. As above in PPL showing asymmetric opaque (?magnetite) exsolution trails.



Limited experimental work has shown that amphiboles are among the strongest of silicate minerals. Plastic deformation by mechanical twinning on (101)[101] is only activated if the resolved stress exceeds 2-4 kb at 400-600°C, $\epsilon = 10^{-5} \text{ s}^{-1}$ and 5-15 kb confining pressure (Nicolas & Poirier 1976). Distinct weakening occurs above 800° C or at high pore fluid pressure.

It appears that, over most of the Forth Metamorphics, although the temperature and strain rate were high enough to induce local plastic deformation in quartz, conditions were not sufficiently extreme to initiate intracrystalline slip in amphibole.

Shear indicators:

Many of the microstructural features described above can be used to determine the sense of shear (Simpson 1986).

The orientation of quartz deformation bands record the last increment of ductile strain during D2. In eight oriented quartzites from widely scattered localities with variable S2 orientation the bands are oriented at 30-50° to the mylonitic foliation and indicate left lateral, westward transport. This sense of shear is supported by weak muscovite shear bands, rare asymmetrical σ -type skeletal garnet porphyroblasts and asymmetric mica 'fish' (Pl.4.2).

In 75671, the asymmetric morphology and strong sub-grain preferred orientation in kink-banded amphibole also supports left lateral shear.

4.1.2 MACROSTRUCTURE/CORRELATION:

The strong deformation and regional metamorphism in the Forth Metamorphics is similar to that in the Tyennan Region and is generally considered to be of Precambrian age (Spry 1962, Burns 1963, 1964, Turner 1989 - see Ch).

As noted by Burns, the most striking structural feature of the Forth Metamorphics is the almost complete transposition and overprinting of the early S1 fabric by the late S2 crenulation cleavage. Fold axial structures are restricted in occurrence and their present orientation suggests isoclinal folding about a shallowly N-S plunging axis.

Quartz mylonites are widespread east of the Claytons Rivulet and shear indicators consistently support west-directed tectonic transport. Schist belts were high strain zones, in which there was almost complete transposition of D1 structures during D2. Despite the development of strong mesoscopic LS fabrics, the amphibolites appear to have behaved as relatively competent blocks,

throughout most of the D2 deformation. Mylonitic fabrics are only developed in a narrow belt, along the west bank of the Forth River, in close association with garnet-cpx gneiss interbands and high grade pelitic bands in mylonitic quartzites. Late D2 K-metasomatism in this area - supported by mineralogical and geochemical constraints - may have resulted as the metabasites were thrust into a locally alkali and silica-rich environment buffered by adjacent pelitic lithologies.

In the Claytons Valley, pods of coarse-grained chloritoid paragonite staurolite garnet schist in a sequence of quartz mylonites may indicate the axis of another ductile shear zone.

The westward tectonic transport in the Forth Metamorphics is concordant with sinistral transpressive shear bands in the Ulverstone Metamorphics at Picnic Point (Berry *et al* 1990). Elsewhere in Tasmania, however, large scale Precambrian fold vergence and local syn-metamorphic mylonitic textures have generally indicated eastward transport (Turner 1989): in the central part of the Tyennan Region, for example, the high grade Franklin Metamorphic Complex appears to override the lower grade Scotchfire Metamorphic Complex along a west dipping reverse mylonite zone (Kamperman 1983, Turner 1989).

In the context of local Precambrian tectonics, westward transport is more consistent with the present east to west pattern of (high grade) Forth Metamorphics -> (lower grade) Ulverstone Metamorphics - > (un-metamorphosed) Rocky Cape Group as well as metamorphic P-T zonation within the Forth complex (see Chapter 5).

Woodward *et al* (*in review*) have re-evaluated the possibility, suggested by gravity data (Leaman 1989), that the entire Forth Region is a rootless allochthonous block, emplaced during two separate Paleozoic thrusting events. An exotic structural provenance may partly reconcile the regionally anomalous tectonic features of the block, but this possibility cannot be assessed in the present study.

4.2 POST-METAMORPHIC STRUCTURE:

Overprinting of syn-metamorphic structures by later more brittle-style deformation has been reported from several Precambrian areas in Tasmania. Near Frenchman's Cap, schists and quartzites of the Mary Group are deformed by large scale folds and faults which also affect overlying Lower Paleozoic sediments and are considered to be of Devonian age (Spry & Gee 1964).

In the Forth Region, post-metamorphic deformation is evident on a number of scales ranging from macroscopic rotation of S2 to outcrop-scale faults and small wavelength concentric or kink-style folds. Late cleavage development is more common in schistose lithologies but also affects retrogressed amphibolites in the Lower Claytons Rivulet. The quartzites are faulted and have locally

developed fracture cleavage but show limited evidence of folding. Massive garnet amphibolites are generally unaffected by the late deformation, although microfolds are present in well-layered micaceous units near Goldie Creek.

The purpose of the following discussion is to describe the style, orientation and relative chronology of post-S2 structures and attempt to correlate these with known or inferred deformation events in Northern Tasmania.

4.2.1 DOMINANT POST-S2 DEFORMATION (D3):

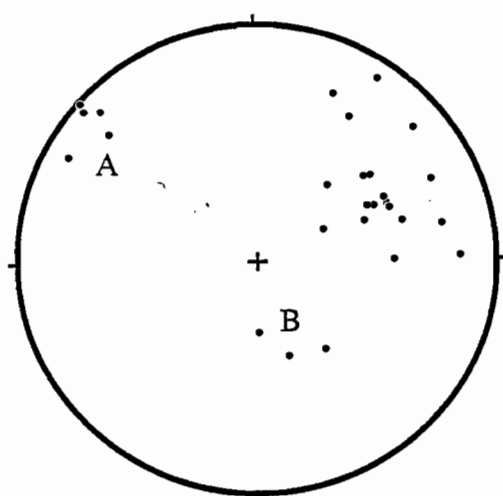
4.2.1.1 FOLDING AND CLEAVAGE DEVELOPMENT:

Along Castra Road, the dominant late structure in schist is a moderately south-west dipping crenulation cleavage, expressed as a set of well-developed shallow SSE and minor NNW plunging crenulation lineations on S2 (fig.4.5). The late cleavage, provisionally labelled S3, may be locally dominant forming discrete zones of strongly penciled schist.

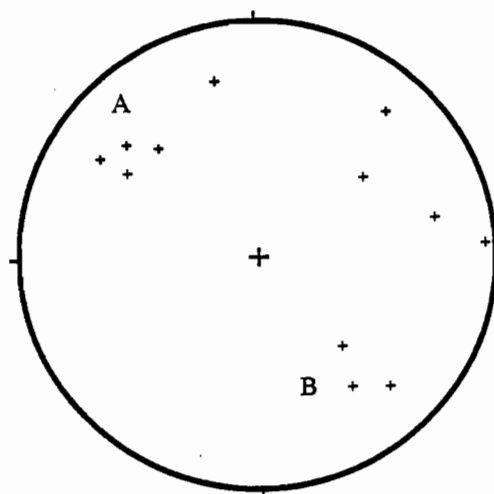
Further east, mesoscopic folds have a somewhat irregular axial plane orientation and show little cleavage development. They generally plunge moderately to the south west (fig.4.5) and are spatially associated with zones of locally anomalous E-W striking S2 orientation. In schist, the folds vary from 1-2m wavelength open angular kinks to small scale crenulations in the S2 schistosity. Near Goldie Creek small wavelength steeply plunging folds in micaceous amphibolite have a concentric profile with limited vertical extent and are bounded by discrete decollement planes.

4.2.1.2 S3 MICROSTRUCTURE:

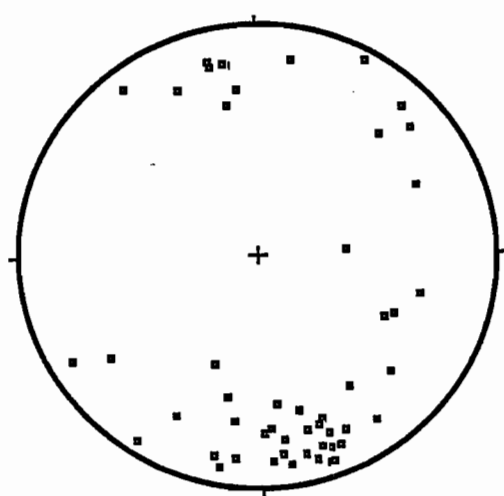
In 75600 from the Claytons Rivulet (DQ325394), S2 is folded into asymmetric close to tight crenulations which define a weak S3 cleavage in hand specimen. In thin section, the crenulation hinges are defined by polygonal recrystallised muscovite and quartz is locally recrystallised as fine-grained patches of optically and dimensionally oriented grains, parallel to the fold axial plane (Pl.4.1). The quartz preferred orientation may have been controlled by a pre-existing S2 fabric, although the apparent recrystallisation of both quartz and muscovite suggests at least lower greenschist facies conditions during deformation (Wilson 1973, Vernon 1976). This is supported by the presence of coarse 1mm clots of ragged chlorite parallel to the crenulation axial planes, possibly formed during retrogressive shearing of garnet.



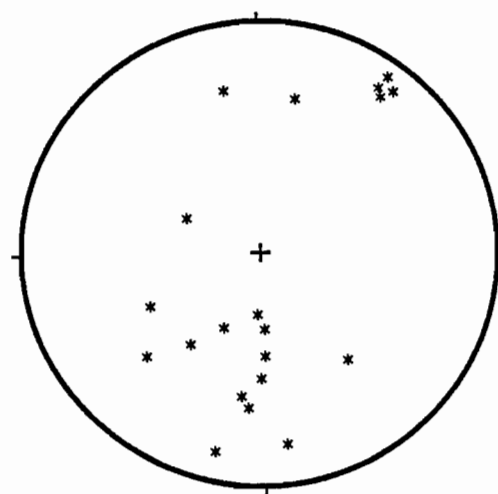
S3 cleavage



F3 - axial planes



L23 - crenulation lineations



F3 - hinges

Figure 4.5: Late brittle-style structural elements - Forth Metamorphics (groups A and B discussed below).

In samples where S3 is not mesoscopically obvious, S2 may be weakly overprinted by open symmetrical crenulations and kink bands producing undulose extinction in S2 muscovite.

4.2.1.3 SERPENTINITE:

The field setting of the ultramafics has been discussed in chapter 2, and the local geology of the Claytons Rivulet body is shown in figure 4.7.

Fabric:

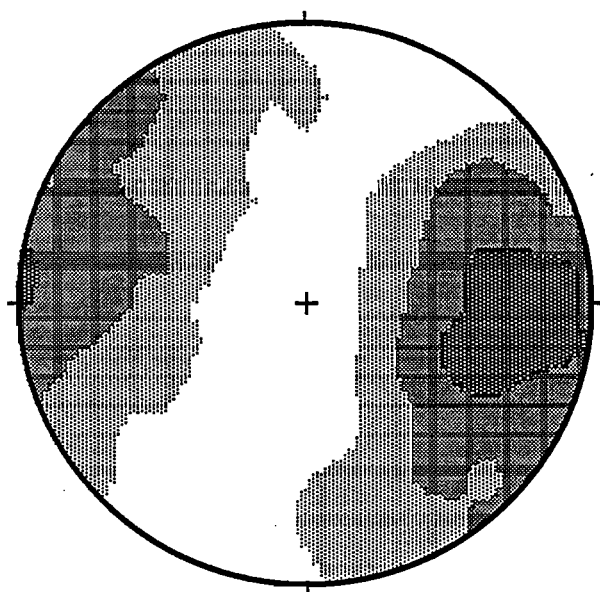
At DQ364385, original igneous textures are preserved in bodies of coarse-grained massive serpentinite with 2cm long bastite pseudomorphs after ?orthopyroxene. Elsewhere, small domains of medium to coarse massive serpentinite are locally preserved between striated slip surfaces in foliated units and these may have aligned xenoliths of banded ?amphibolite (DQ331405) or a preferred orientation of bastite pseudomorphs (Burns 1964).

In outcrop, the serpentinite has a complex anastomosing shape-fabric foliation defined by the long dimension of asymmetric 4 x 7 x 2 cm lenses of fine-grained serpentine. The lenses are bounded by a conjugate set of WNW to WSW and ESE dipping slip surfaces with predominantly down-dip striations and fibre lineations (fig.4.6). The modal shape fabric foliation is dominated by west dipping surfaces, on which the fibres indicate reverse movement.

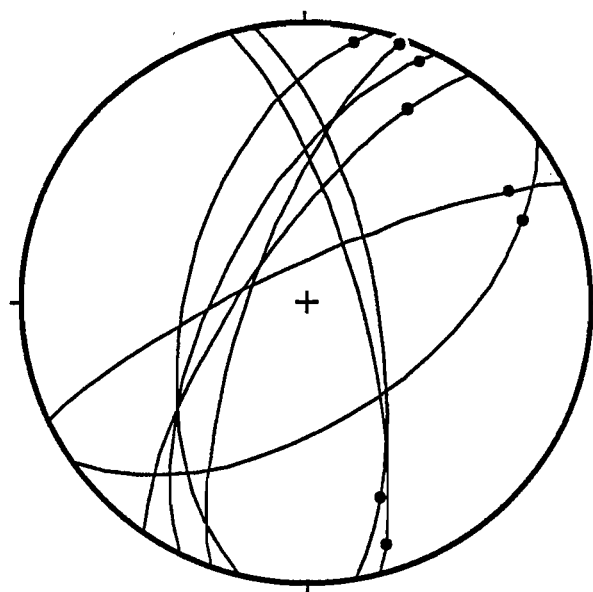
The lenses may enclose a complex system of internal shears and in places have a penetrative cleavage which dips more steeply west than the shape fabric. Where present, the cleavage is rotated towards the margins of the lenses and indicate reverse west-over-east movement.

Contacts:

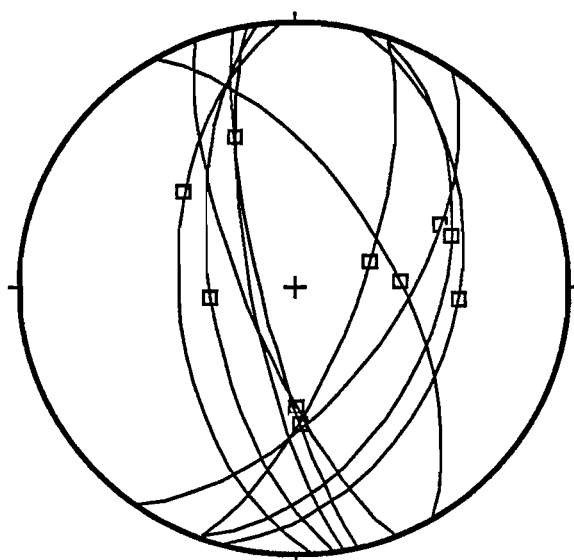
Close to its western margin, the serpentinite is interlayered with slivers of quartzite, strongly foliated epidote amphibolite and minor garnet mica schist. The amphibolites, interlayered with the quartzite, are fine-grained, well foliated rocks with a sub-horizontal amphibole lineation sub-parallel the late crenulation lineation in adjacent schist. The lineation is parallel to the axes of tight microfolds in a weak mesoscopic banding defined by lenses of coarse amphibole, layers of albite or trails of small garnet porphyroblasts.



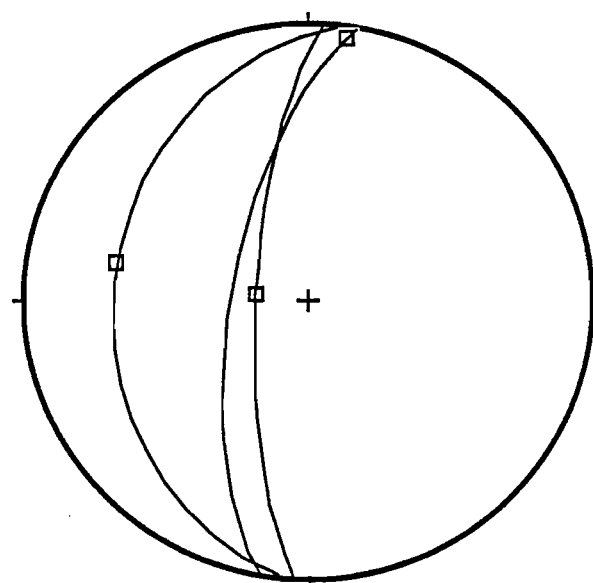
(a) Poles to foliation ($n = 41$, $ci = 2\sigma$)



(b) D4 striations



(c) D3 fibres and striations



(d) Forth Valley striations

Figure 4.6: Serpentine structures from Claytons Rivulet. (a) Poles to shape fabric foliation. (b) Late dextral striations. (c) Dominant down-dip fibres and striations. (d) Forth Valley structures.

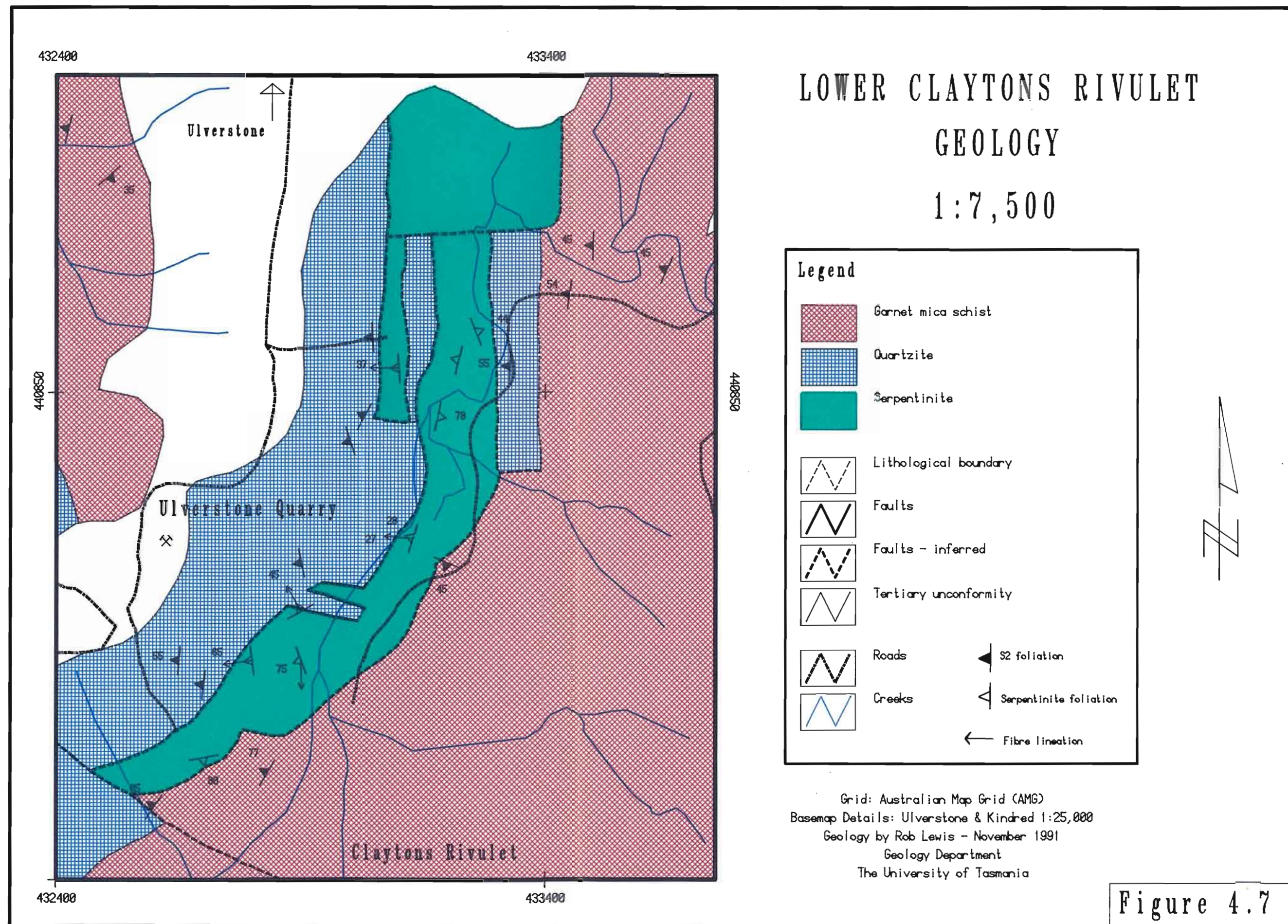


Figure 4.7

In thin-section, the coarse lenses enclose weakly undulose 1.5mm asymmetric amphibole porphyroclasts which are marginally replaced and cross-cut by thin bands of fine-grained amphibole. The coarse domains are moulded by a strongly foliated matrix of fine-grained amphibole, granular epidote, sericitised albite and trails of ?hematite. In 75612, unaltered rims of 1mm garnet porphyroblasts enclose cores of fine-granular epidote and are moulded by the foliation. In places, the altered garnets are fractured and displaced across 1mm bands of ultra fine-grained amphibole. The mineralogy and structure of these amphibolites differ markedly from unaltered garnet amphibolites further east and is consistent with retrograde shearing along an east-west trending axis. The interlayered sequence passes westward, through a gap in exposure, to be structurally overlain by massive quartzite. 30m above the inferred contact, the quartzite is cross-cut by a series of undulating thrust surfaces above deeply weathered bands of very coarse garnet-mica schist. The base of massive quartzite units are marked by a thin laminated zone which has weakly developed dip slip striations and, in places, a down dip tourmaline lineation. Foliated schist bands below the slip plane are up to 30 cm wide and, in places have an internal west dipping foliation oblique to their margin. The geometry of this zone is shown in figure 4.8.

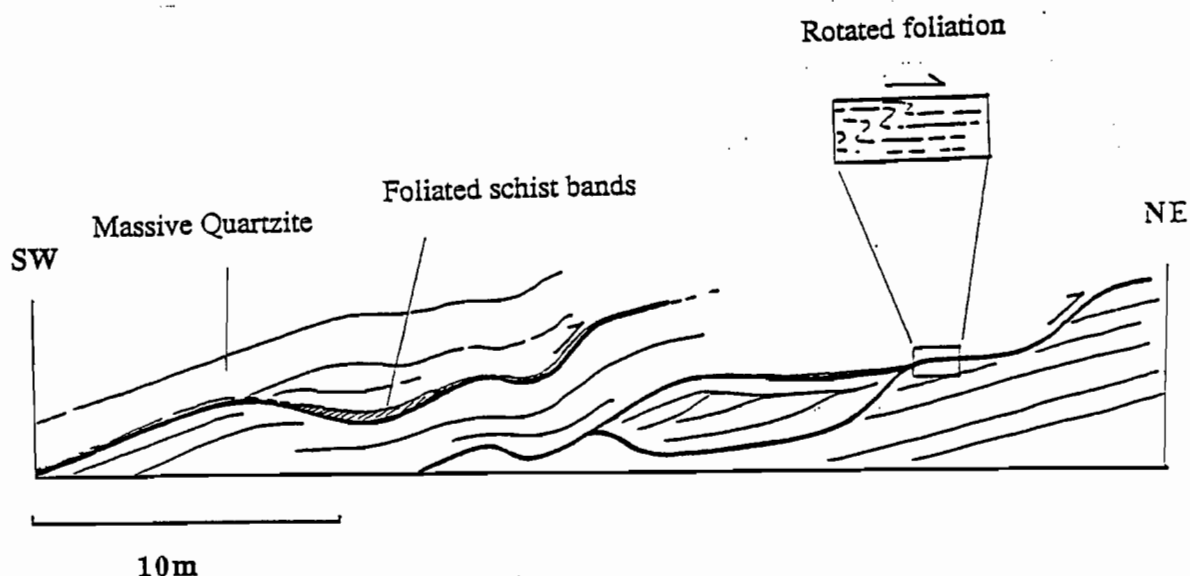


Figure 4.8: Thrust zone in quartzite 30m above the western serpentinite contact (DQ331409).

4.2.1.4 FAULTING:

The thrust related structures, described above, may be correlated with a small set of south-west dipping reverse faults and shear zones in schist and quartzite (fig.4.9).

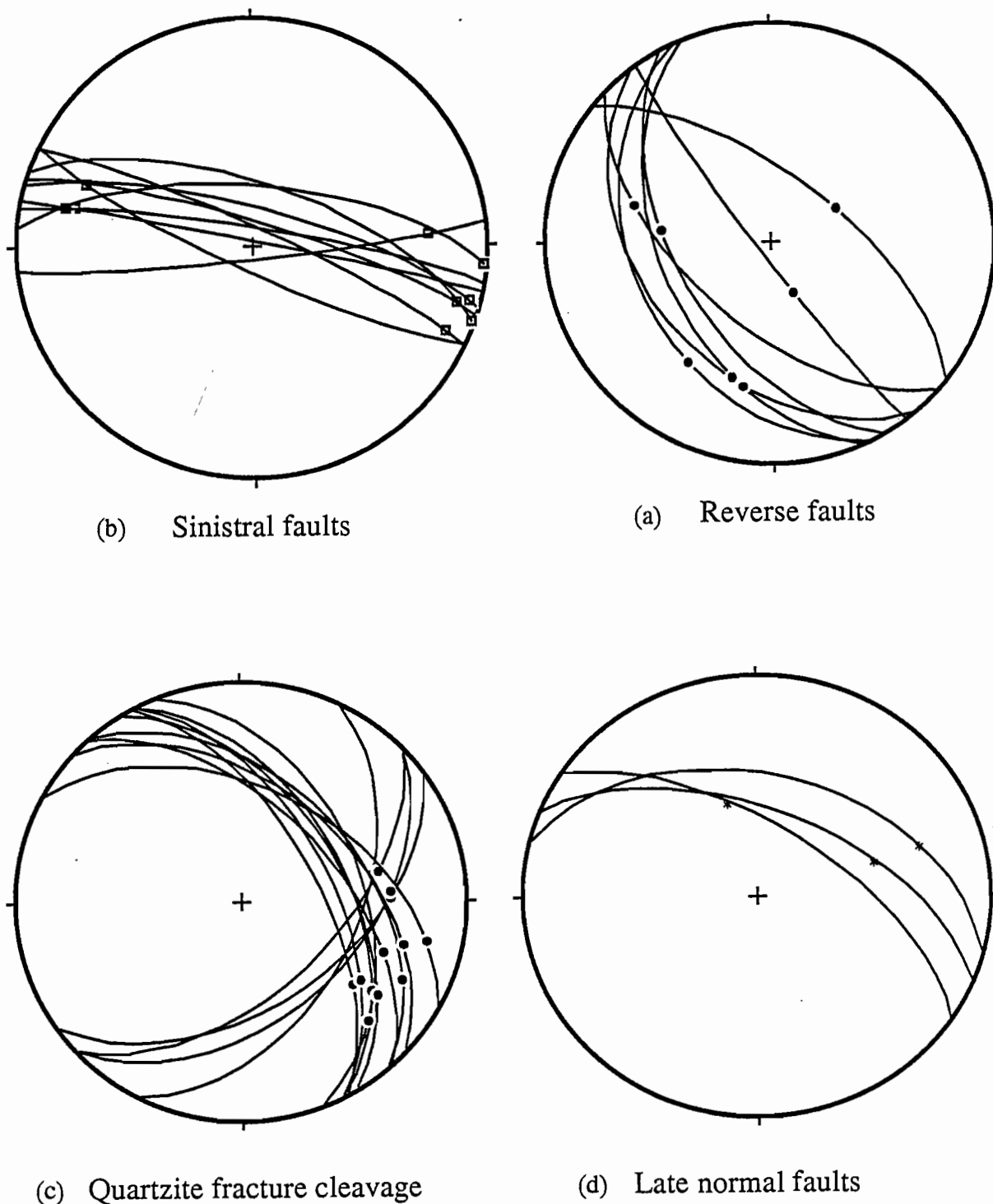


Figure 4.9: Fault-related structures - Forth Metamorphics. (a) D3 reverse faults. (b) D3 sinistral faults. (c) ?D3 fracture cleavage in quartzite. (d) Late normal faults.

A second group of east-west striking faults with shallow, predominantly sinistral strike-slip fibres and striations are common near the western contact of the Claytons River serpentinite, where they cut both quartzite and serpentinite (fig.4.9b). The possibility of more extensive strike-slip faulting is suggested by discontinuities in the distribution of large scale lithological units and local zones of anomalous E-W striking S2 cleavage.

Burns (1964) inferred a macroscopic south-west plunging antiform in S2 near the south-west margin of the Forth Metamorphics - based on the interpolation of widely scattered S2 traces - and correlated this with the mesoscopic south west plunging folds, described above. The present study supports an alternative model, in which the S2 rotation is restricted to discrete E-W trending strike slip zones. These zones are the locus of late mesoscopic folding about steeply SW plunging axes and separate relatively undeformed (predominantly west dipping) blocks in which early lineations have maintained their original pitch with respect to S2.

On Porcupine Hill, two sets of NE and SE dipping 5-10cm spaced fracture cleavages are developed in quartzite and have striations and quartz fibre ledges suggesting reverse movement (fig4.9c). The orientation of these slip features has been compared with fault plane and serpentinite striations using the fault striation analysis program of Etchecopar *et al* (1981) (table 1, fig.4.10).

DATA	No.	Min. %	Random Tries	σ_1	σ_2	σ_3	R	Err. (deg)
All	35	80	200	10.271	12.179	75.040	0.2	14
Serpentinite	10	80	300	5.275	14.184	76.025	0.8	15
Sinistral faults	8	80	200	6.269	18.177	71.018	0.2	8
Fracture cleavage	13	100	300	7.097	41.001	48.195	0.2	9

Table 1: Results of fault striation analysis.

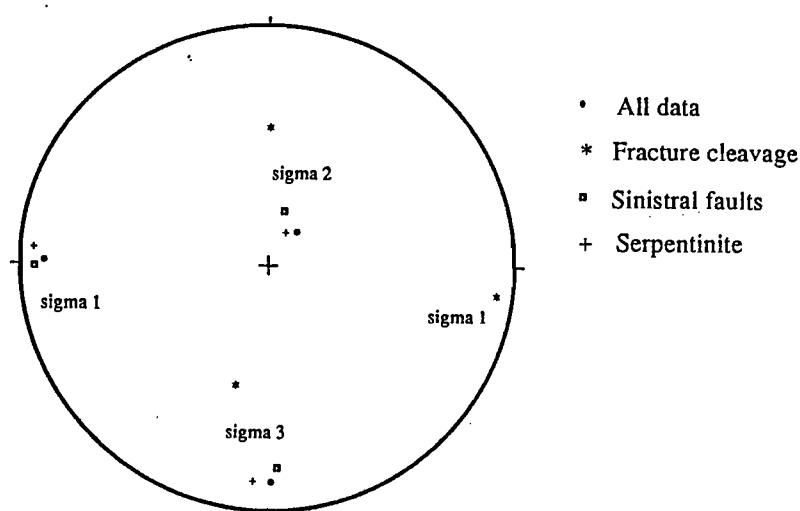


Figure 4.10: Best fit stress tensors for all striation data, fracture cleavage in quartzite, sinistral strike slip faults and serpentinite striations.

These results are broadly consistent with E-W compression, under a thrust regime with σ_3 steep or sub-vertical. Uncertainties are significant but not unreasonable, considering the geographical extent of the dataset, the range of lithological types and a probable non-homogeneous stress field due to the pre-existing anisotropic S2 fabric.

4.2.1.5 CORRELATION:

The east-directed thrust structures, described above, may correlate with a complex sequence of WNW dipping reverse faults and fault zones exposed along the north coast between Burnie and Ulverstone (fig.4.11). Associated minor conjugate thrust surfaces in this area range from NE to NW striking and in the footwall of the Ulverstone Fault are associated with a NNE to NNW striking late crenulation cleavage (S3) in the Ulverstone Metamorphics. Inland, the coastal faults coalesce, trend from NE through to NW and parallel folds of the Devonian West Coast Range - Valentines Peak Trend (Williams *et al* 1989).

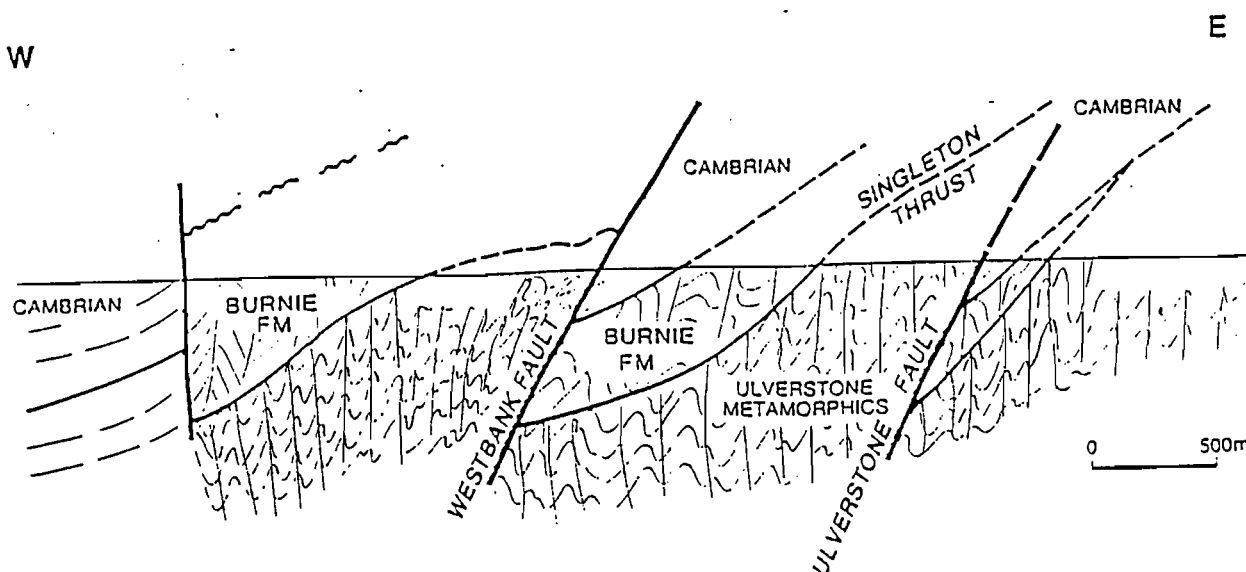


Figure 4.11: Structural profile across the northwestern portion of the Forth Block (from Burns 1963).

The present study supports the eastward continuation of this belt. Coarse grained schists and (now retrogressed) amphibolites of the Forth Metamorphics appear to overly ?Cambrian serpentinite across a major thrust surface in the lower reaches of the Claytons Rivulet and this structure may be laterally continuous with a large reverse fault in Cambro-Ordovician sediments south of the metamorphics (Burns 1964).

The apparent lateral variation in both metamorphic grade and D2 fold style east of Buttons Rivulet may indicate additional overthrusting of higher grade Forth assemblage by garnetiferous lithologies on the eastern margin of the Ulverstone Metamorphics. The thrust belt continues at least as far as the Forth Valley, where Forth Metamorphics overlie a smaller serpentinite block.

This model is shown schematically in figure 4.12.

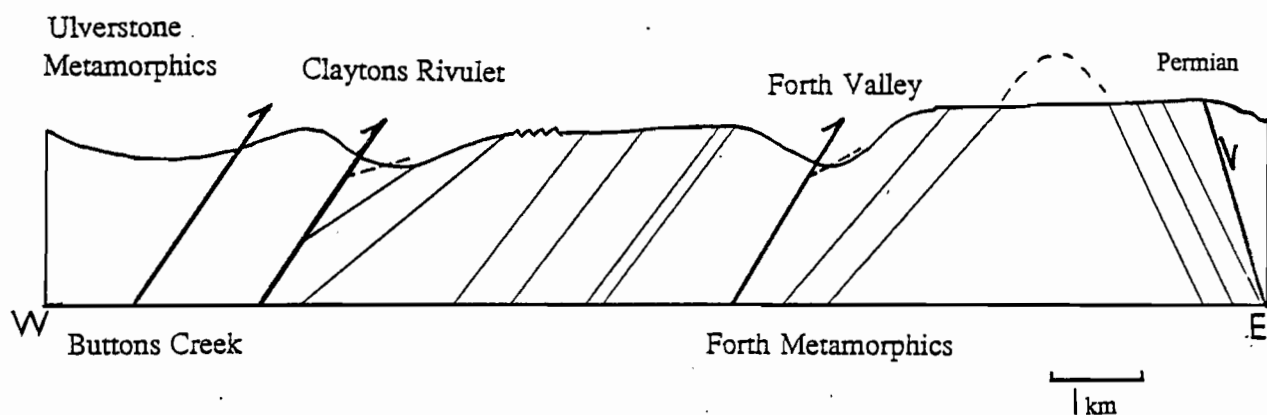


Figure 4.12: Schematic composite section across the Forth Metamorphics (section line from fig.2.2).

4.2.2 MINOR DEFORMATIONS:

4.2.2.1 GROUP A:

In the lower Clayton Rivulet, north-east of the serpentinite zone, a moderately north to north-west dipping spaced crenulation cleavage is locally associated with asymmetric close to tight 1-2m wavelength folds and north dipping shear zones in medium grained porphyroblastic albite mica schist. The folds have angular hinge zones, planar limbs and rotate S2 which, in this location, is a 0.5mm spaced crenulation cleavage sub-parallel to pale-dark compositional banding. Fold axes and associated crenulation lineations on S2 plunge shallowly to the north east and south west. North-west

dipping cataclasite zones with reverse sense of shear are found further south in weakly foliated quartzite.

A locally developed late crenulation cleavage of similar orientation is found in the footwall of the Ulverstone Fault Zone and it is possible that the west over east vergence at this locality is related to the dominant thrust event.

4.2.2.2 GROUP B - ?CAMBRIAN:

A small body of strongly foliated serpentine chlorite tremolite schist occurs 500m south of the Forth River serpentinite. The unit contains abundant chromitiferous magnetite and is correlated with the ultramafics on geochemical grounds (Chapter 3). A penetrative west dipping foliation is concordant with S2 in the enclosing amphibolites, and carries a strong *down-dip* tremolite lineation (cf. Lower Claytons epidote amphibolites). In outcrop, the foliation is deflected into steeply west dipping 1cm spaced sinistral shear bands which, in their present orientation, suggest westward transport.

In thin-section, the foliation is defined by an anastomosing matrix of medium-grained chlorite enclosing 1-2mm long lensoid domains of unfoliated fibrous serpentine. Idioblastic tremolite prisms, up to 1.5mm long, lie in the foliation and have spaced transverse fractures filled with fine-grained serpentine suggesting extensional strain. This is also indicated by weak chlorite shear bands of predominantly sinistral orientation. Chlorite, in places, forms symmetrical pressure shadows on idioblastic magnetite suggesting a moderate flattening component of strain.

The mineralogy and fabric of this unit are consistent with retrograde west-directed shearing of an originally ultramafic assemblage in a water-saturated environment.

Near the north-eastern margin of the metamorphics, S2 in interlayered quartzite and mica schist is folded into 0.5m wavelength NW vergent tight concentric folds. The most strongly folded quartzites are restricted to within 1m of strongly weathered south-east dipping schist bands which have a penetrative steeply south-east dipping cleavage oblique to compositional banding. The concentric folds grade into open angular kinks in quartzite away from the foliated schist bands. Fold vergence and the cleavage orientation suggest that the schist bands acted as minor thrust surfaces during westward movement.

The relatively ductile late fold-style at this locality, is unlike the more brittle-style deformation in quartzites further west.

Although limited, the evidence for post-S2 westward transport is in general agreement with current tectonic models suggesting emplacement of the ultramafics from the east (Berry & Crawford 1988, Elliott *et al* - in review).

4.2.2.3 POST-S3 FAULTS:

In the Claytons Rivulet, the west dipping foliation in serpentinite is overprinted by upright, roughly N-S striking zones with dextral strike-slip fibres and lineations (fig.4.6b). Steeply east dipping surfaces with strike slip striations are also found in albitic schist east of the serpentinite block.

In quartzites on Porcupine Hill, NNW to NNE trending dextral faults, up to 2m wide, contain a jumble of 30-50cm rotated blocks in a siliceous matrix of granulated quartzite and vein quartz.

Faults of this sense and orientation occur in Cambrian sediments south of the metamorphics and further west, in the Dial Range and have been correlated with south-west vergent thrusts of the latest Devonian Deloraine-Railton Trend (Williams *et al* 1989).

4.2.2.4 POST-PERMIAN EXTENSIONAL FAULTS:

A NNE dipping 5-10m wide zone of strongly foliated quartz-muscovite cataclasite is well-exposed close to the eastern margin of the metamorphics at DQ409373. Within the fault zone, numerous undulating striated surfaces enclose lenticular domains from 10cm to several metres in length, in which an internal cataclastic foliation dips more shallowly east. An early set of etched dip slip striations are overprinted by weak striations on a clay polish and both indicate normal movement (fig.4.9d). The fault is concordant with Post-Permian extensional faults, in the Devonport Basin (e.g. Aberdeen Fault) east of the metamorphics.

4.3 STRUCTURAL SUMMARY:

The structural history of the Forth Metamorphics, as outlined above, is summarised in table 4.2. Geologic thermobarometry, mineral compositional zonation and reaction textures, discussed in Chapter 5, have been used to constrain the P-T history of the area and help to clarify the tectonic significance of this sequence. Aspects of the Precambrian (and Paleozoic) tectonics are thus deferred to Chapter 6.

D1-2: Precambrian ductile strain.

Early isoclinal fold phase regionally rotated during west directed D2 transport. N-S trending west vergent mesoscopic folds developed between mylonitic shear zones along which high grade assemblages were emplaced.

?Cambrian Thrusting.

Serpentinite emplaced over the Forth Metamorphics from the east. Thrusting may have delaminated basement and transported Forth Metamorphics over the Ulverstone Metamorphics at this time (see Chapter 6).

D3: West Coast Range - Valentines Peak Trend .

East-directed backthrusting of Ulverstone Metamorphics over Forth Metamorphics and the latter over remnants of serpentinite (?thrust sheet). Eastward continuation of coastal thrust belt.

D4: Deloraine-Railton Trend.

Minor N-S trending dextral strike-slip faults.

D5: Post-Permian Extension:

Down-faulting of eastern margin against Permian sediments - may involve several periods of movement continuing into the Tertiary.

Table 4.2: Structural sequence - Forth Metamorphics.

CHAPTER 5

METAMORPHIC PETROLOGY.

The aim of this chapter is to document and evaluate critical metamorphic phase assemblages in the Forth Metamorphics and outline the P-T history of the area.

The first section describes the petrography and mineral chemistry of the common phases with an emphasis on specific lithologies. Peak metamorphic conditions, calculated from traditional thermobarometric methods, are discussed in 5.2 and the petrogenesis of critical assemblages is evaluated in 5.3.

5.1 PETROGRAPHY/MINERAL CHEMISTRY:

5.1.1 METAPELITES:

Over most of the Forth Metamorphics, pelitic lithologies are deeply weathered and unsuitable for petrologic work. Despite sampling difficulties, three relatively fresh samples (75637, 75641, 75602) have been selected for detailed thin section study, microprobe and wholerock geochemical analysis.

All mineral analyses described in this and following sections have been obtained using a Cameca SX50 microprobe under operating conditions of 15kV and 20mA, with an on-line data reduction system.

5.1.1.1 DESCRIPTIVE PETROGRAPHY AND MINERAL CHEMISTRY:

Metapelites assemblages include muscovite + quartz +/- biotite +/- garnet + rutile. Additional phases are of restricted occurrence and described in terms of specific lithologies.

Muscovite is the dominant phyllosilicate phase, occurring as sheaves of 0.3 - 2.0 mm dimensionally oriented grains defining the S2 schistosity. Early S1 muscovite is preserved in microlithons and rarely as small oriented inclusions in porphyroblastic garnet.

Post-S2 muscovite growth is indicated by coarse sub-idioblastic single crystals with uniform extinction, oriented at a high angle to the foliation. Post-kinematic sericite occurs as rims on kyanite (75641, 75676) and forms 1mm rounded, undeformed clots after ?albite in 75658.

Aspects of muscovite composition are shown in figure 5.1. All muscovites analysed have less than ideal stoichiometry (i.e. $\text{Na} + \text{K} < 1$) and are phengitic; being intermediate solutions between muscovite $((\text{K}(\text{Al}_2)(\text{Si}_3\text{Al})\text{O}_{10}(\text{OH})_2)$ and celadonite $(\text{K}(\text{Al}(\text{Mg},\text{Fe}))\text{Si}_4\text{O}_{10}(\text{OH})_2)$. This involves the Tschermakite exchange vector $\text{Si}^{\text{T}}(\text{Mg},\text{Fe})^{\text{M1}}\text{Al}^{\text{T}}_{-1}\text{Al}^{\text{M1}}_{-1}$, and is expressed in terms of Si occupancy on the tetrahedral site (Si^{4+}) (Deer et al 1980). All muscovites co-exist with ferromagnesian phases and phengite saturation should be largely independent of bulk rock composition (Velde 1967).

Increased phengite substitution is accompanied by a weak trend of decreasing $\text{Na}/(\text{Na}+\text{K})$ (i.e. paragonite substitution). The highest Na and lowest Si occur in albite-bearing schist (75637) which, on independent geothermobarometric grounds appears to have equilibrated at higher P-T than kyanite-bearing assemblages (see below). These observations are broadly consistent with Velde (1965, 1967) who demonstrated a general decrease in Si^{4+} with increasing P-T.

Miyashiro (1973) has compiled analyses of metamorphic muscovites and argued that these could be discriminated in terms of FeO^* and Al_2O_3 . The majority of muscovites plot in the garnet-zone field, although the range is not tightly constrained. Alteration rims on kyanite are more aluminous and coarse weakly pleochroic pale green S2 phengites, in sample 75665, have up to 8% FeO.

Biotite is a ubiquitous, but minor phase, occurring as deep brown 0.1-0.3 mm matrix grains, aligned parallel to S2, and as rare inclusions in large garnet porphyroblasts. Matrix biotite is often interleaved with sheaves of ragged chlorite and where the latter is not petrographically obvious, biotite shows mottled pale green-brown pleochroism indicating sub-microscopic intergrowth.

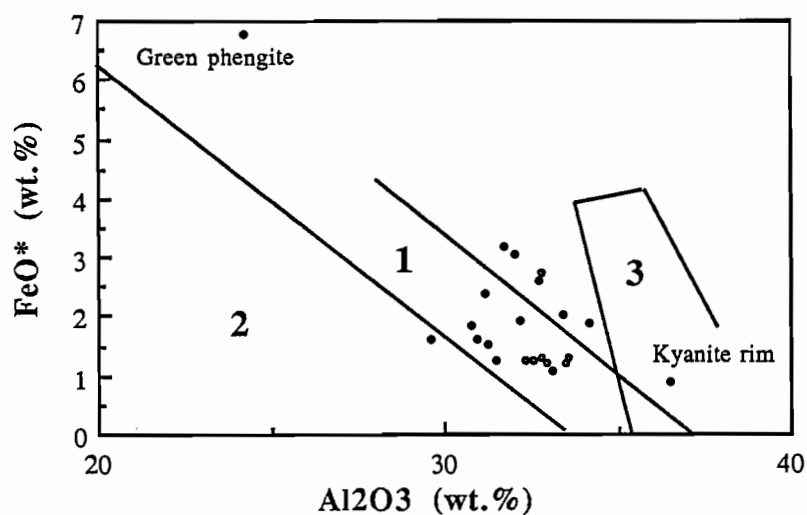
There is considerable variation in biotite chemistry, but fresh single crystals are substantially unzoned. Within individual thin-sections, biotites in progressively closer proximity to garnet show an increase in Mg# (e.g. 75637 and 75641), suggesting local re-equilibration during cooling (Schreurs 1985).

Fe and Mg on the octahedral site are diluted by up to 0.11 Ti and 0.47 Al_{vi} (11 cation basis) indicating partial solution towards eastonite $(\text{K}(\text{Mg}_2\text{Al})(\text{Si}_2\text{Al}_2)\text{O}_{10}(\text{OH})_2)$ and siderophyllite $(\text{K}(\text{Fe}_2\text{Al})(\text{Si}_2\text{Al})\text{O}_{10}(\text{OH})_2)$.

Garnet is a common component of most schists, occurring as 1-2 mm porphyroblasts, making up 20-40% by volume. Larger 10-15mm porphyroblasts occur in 75602 and weathered schist bands at DQ331409 have 20-30mm limonite clots with a dodecahedral habit, probably after garnet. In hand

specimen, the blasts appear pink when fresh, but are often encrusted with a surficial film of red-brown iron oxides or an olive green mantle of chlorite.

(a)



(b)

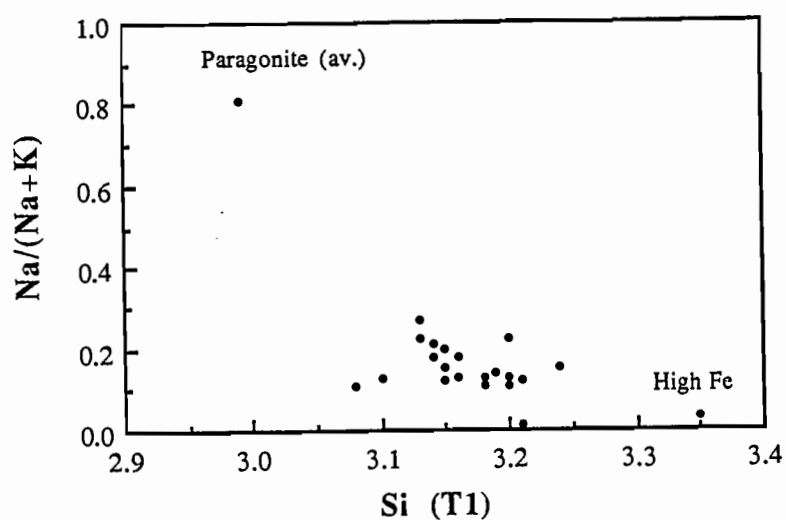


Figure 5.1: Composition of phengites from Forth metapelites - (a) FeO^* vs. Al_2O_3 . Fields are: (1) almandine zone, (2) glaucophane zone, (3) staurolite-sillimanite zones (after Myashiro 1973) (b) $\text{Na}/(\text{Na} + \text{K})$ vs. Si^{4+} (cations).

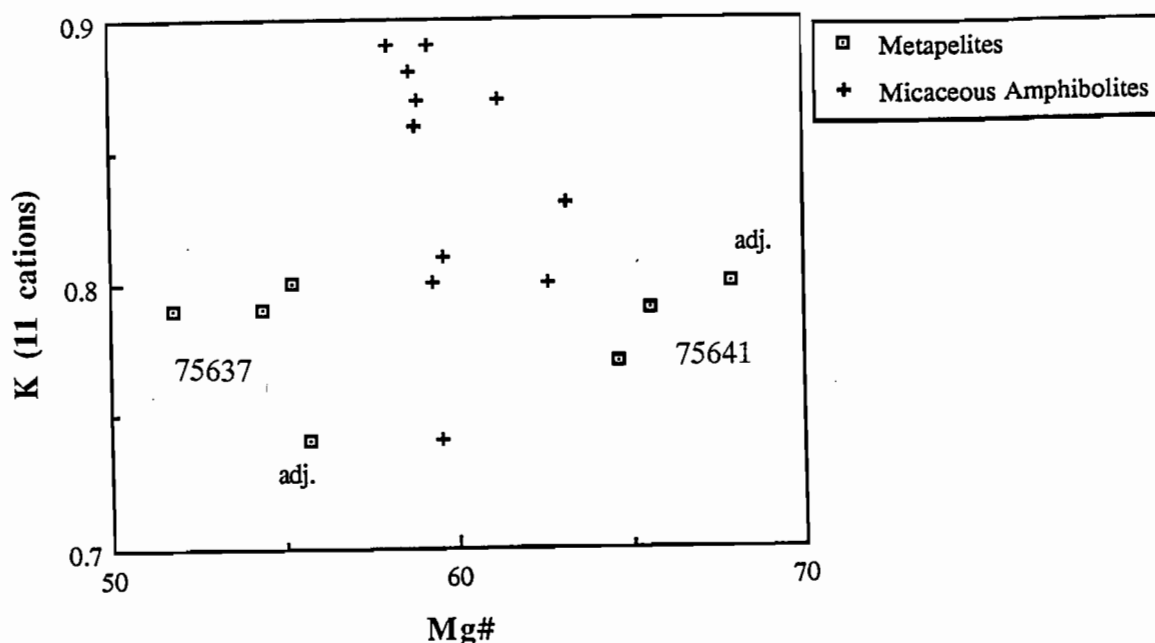


Figure 5.2: Biotites - K vs. Mg# (11 cations) for metapelites and micaceous amphibolites.

In thin section, the garnets are rounded or angular, sub-idioblastic to idioblastic grains, wrapped around by the S2 foliation and bounded by quartz pressure shadows. Cores are optically defined by abundant linear or sigmoidal inclusion trails of elongate quartz + rutile +/- muscovite, which form an internal foliation (Si) at a high angle to the matrix schistosity (Se). These inclusion-rich domains are bounded by 0.1-0.2mm wide, optically distinct, inclusion-free rims. Sigmoidal inclusion trails have been cited as evidence for rotation during growth (Spry 1969), although Bell *et al* (1986) proposed an alternative model of static growth during heterogeneous strain partitioning. Whatever the case, these structures and the fact that garnet is wrapped around by S2 indicate early to syn-D2 garnet growth. In quartzites and quartz-rich interbands in schist, porphyroblasts have a skeletal morphology and are often rimmed by chlorite or intergrown with biotite.

All pelitic garnets are almandine rich with relatively high grossular, low pyrope and variable spessartine components (fig.5.3).

A marked and consistent 'prograde' chemical zonation is evident from core-rim analyses and microprobe traverses of selected optically zoned grains, and involves an increase in Fe, Mg and Mg# and corresponding decrease in Ca and Mn from core to rim.

At temperatures above 800° C, zonation of this type may result from selective volume diffusion of an originally homogeneous composition (Tracy 1982). Thermometry results, presented below, indicate

lower temperatures (700° C) for the metapelites and under these conditions compositional variation is commonly due to continuous prograde exchange reactions (Spear & Peacock 1990). The zonation is thus considered to be a genuine growth feature.

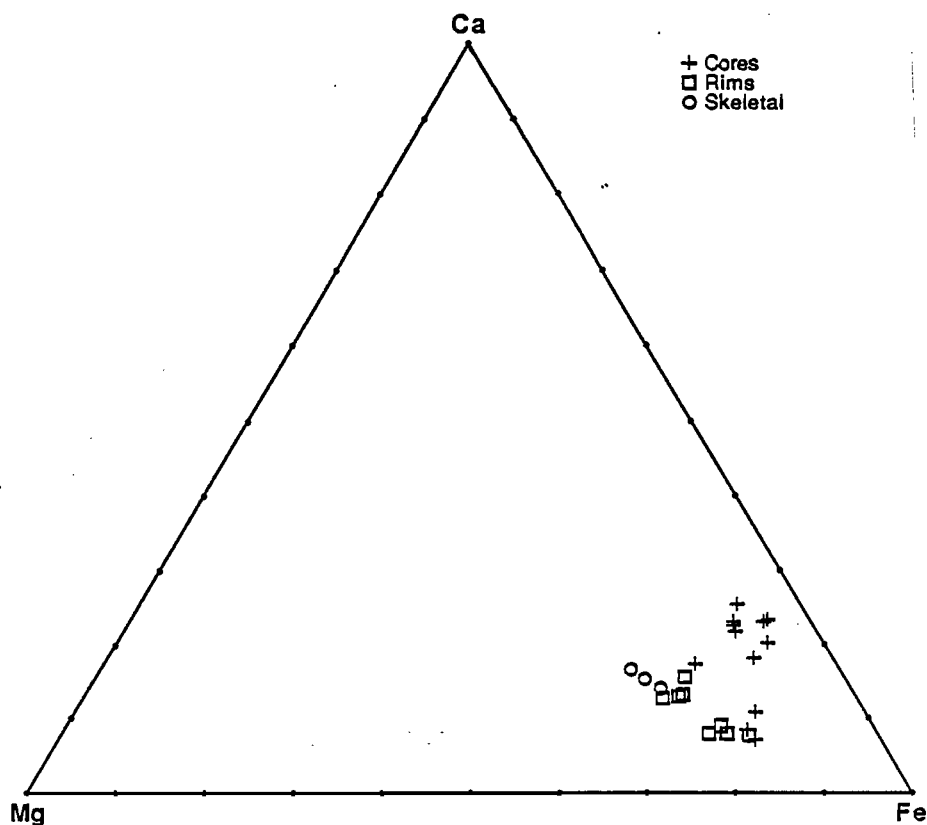


Figure 5.3: Cationic CFM (Ca-Fe-Mg) diagram of pelitic core, rim and skeletal garnet compositions.

The core to rim trend is reversed where garnet abuts matrix biotite, with Mn in particular showing a local marginal increase, and is probably due to retrograde cooling (Spears & Peacock 1990).

Plagioclase is only identifiable as a matrix phase in 75600, where 0.2mm xenoblastic strain free grains may be distinguished from quartz by a thin selvage of iron oxides, slight turbid alteration and rare multiple twinning. S2 muscovite terminates abruptly at the grain boundaries, and although there is a weak grain elongation, the plagioclase appears to have grown post-S2.

Pale 1-8mm porphyroblasts are a major component of some lithologies but only common where the rocks lack garnet (but see 75637 below). In most cases, the original composition is uncertain as the blasts are pervasively altered to a boxwork of fine-grained white mica and unoriented ?kaolinite or pseudomorphed by sericite.

Fresh grains, where preserved, are almost pure albite (75653), although this may reflect selective weathering of Ca-rich compositions. Grains or alteration clots have abundant quartz inclusions and are rounded to augen shaped morphology which is wrapped around by S2. Albite in 75653 forms 1.5mm long asymmetric porphyroblasts, with aspect ratios of up to 8:1, set in a strongly mylonitic matrix of quartz + muscovite. Most grains are strain free but are locally kinked or show polysynthetic twinning and contain consistently oriented sigmoidal opaque inclusion trails suggesting rotation during growth. Similar textures are preserved in weathered samples (75656) and suggest early-syn-D2 albite growth.

Chlorite occurs in intimate intergrowth with D2 biotite, as randomly oriented weakly undulose matrix grains and along fractures or as rims on garnet, suggesting post-S2, retrograde growth.

Coarse clots of kink-banded chlorite, parallel the late S3 crenulation cleavage in 75600 and microstructural features indicate lower greenschist facies conditions during deformation. This is consistent with syn-S3 chlorite growth, although the chlorite may have grown under earlier static conditions and been sheared and recrystallised during S3.

Late chlorites are of ripidolite composition, according to the classification of Deer *et al* (1967), and have higher Mg# than associated garnet and biotite.

Minor Phases:

In the Forth Schists, rutile is the dominant Ti-bearing phase, making up to 5% of some samples. It occurs as disseminated slightly elongate matrix grains up to 0.2mm long, as rare 0.5mm xenoblastic clots and as inclusion trails in garnet and kyanite which define a linear S_e at a high angle to S2. These features support pre-S2 growth.

Accessories include tourmaline, granular zircon and in 75602, abundant fine-grained disseminated titaniferous hematite (11.5 wt.% TiO_2). Tourmaline, where present forms scattered 0.1mm idioblastic granules (75602) or rare 1mm idioblastic prisms with a distinct optical zoning from blue-green cores to yellow rims. In mylonitic units, prismatic tourmaline has a strong preferred orientation, transverse extensional fractures and the rims may represent syn-D2 overgrowths on originally detrital grains.

Plate 5.1: Pelitic mineral textures. Scale bar 0.5mm.

A. Skeletal garnet, chloritoid (blue), S2 chlorite and staurolite atoll (pale yellow) in 75596 - PPL (DQ321367).

B. Detail of chloritoid in (a) showing strong undulose extinction but relatively strain-free staurolite atoll (uniform extinction) - XN.

C. Chloritoid (circled) largely replaced by coarse staurolite (pale - high relief) in 75602 - PPL (DQ331368).

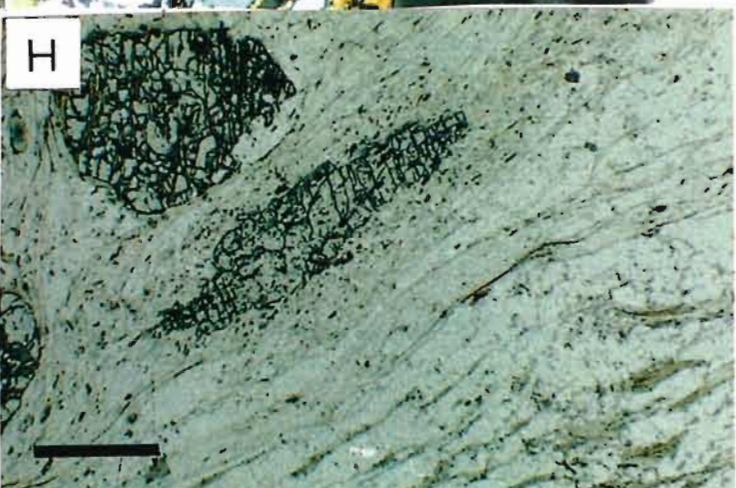
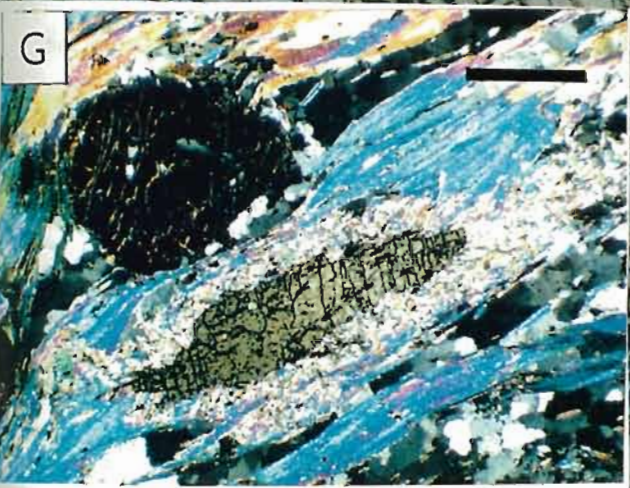
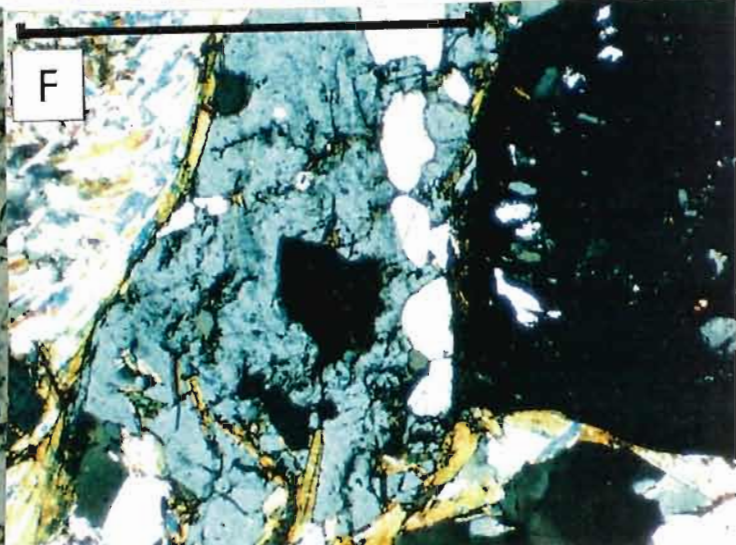
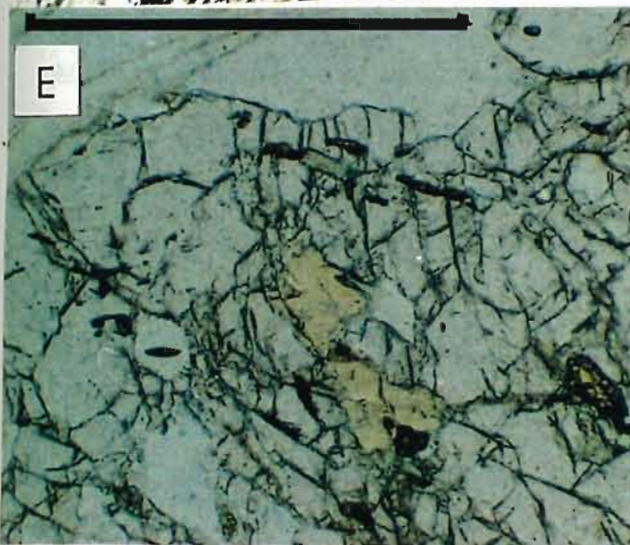
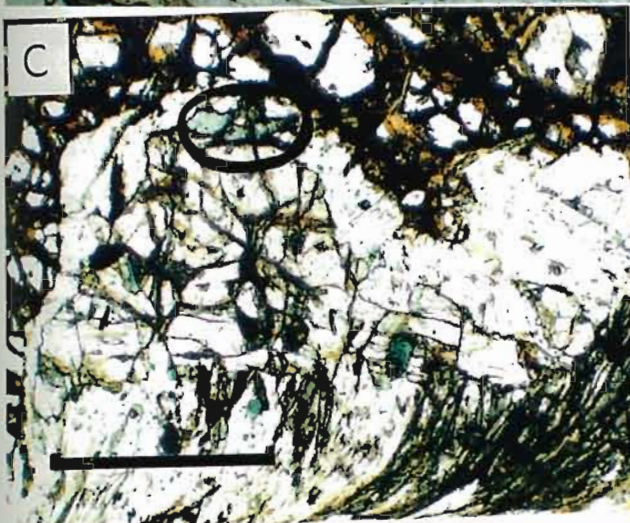
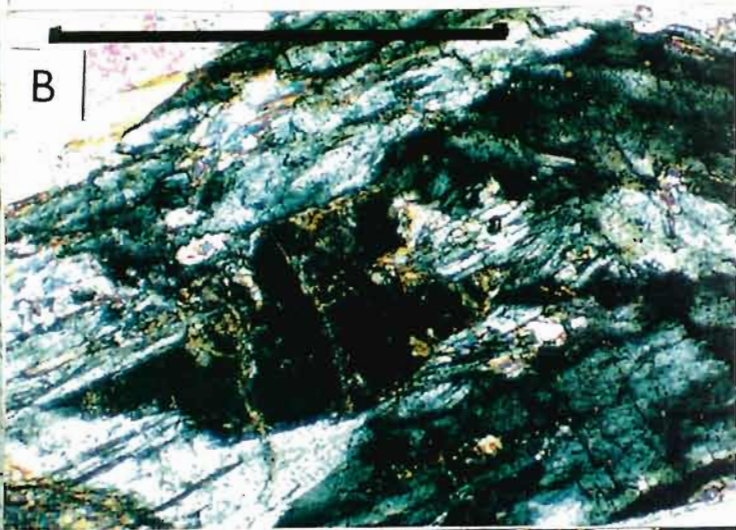
D. As above, showing paragonite rim (high order birefringence and single cleavage) between staurolite/chloritoid and garnet (dark) - XN.

E. Staurolite and rutile inclusions in garnet. Matrix has kyanite but no staurolite - PPL. (75461 - DQ368361)

F. Co-existing albite and garnet porphyroblasts in 75637 - XN (DQ372366).

G. Kyanite and garnet in 75461 - XN. Note late sericite rims on kyanite (DQ368361).

H. As above in PPL showing high grade syn-S2 assemblage of garnet + kyanite + muscovite + biotite (lower right - partly chloritised) + quartz + rutile (small dark brown granules).



5.1.1.2 CRITICAL ASSEMBLAGES:

Chloritoid-bearing schists:

Pods of coarse chloritoid-bearing schists are present at DQ329363 (75602) and further west at DQ323384 (75596).

75596 is a medium-grained schist with the assemblage garnet + muscovite + chloritoid + chlorite + staurolite + rutile + ?paragonite. A 2-3mm spaced crenulation cleavage (S2), defined by alternating bands of anastomosing coarse muscovite + chlorite and domains of strongly undulose quartz, wrap around elongate compact to skeletal 1-3mm garnet porphyroblasts, and enclose lensoid microlithons which preserve an earlier fabric (S1) at 45° to S2. Chloritoid occurs in microlithons as elongate undulose xenoblastic 0.5mm grains oriented parallel to S1 and is intergrown with clots of fine-grained decussate ?paragonite, 0.2mm granular staurolite, late coarse muscovite and randomly oriented chlorite. The chloritoid appears to have developed syn-S1, but is locally rotated parallel to S2. Staurolite atolls within chloritoid are substantially undeformed, suggesting late-S2 growth (Pl.5.1).

75602 is more coarse-grained and contains the assemblage garnet + muscovite + chloritoid + staurolite + paragonite + quartz + chlorite + titaniferous hematite. The microtexture is dominated by a coarse domainal schistosity (S2) which wraps around 15mm garnet porphyroblasts and matrix chloritoid. Chloritoid also occurs as unaltered idioblastic 0.3-0.5mm inclusions in garnet having a tabular or platy habit, slightly oblique extinction (up to 10°) and striking blue-green pleochroism. Tabular matrix grains, up to 2mm long, are oriented sub-parallel or more rarely at a high angle to the dominant foliation, and occurs in complex intergrowth with paragonite, staurolite and chlorite (Pl.5.1).

Paragonite forms clots of fine-grained decussate flakes enclosed within chloritoid/staurolite composite grains and as 0.2mm rims between staurolite and garnet (Pl.5.1). Small scale microprobe traverses indicate rare submicroscopic interlayering of paragonite and muscovite in matrix white mica.

Staurolite occurs as coarse matrix grains (up to 1mm), always intergrown with and apparently pseudomorphing chloritoid and also as very rare inclusions in garnet. Matrix muscovite weakly wraps around the grains or terminates abruptly on grain boundaries and these textures suggest that staurolite developed late in D2, after garnet growth, and at the expense of chloritoid.

Chlorite textures are complex and suggest several periods of growth. In 75596, and to a lesser extent 75602, chlorite forms dimensionally oriented 'fish-like' clots of undulose or strongly kink-banded

	Ctd-inc		Ctd-mtx		Staur.		Ga.		Parag.	Mus.	Cht.	Hem.	W/R
	core	rim	core	rim	core	rim	core	rim					
SiO2	25.01	25.21	24.86	25.10	28.87	29.77	38.27	38.46	46.54	47.13	26.73	0.19	58.96
TiO2	0.03	0.01	0.04	0.02	0.52	0.61	0.12	0.09	0.11	0.26	0.03	11.50	0.91
Al2O3	40.13	38.74	40.26	39.83	53.00	53.34	21.23	21.34	38.98	32.71	22.10	0.07	20.25
Fe2O3	-	-	-	-	0.20	0.20	0.49	0.40	-	-	-	87.40	7.42
MgO	5.42	4.95	4.82	4.08	1.89	1.40	3.85	4.44	0.27	1.44	20.06	-	2.12
CaO	-	-	0.01	-	-	0.01	5.82	5.33	0.25	-	-	0.01	0.02
MnO	0.17	0.11	0.04	0.06	0.04	0.02	1.95	0.99	0.01	0.04	0.03	0.02	-
FeO	20.09	23.03	21.34	22.38	11.02	9.51	29.43	29.87	1.34	3.38	19.68	-	-
Na2O	-	-	-	-	-	-	-	-	5.91	1.32	-	-	4.27
K2O	-	-	-	-	-	-	-	-	2.06	8.81	-	-	0.05
Σ	90.85	92.05	91.37	91.48	95.54	94.86	101.16	100.92	95.47	95.09	88.63	99.19	94.00
Cations													
Si	1.03	1.04	1.02	1.08	8.07	8.30	3.01	3.01	2.99	3.14	2.67	-	
Ti	-	-	-	-	0.11	0.13	0.01	0.01	0.01	0.01	-	0.22	
Al	1.94	1.88	1.95	2.02	17.47	17.52	1.97	1.97	2.95	2.57	2.60	-	
Fe3	-	-	-	-	0.04	0.04	0.03	0.03	-	-	0.25	1.70	
Mg	0.33	0.30	0.30	0.26	0.79	0.58	0.45	0.52	0.03	0.14	2.99	-	
Ca	-	-	-	-	-	-	0.49	0.45	0.02	-	-	-	
Mn	0.01	-	-	-	0.01	0.01	0.13	0.07	-	-	-	-	
Fe2	0.69	0.79	0.73	0.80	2.58	2.22	1.90	1.93	0.07	0.19	1.65	-	
Na	-	-	-	-	-	-	-	-	0.74	0.17	-	-	
K	-	-	-	-	-	-	-	-	0.17	0.75	-	-	
Σ	4.00	4.01	4.00	4.17	29.07	28.80	7.99	7.99	6.98	6.97	10.16	1.92	
No. O	6	6	6	6	46	46	12	12	11	11	14	3	
XMg	32.4	27.5	29.1	24.5	23.4	20.7	19.1	21.2	30.0	42.4	64.4	-	

Table 5.1: Bulk rock geochemistry and representative mineral analyses of garnet, chloritoid, staurolite, muscovite, paragonite, S2 chlorite and hematite from 75602.

	Ga.			Mus.	Ser.	Bt.	Cht.	Staur.	Rt.	Ky.	W/R
	core	rim	sk.								
SiO₂	38.06	38.71	38.10	48.34	47.99	39.98	27.44	27.41	0.05	37.28	64.87
TiO₂	0.43	0.67	0.04	0.45	0.09	0.85	0.06	0.56	96.90	-	0.80
Al₂O₃	21.32	21.94	22.53	32.78	36.46	18.95	22.22	53.90	-	63.07	17.21
Fe₂O₃	0.34	-	-	-	-	-	-	0.20	-	-	6.76
MgO	2.10	5.75	5.69	2.17	1.06	13.79	20.78	0.88	-	-	2.48
CaO	7.87	4.48	5.33	-	0.01	0.08	-	0.01	-	-	0.83
MnO	1.32	0.23	0.37	0.01	-	-	0.01	0.08	-	-	-
FeO	29.66	28.73	27.94	1.30	0.92	13.52	18.04	12.70	0.43	-	-
Na₂O	-	-	-	0.95	0.94	0.28	-	0.01	-	-	0.53
K₂O	-	-	-	9.77	9.68	8.40	-	0.01	-	-	3.63
Σ	101.10	100.50	100.00	95.77	97.15	95.85	88.55	95.76	97.38	100.35	97.11
Cations											
Si	3.00	2.95	2.90	3.18	3.10	2.87	2.72	7.72	-	1.00	
Ti	0.03	0.04	-	0.02	-	0.05	-	0.12	1.00	-	
Al	1.98	1.97	2.02	2.54	2.78	1.60	2.59	17.91	-	2.00	
Fe₃	0.02	-	-	-	-	-	-	0.04	-	-	
Mg	0.25	0.65	0.64	0.21	0.10	1.48	3.07	0.37	-	-	
Ca	0.66	0.37	0.44	-	-	0.01	-	-	-	-	
Mn	0.09	0.01	0.03	-	-	-	-	0.02	-	-	
Fe₂	1.95	1.83	1.78	0.07	0.05	0.81	1.49	2.99	-	-	
Na	-	-	-	0.12	0.12	0.04	-	-	-	-	
K	-	-	-	0.82	0.80	0.77	-	-	-	-	
Σ	7.98	7.83	7.82	6.96	6.95	7.63	9.87	29.17	1.00	3.00	
No. O	12	12	12	11	11	11	14	46	2	5	
Mg#	11.36	26.28	26.61	75.00	66.67	64.63	67.32	11.01	-	-	

Table 5.2: Whole rock and representative mineral analyses of garnet, kyanite, muscovite, biotite, rutile and staurolite from 75641.

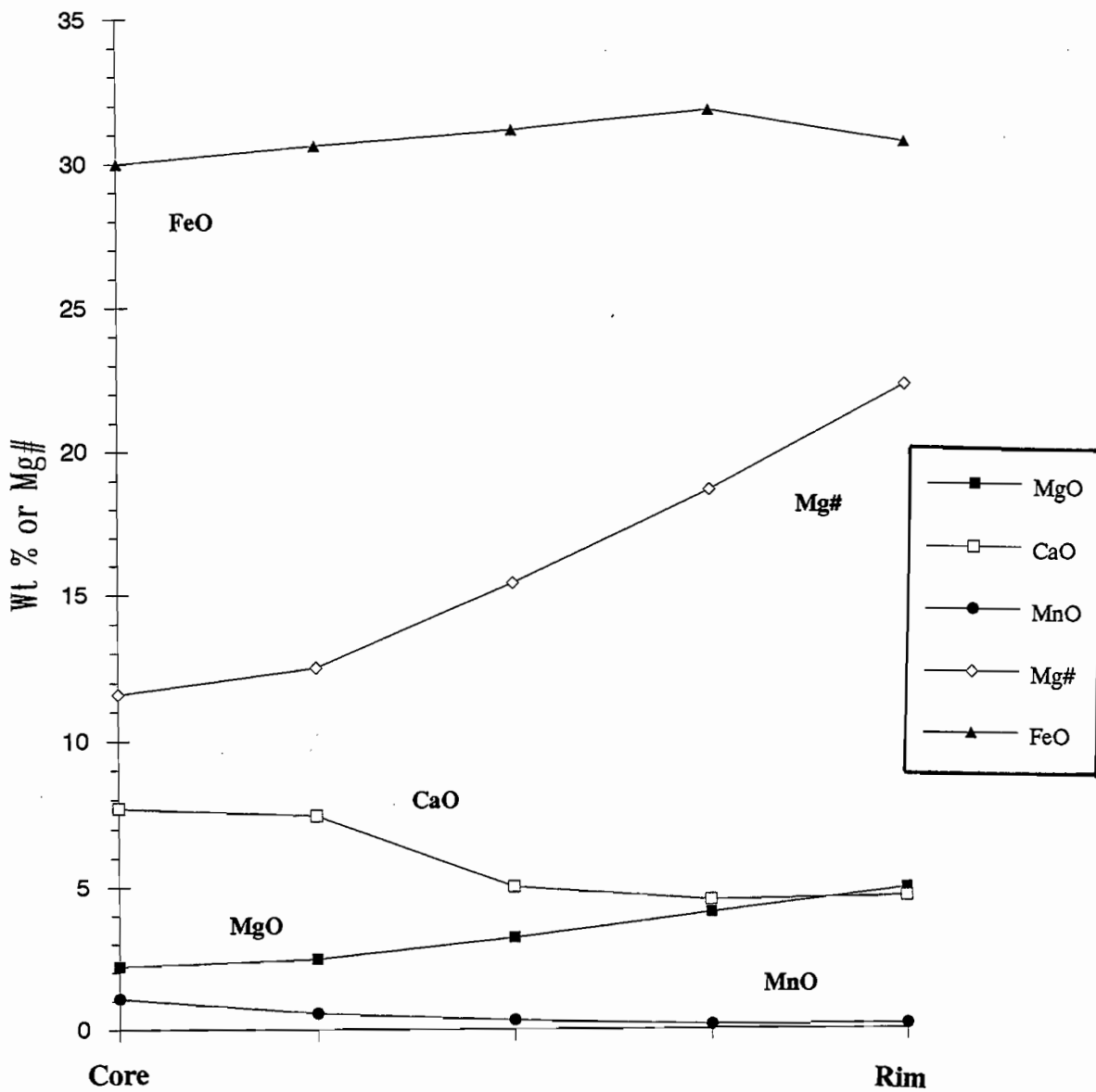


Figure 5.5: Garnet zonation in porphyroblast from 75641.

A single staurolite inclusion, located half-way between core and rim of a large garnet porphyroblast, was identified in 75641 (Pl.5.1) and as plagioclase was not detected either optically or during microprobe analysis, garnet appears to be the sole reservoir for Ca in this assemblage.

Garnet albite schist:

Despite their widespread occurrence, co-existing garnet and albite porphyroblasts were only found in one sample (75637 - table 5.3).

Albite occurs both as equant or tabular, sub-idioblastic porphyroblasts up to 1.5mm across and as irregular polygranular or skeletal aggregates of 0.3-0.5mm grains.

Garnet porphyroblasts are up to 1.5mm across, with an equant rounded morphology and sigmoidal inclusion trails suggesting > 180° C of rotation during growth. Chemical zonation is similar to that described above.

	Ga.		Plag.		Mus.	Bt.	Cht
	core	rim	core	rim			
SiO₂	37.87	38.33	68.60	68.82	48.54	38.57	25.86
TiO₂	0.07	0.03	0.03	0.02	0.73	1.72	0.02
Al₂O₃	21.15	21.46	19.67	19.61	32.07	16.99	20.61
Fe₂O₃	0.25	0.06	0.03	0.03	-	-	-
MgO	2.49	4.76	-	-	2.16	12.01	15.85
CaO	5.03	2.69	0.27	0.21	-	0.06	0.03
MnO	1.01	0.11	-	0.01	0.03	0.03	0.01
FeO	32.60	32.62	-	-	2.08	17.89	26.54
Na₂O	-	0	11.26	11.24	1.50	0.21	0.08
K₂O	-	0	0.06	0.05	8.24	8.41	0.04
Σ	100.47	100.06	99.91	99.99	95.36	95.90	89.04
Cations							
Si	3.01	3.02	3.02	3.03	3.26	2.91	2.73
Ti	-	0	-	-	0.04	0.10	-
Al	1.99	2	1.02	1.02	2.54	1.51	2.56
Fe₃	0.02	0	-	-	-	-	-
Mg	0.30	0.56	-	-	0.21	1.35	2.49
Ca	0.43	0.23	0.01	0.01	-	0.01	-
Mn	0.07	0.01	-	-	-	-	-
Fe₂	2.17	2.15	-	-	0.12	1.14	2.04
Na	-	0	0.96	0.96	0.19	0.03	0.02
K	-	0	-	-	0.70	0.81	0.01
Σ	7.99	7.97	5.01	5.02	7.08	7.87	9.85
No. O	12	12	8	8	11	11	14
Mg#	12.1	20.7	-	-	63.6	54.3	55.0

Table 5.3: Representative mineral analyses of muscovite, biotite, rutile, albite and garnet from 75637.

All porphyroblasts are wrapped around by the foliation (Pl.4.1) and, in places, albite grains have irregular boundaries with S2 muscovite, suggesting partial dissolution. Albite and garnet are commonly separated by septa of polygonal quartz, but where in contact, have sharp boundaries and appear to be in textural and chemical equilibrium (Pl.5.1).

Microolithons of S1 muscovite in 75637 have similar chemistry to the dominant S2 foliation and both have higher paragonite solution than other schists, with $\text{Na}/(\text{Na} + \text{K})$ up to 0.31.

5.1.2 METABASITES:

5.1.2.1 AMPHIBOLITES:

The amphibolites are medium to coarse granoblastic or foliated rocks with the assemblage amphibole + plagioclase + zoisite + quartz + sphene +/- garnet +/- epidote +/- clinopyroxene. Foliated units are banded due to the segregation of coarse garnet-hornblende and quartz-plagioclase-zoisite domains. Representative mineral assemblages are given in tables 5.4-5.5 and compositional variation of garnet, amphibole and clinopyroxene are shown in figure 5.6.

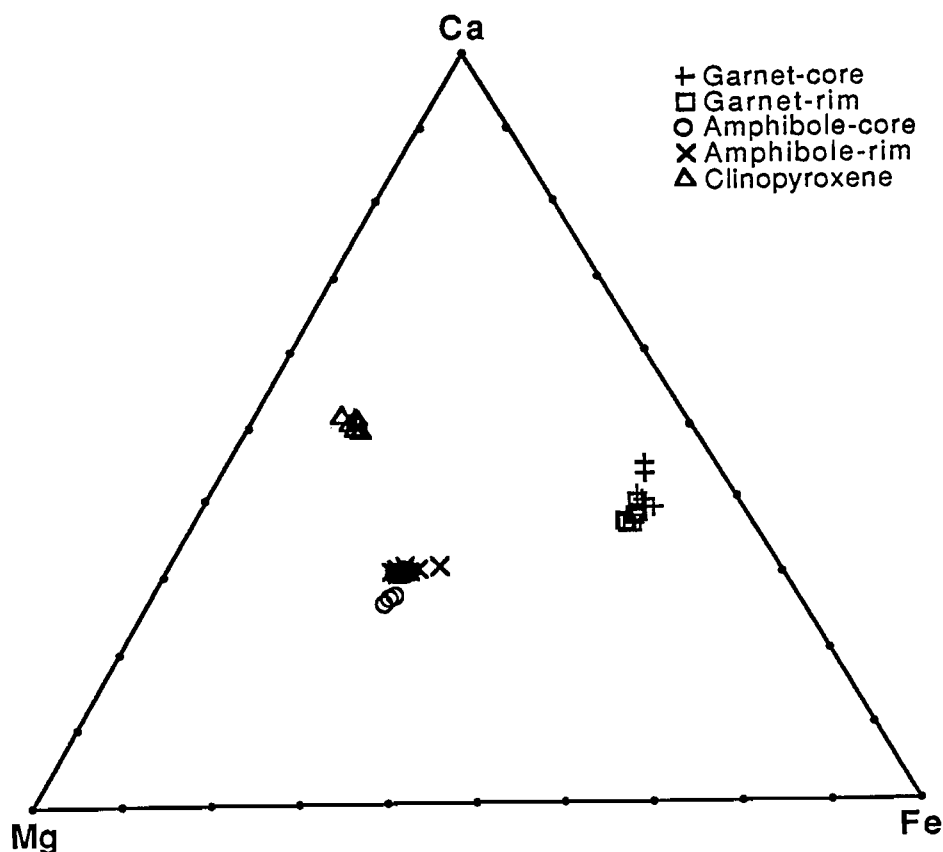


Figure 5.6: Cationic CFM diagram of representative garnet, amphibole and clinopyroxene for garnet amphibolites.

	Ga.		Amp.		Cpx		Plag.			Zo.	K-fsp
	core	rim	core	rim	core	rim	core	rim	inc.(g)		
SiO₂	38.85	39.02	44.62	44.88	53.36	52.89	64.48	64.55	68.65	39.58	62.11
TiO₂	0.20	0.14	0.78	0.58	0.13	0.14	0.01	0.01	-	0.11	0.07
Al₂O₃	21.46	21.64	13.46	13.64	5.05	4.93	22.57	22.20	19.73	32.92	15.26
Cr₂O₃	0.08	0.01	0.07	0.07	0.07	0.08	0.02	0.01	0.03	0.05	0.01
Fe₂O₃	0.64	0.54	-	-	0.94	0.82	0.03	0.21	0.18	1.88	2.70
MgO	2.60	3.59	11.33	10.76	11.09	11.14	-	-	0.01	0.02	2.27
CaO	13.35	12.91	11.25	11.32	21.09	20.69	3.52	3.26	0.15	25.32	5.00
MnO	3.02	0.84	0.07	0.05	0.05	0.01	-	0.01	-	0.04	-
FeO	20.66	22.09	13.07	13.46	6.42	6.70	-	-	-	-	-
Na₂O	-	-	2.59	2.46	2.30	2.22	9.33	9.39	11.15	-	0.46
K₂O	-	-	0.34	0.36	-	-	0.04	0.04	0.11	-	12.22
Σ	100.86	100.78	97.58	97.58	100.50	99.62	100.00	99.68	100.00	99.92	100.10
Cations											
Si	3.01	3.01	6.51	6.55	1.96	1.96	2.85	2.85	2.95	2.97	2.92
Ti	0.01	0.01	0.09	0.06	-	-	-	-	-	0.01	-
Al	1.96	1.97	2.31	2.35	0.22	0.22	1.17	1.16	0.99	2.91	0.85
Fe₃	0.04	0.03	-	-	0.03	0.02	-	0.01	0.01	0.11	0.10
Mg	0.30	0.41	2.46	2.34	0.61	0.61	-	-	-	-	0.16
Ca	1.11	1.07	1.76	1.77	0.83	0.82	0.17	0.15	0.01	2.03	0.25
Mn	0.20	0.06	0.01	0.01	-	-	-	-	-	-	-
Fe₂	1.34	1.43	1.60	1.65	0.20	0.21	-	-	-	-	-
Na	-	-	0.73	0.70	0.16	0.16	0.80	0.80	0.93	-	0.04
K	-	-	0.06	0.07	-	-	-	-	0.01	-	0.74
Σ	7.97	7.99	15.53	15.50	4.01	4.00	5.00	4.97	4.90	8.03	5.06
No. O	12	12	23	23	6	6	8	8	8	13	8
Mg#	18.3	22.3	60.6	58.6	75.3	74.4	-	-	-	-	-

Table 5.4: Representative mineral analyses of garnet, amphibole, clinopyroxene, plagioclase, zoisite and K-feldspar from 75628

	Plag.		Amp.		Epidote	
	core	rim	core	rim	core	rim
SiO₂	67.20	68.35	44.90	45.32	36.53	37.39
TiO₂	0.03	0.01	0.52	0.58	0.09	0.14
Al₂O₃	20.64	19.98	11.33	10.84	22.96	25.31
Fe₂O₃	0.06	0.10	-	-	13.05	9.82
MgO	0.01	-	12.09	12.17	-	-
CaO	1.44	0.64	9.81	10.01	23.72	23.91
MnO	0.03	-	0.25	0.22	0.18	0.10
FeO	-	-	12.78	12.95	-	-
Na₂O	10.57	11.00	3.13	2.88	-	-
K₂O	0.02	0.03	0.42	0.43	-	-
Σ	100.00	100.11	95.23	95.40	96.53	96.67
Cations						
Si	3.00	3.03	6.70	6.75	2.96	2.99
Ti	-	-	0.06	0.07	0.01	0.01
Al	1.08	1.05	1.99	1.90	2.20	2.38
Fe₃	-	-	-	-	0.80	0.59
Mg	-	-	2.69	2.70	-	-
Ca	0.07	0.03	1.57	1.60	2.06	2.05
Mn	-	-	0.03	0.03	0.01	0.01
Fe₂	-	-	1.60	1.61	-	-
Na	0.92	0.95	0.91	0.83	-	-
K	-	-	0.08	0.08	-	-
Σ	5.07	5.05	15.63	15.57	8.04	8.03
No. O	8	8	23	23	13	13
Mg#	-	-	62.7	62.6	-	-

Table 5.5: Mineral analyses of amphibole, plagioclase and epidote from 75617.

Garnet occurs as idioblastic porphyroblasts up to 2mm in diameter which are often crowded with inclusions of quartz, rutile, sphene and more rarely amphibole. Inclusions are either randomly oriented or distributed in concentric bands suggesting crystallographic control. In mylonitic units matrix amphibole wraps around the porphyroblasts which have closely spaced sub-parallel fractures normal to the foliation.

The garnets are almandine-rich but have up to 14.5% CaO and cores of up to 5% MnO. The blasts are compositionally zoned, in a similar manner to the pelitic garnets, with a decrease in CaO and MnO and corresponding increase in Fe, Mg and Mg# from core to rim.

Amphibole is the dominant matrix phase, and forms a granoblastic to foliated mosaic of xenoblastic or prismatic deep olive green pleochroic grains up to 1.5mm long, having curvilinear grain boundaries and equilibrium triple point textures (Pl.5.2).

The amphiboles are aluminous and plot in the tschermakitic to pargasitic hornblende field of Deer *et al* (1967) (fig.5.7 & 5.11 below). Compositional zoning is subtle but shows a slight decrease in Mg# from core to rim. In 75617, amphibole is less calcic and co-exists with abundant epidote, which appears to be a more favourable reservoir for Ca and Al. The amphibole has lower Al_{iv} than the main amphibolite trend, suggesting that alkali site occupancy is charge balanced to a greater extent by octahedral Fe³⁺.

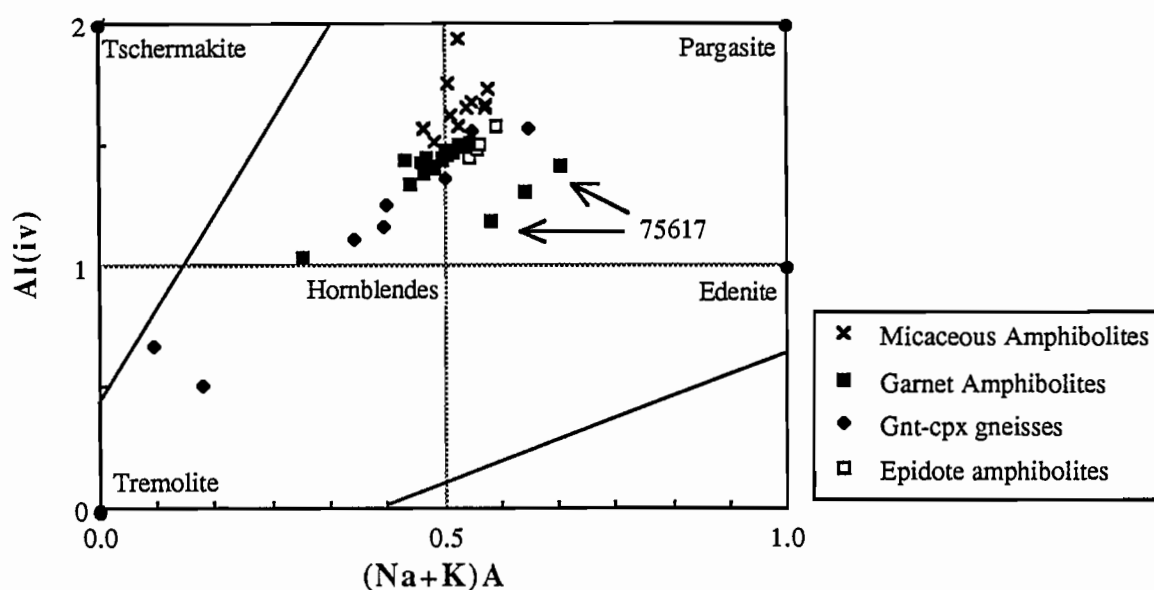


Figure 5.7: Amphibole compositions of garnet amphibolites, garnet clinopyroxene gneisses and micaceous amphibolites. Al_{iv} vs. (Na + K)_A.

Plagioclase is a relatively minor component of garnet-bearing amphibolites, occurring as rarely twinned 0.5mm xenoblastic matrix grains either interstitial to amphibole or segregated into granoblastic quartz and zoisite-rich bands. Garnet in 75628 co-exists with relict matrix clinopyroxene and contains rare inclusions of almost pure albite, suggesting an early garnet-cpx-albite assemblage.

Matrix plagioclase, in apparent textural equilibrium with garnet rims is more calcic, zoned from cores of An₁₇ to rims of An₁₅. In garnet-free units, intermediate albite compositions (cores of An₇ to rims of An₃) are associated with abundant granular epidote (75617).

Zoisite/clinozoisite is common in quartz+plagioclase bands of foliated units as 1-1.5mm idioblastic prisms, showing optical zonation in plane polarised light. Cores have anomalous purple interference colours and straight extinction and are sharply bounded by clinozoisite rims with dark grey birefringence and slight oblique extinction. Both core and rim compositions are aluminous but contain up to 2.8wt% Fe₂O₃. The optical zonation is not manifest chemically and appears to result from crystallographic variation.

Epidote is only present in massive garnet-absent units (e.g. 75617) where it forms equant 0.2-0.5mm optically zoned grains with yellow-green cores (13% Fe₂O₃) and pale yellow rims (9.8% Fe₂O₃).

Clinopyroxene makes up to 5% of 75628 where it forms scattered xenoblastic grains up to 0.5mm in diameter, with a dusty appearance due to abundant fine-grained inclusions. Grains are intergrown with small clots of fine-grained sphene, zoisite and rare K-feldspar, and in places are marginally corroded by amphibole. Locally, however, the clinopyroxene has sharp apparently unreacted contacts with hornblende, plagioclase and garnet. The equivocal textural evidence makes it uncertain whether clinopyroxene is in chemical equilibrium with associated phases.

The clinopyroxene is slightly higher in Na and Al but otherwise similar in composition to that of the garnet - clinopyroxene gneisses, discussed below.

Sphene is the dominant Ti-bearing phase occurring as abundant 0.1-0.2mm long diamond shaped grains, concentrated along grain boundaries and often aligned parallel to the amphibole foliation. Inclusions of sphene also occur in strongly fractured garnet porphyroblasts.

Rutile is rare as a matrix phase and where present forms small granular cores in sphene (Pl.5.1). Unaltered rutile is restricted to inclusions in unfractured garnet, and to a lesser extent hornblende, plagioclase and epidote. Textural evidence suggests that rutile was the dominant prograde Ti-phase, armoured in unfractured early phases but replaced by sphene post-porphyroblasts growth.

K-Feldspar was detected during microprobe analysis and occurs as small grains intergrown with relict clinopyroxene in 75622. The dominant opaque phase is pyrrhotite which forms 0.2-0.5mm xenoblastic clots, intergrown with minor chalcopyrite and associated with late calcite in fractures. The latter forms atoll textures with garnet and partly replaces plagioclase in 75671.

5.1.2.2 GARNET-CLINOPYROXENE GNEISSES:

The garnet clinopyroxene gneisses are texturally and mineralogically heterogeneous with alternating bands of granoblastic garnet + clinopyroxene and more foliated zoisite + quartz domains. Minor phases include sphene, pyrrhotite and rare rutile with amphibole both as inclusions in garnet and as secondary replacement of clinopyroxene. Representative mineral analyses are given in tables 5.6-5.8.

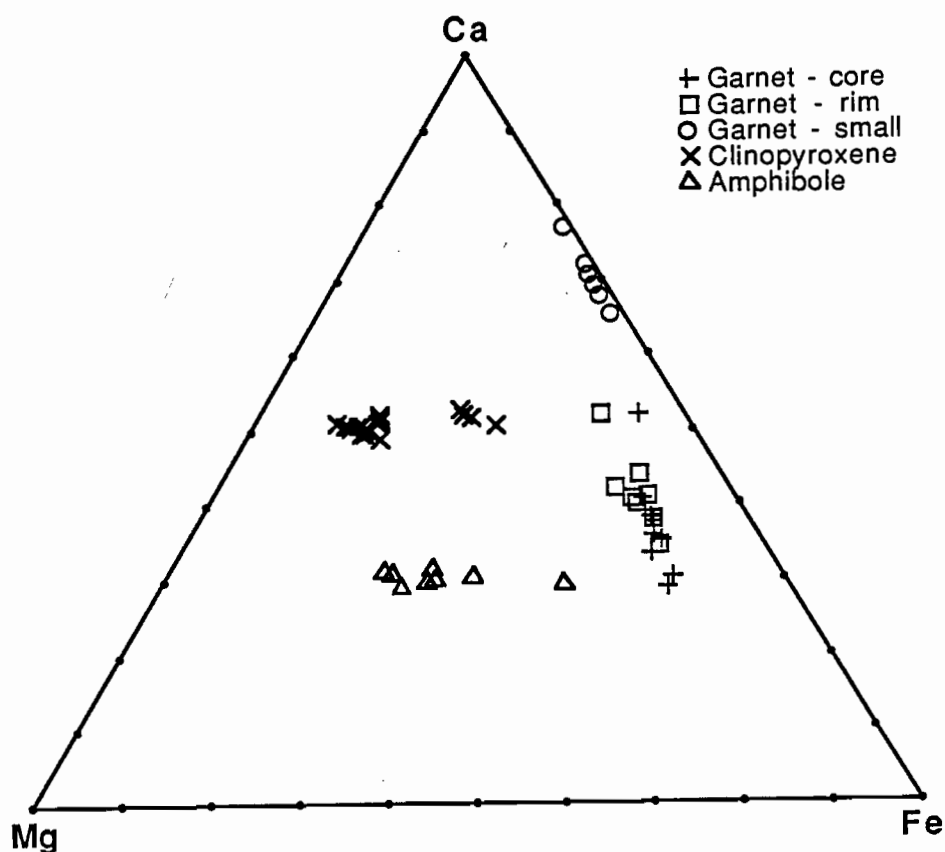


Figure 5.8: Cationic CFM diagram of garnet, clinopyroxene and amphibole compositions - garnet clinopyroxene gneisses.

The coarse domains (e.g. 75627) contain equant 1mm garnets, embedded in a granoblastic mosaic of xenoblastic clinopyroxene, with sphene and granular zoisite concentrated along grain boundaries (Pl.5.2). These are separated by foliated bands with zoisite-quartz-minor clinopyroxene and a second population of small equant 0.1-0.3mm garnets dispersed along the foliation.

	Gar.		Cpx		Amp.		
	core	rim	core	rim	core	rim	inc(g)
SiO ₂	37.47	39.04	53.17	53.05	43.72	52.48	45.48
TiO ₂	0.15	0.04	0.07	0.12	0.75	0.09	0.19
Al ₂ O ₃	21.62	21.01	2.21	2.31	13.75	4.26	9.28
Fe ₂ O ₃	-	1.18	1.17	1.04	-	-	-
MgO	2.78	2.27	12.81	12.77	10.35	13.81	6.89
CaO	12.28	15.01	23.39	23.33	11.49	13.43	11.01
MnO	2.21	1.00	0.04	0.03	0.17	0.17	0.26
FeO	23.90	20.33	6.40	6.69	13.99	13.48	21.96
Na ₂ O	-	-	0.95	0.90	1.82	0.89	1.80
K ₂ O	-	-	-	-	1.39	0.24	0.54
Σ	100.41	99.88	100.21	100.24	97.44	98.86	97.41
Cations							
Si	2.95	3.04	1.97	1.96	6.48	7.54	6.89
Ti	0.01	-	-	-	0.08	0.01	0.02
Al	2.01	1.93	0.10	0.10	2.40	0.72	1.66
Fe ₃		0.07	0.03	0.03	-	-	-
Mg	0.33	0.26	0.71	0.71	2.29	2.96	1.56
Ca	1.04	1.25	0.93	0.93	1.83	2.07	1.79
Mn	0.15	0.07	-	-	0.02	0.02	0.03
Fe ₂	1.57	1.33	0.20	0.21	1.74	1.62	2.79
Na	-	-	0.07	0.07	0.52	0.25	0.53
K	-	-	-	-	0.26	0.04	0.10
Σ	8.06	7.95	4.01	4.01	15.62	15.23	15.37
No. O	12	12	6	6	23	23	23
Mg#	17.4	16.4	78.0	77.2	56.9	64.6	35.9

Table 5.6: Representative mineral analyses of garnet , clinopyroxene and amphibole from 75627 - coarse band.

The large garnets contain concentrically oriented inclusions of sphene, quartz and amphibole and in contrast to the amphibolites and schists, show 'reverse' zonation with *increasing* CaO, decreasing FeO and inconsistent change in MgO and Mg# from core to rim. MnO shows 'normal' core-rim zonation (~1.5% - <1%). The high Ca rims are optically distinct and inclusion-free (Pl.5.2).

The smaller garnets are similarly zoned but significantly higher in CaO than larger grains with correspondingly low MgO (0.3%). In 75619 garnets with up to 28% CaO form aggregates of 0.2mm grains rimming and apparently replacing zoisite (Pl.5.2).

Plate 5.2: Metabasite textures. Scale bar 0.5mm.

A. Garnet clinopyroxene gneiss showing equant garnets in a mosaic of xenoblastic clinopyroxene (coarse band) - XN (75627 - DQ361382).

B. Garnets with abundant fine-grained sphene inclusions and relatively inclusion-free cores - XN (75627 - DQ361382).

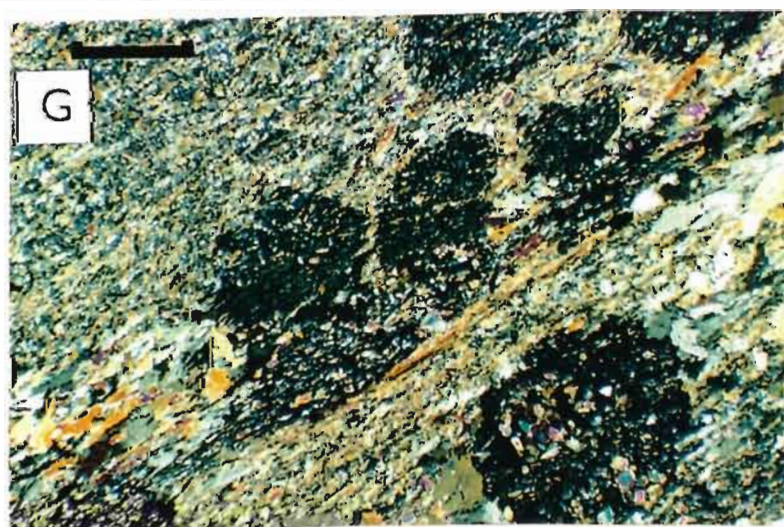
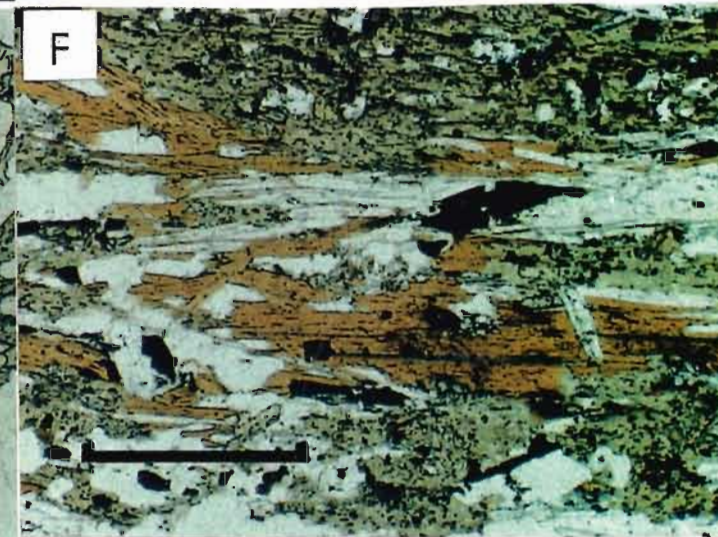
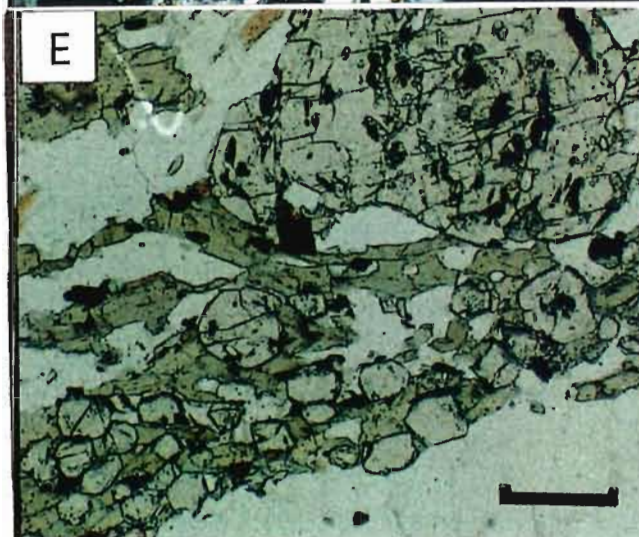
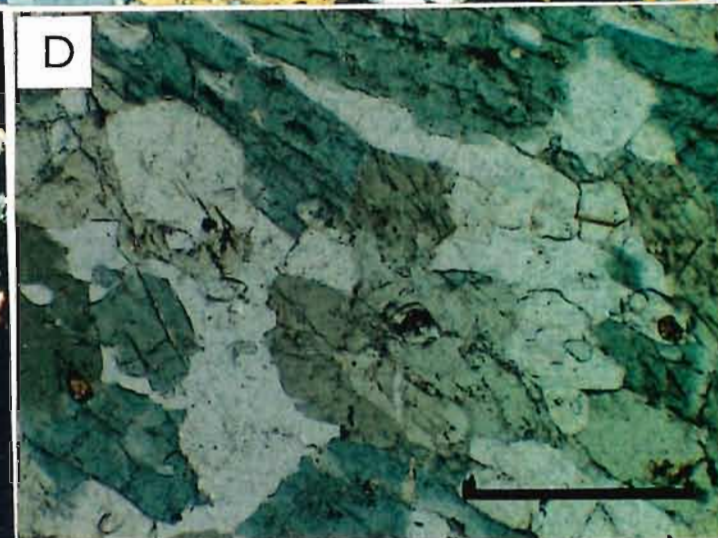
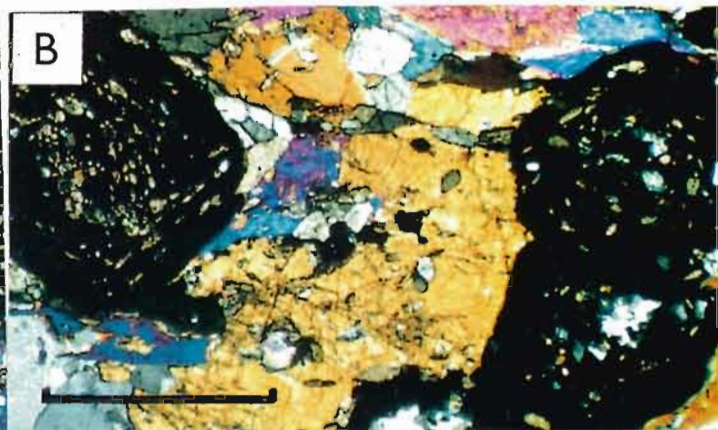
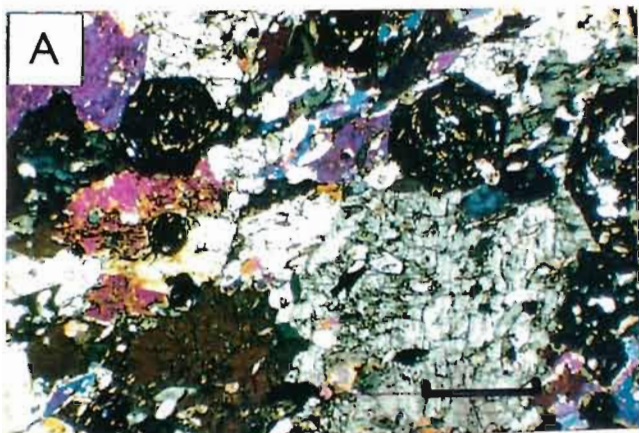
C. Granular high CaO garnet (black) developing as rims on zoisite (yellow grain at centre left with irregular margins). Scattered high birefringent grains are clinopyroxene. Field of view 1.5 mm - XN (75619 - DQ359369).

D. Sphene overgrowths on rutile in garnet-free amphibolite. Note unaltered rutile in core of unfractured amphibole (left) and replacement of rutile in fractured amphibole (centre) and on grain boundary (right) - PPL (75617 - DQ357401).

E. Bimodal garnet size distribution in micaceous amphibolite. Small grains appear to overgrow amphibole and are concentrated along margin of quartz vein (lower right) - PPL (75674 - DQ362376).

F. Interleaved biotite and muscovite replacing strongly degraded amphibole (pale green) - PPL (75631 - DQ362375).

G. Retrogressed garnet amphibolite - Lower Claytons Valley. Relict garnet clots are largely altered to epidote/chlorite and set in a fine-grained albite-epidote-amphibole matrix with local schistose bands - XN (75612 - DQ328401).



	Cpx		Gar.		Zo.	Cht.	Sphene	Amp.		
	core	rim	core	rim				rim(cpx)	rim(gar.)	inc(gar)
SiO ₂	53.39	52.98	38.17	38.43	38.87	26.14	30.38	47.00	45.65	43.34
TiO ₂	0.04	0.06	0.16	0.16	0.13	0.01	37.76	0.34	0.32	0.60
Al ₂ O ₃	2.59	2.15	21.53	21.67	31.08	19.22	1.76	9.18	11.32	13.34
Fe ₂ O ₃	-	0.71	0.24	0.24	3.17	-	-	-	-	-
MgO	12.18	12.04	3.20	2.26	0.10	12.49	-	11.83	11.04	10.52
CaO	22.47	22.94	10.80	15.68	24.88	0.10	29.02	11.51	11.29	11.15
MnO	0.04	0.08	1.40	0.76	-	0.27	-	0.10	0.08	0.06
FeO	7.94	7.79	25.03	21.37	-	29.83	0.26	14.10	14.53	14.68
Na ₂ O	1.16	1.01	-	-	0.01	-	0.04	1.65	1.74	2.16
K ₂ O	-	-	-	-	-	-	0.01	0.57	0.72	1.23
Σ	99.81	99.76	100.53	100.57	98.24	88.06	99.23	96.28	96.69	97.08
Cations										
Si	1.98	1.98	2.99	2.99	2.98	2.77	1.04	6.95	6.75	6.43
Ti	-	-	0.01	0.01	0.01	-	0.98	0.04	0.04	0.07
Al	0.11	0.10	1.99	1.99	2.81	2.40	0.07	1.60	1.97	2.34
Fe ₃	-	0.02	0.01	0.01	0.18	-	-	-	-	-
Mg	0.68	0.67	0.37	0.26	0.01	1.97	-	2.61	2.43	2.33
Ca	0.90	0.92	0.91	1.31	2.04	0.01	0.84	1.83	1.79	1.77
Mn	-	-	0.09	0.05	-	0.02	-	0.01	0.01	0.01
Fe ₂	0.25	0.24	1.64	1.39	-	2.65	0.02	1.74	1.70	1.82
Na	0.08	0.07	-	-	-	-	-	0.47	0.50	0.62
K	-	-	-	-	-	-	-	0.11	0.14	0.23
Σ	4.00	4.00	8.01	8.01	8.03	9.82	2.95	15.36	15.33	15.62
No. O	6	6	12	12	13	14	5	23	23	23
Mg#	73.1	73.6	18.4	15.8	-	42.6	-	60.0	58.8	56.1

Table 5.7: Representative mineral analyses of garnet, clinopyroxene, amphibole, zoisite, sphene, plagioclase and chlorite from 75662.

Clinopyroxene is pale green to colourless and occurs as equant 1-1.5mm strain-free plates or prismatic 0.8mm weakly undulose grains oriented sub-parallel to the zoisite foliation. There is little chemical zonation, but rims have slightly lower Al₂O₃. Fe-rich, Al-poor clinopyroxene is present in 75619, in association with anomalously high Ca-garnets.

	Zoisite		Cpx.		Gar.	
	core	rim	core	rim	core	rim
SiO ₂	38.25	38.40	50.83	50.79	38.52	38.49
TiO ₂	0.18	0.22	0.01	0.00	0.12	0.19
Al ₂ O ₃	28.73	28.82	0.59	0.75	21.32	20.94
Fe ₂ O ₃	6.54	6.22	1.40	1.07	1.19	1.77
MgO	0.02	0.02	8.06	8.10	0.28	0.25
CaO	24.47	24.69	24.13	24.11	26.19	28.08
MnO	0.05	0.01	0.14	0.09	1.00	0.75
FeO	-	-	14.36	14.59	12.64	10.43
Na ₂ O	-	-	0.22	0.16	-	-
Σ	98.25	98.38	99.73	99.66	101.26	100.90
Cations						
Si	2.97	2.97	1.97	1.97	2.96	2.96
Ti	0.01	0.01	-	-	0.01	0.01
Al	2.63	2.63	0.03	0.03	1.93	1.90
Fe ₃	0.37	0.36	0.04	0.03	0.07	0.10
Mg	0.00	0.00	0.47	0.47	0.03	0.03
Ca	2.04	2.05	1.00	1.00	2.16	2.31
Mn	0.00	0.00	0.00	0.00	0.07	0.05
Fe ₂	-	-	0.47	0.47	0.81	0.67
Na	-	-	0.02	0.01	-	-
Σ	8.02	8.02	4.00	4.00	8.03	8.03
No. O	13	13	6	6	12	12
Mg#	-	-	50.0	49.7	3.8	4.1

Table 5.8: Representative mineral analyses from 75619 - foliated band.

Mukhopadhyay (1990) has argued that the name eclogite *sensu stricto* should be reserved for rocks containing omphacitic (i.e. high-Na) clinopyroxene. Clinopyroxene analyses, as illustrated in figure 5.9, have low Na-content (<1%) and in accordance with this convention (and the banded field appearance), this rocktype is referred to as garnet-clinopyroxene gneiss. Clinopyroxene in the garnet amphibolites is more 'eclogitic', and this is discussed in section 5.3.

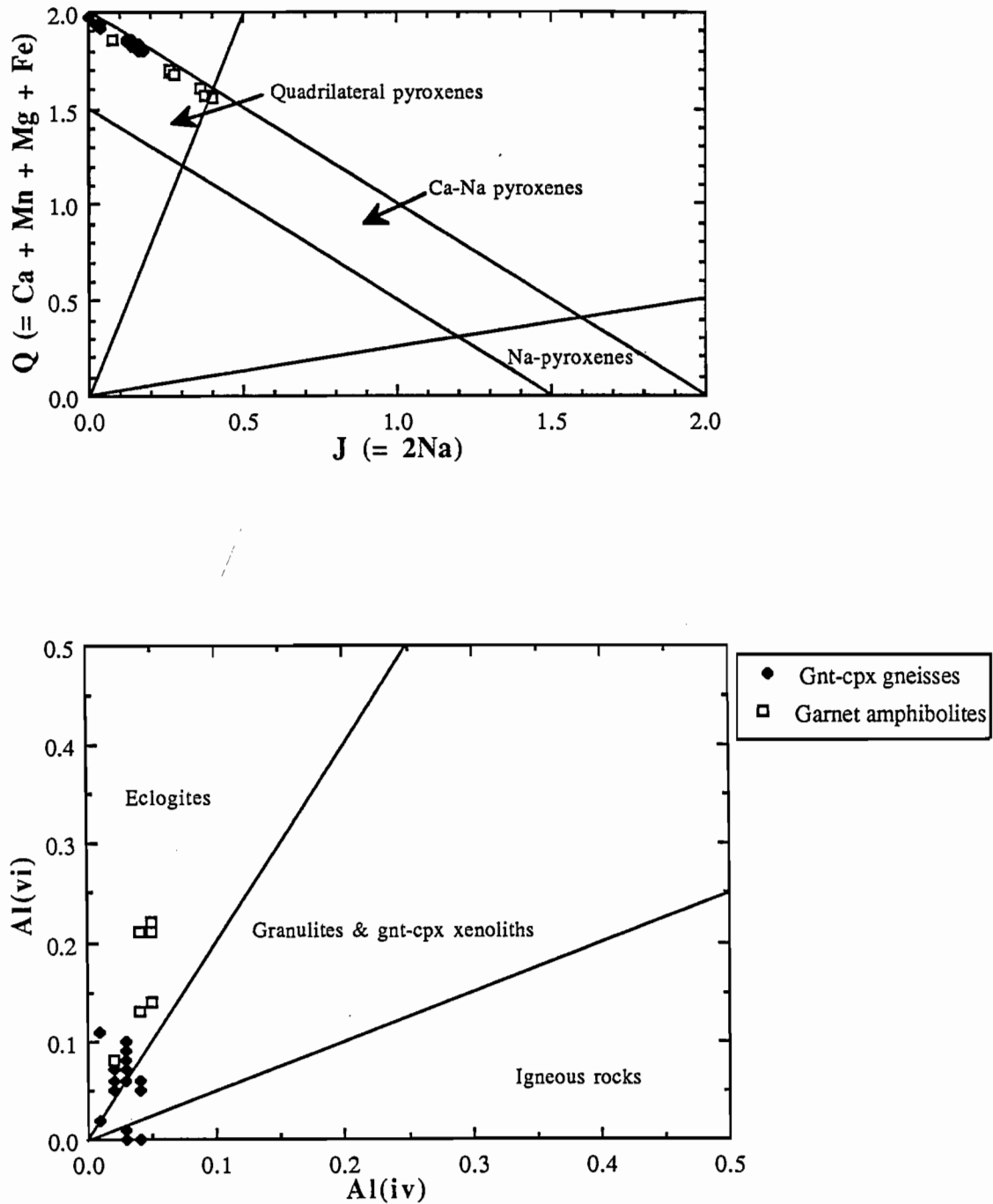


Figure 5.9: Clinopyroxene compositions - gnt-cpx gneisses and garnet amphibolites. (a) $Q (= Ca + Mn + Mg + Fe^{2+})$ vs. $J (= 2Na)$. (b) $Al_{iv} (= 2 - Si)$ vs. $Al_{vi} (= Al_{tot} - Al_{iv})$.

Several varieties of amphibole are evident on both textural and chemical grounds. Both garnet and clinopyroxene contain 0.2mm inclusions of deep blue-green Fe-rich hornblende (up to 21% FeO). Clinopyroxene in coarse domains is partially replaced by xenoblastic amphibole showing an optical

colour zonation from dark olive green cores of pargasitic hornblende (13.5% Al_2O_3) to pale blue-green rims of tremolite-actinolite (4.5% Al_2O_3) (fig.5.11). The low-Al rims appear to be preferentially developed against clinopyroxene and elsewhere, texturally late amphibole is similar in composition to the enclosing garnet amphibolites (e.g. 75662).

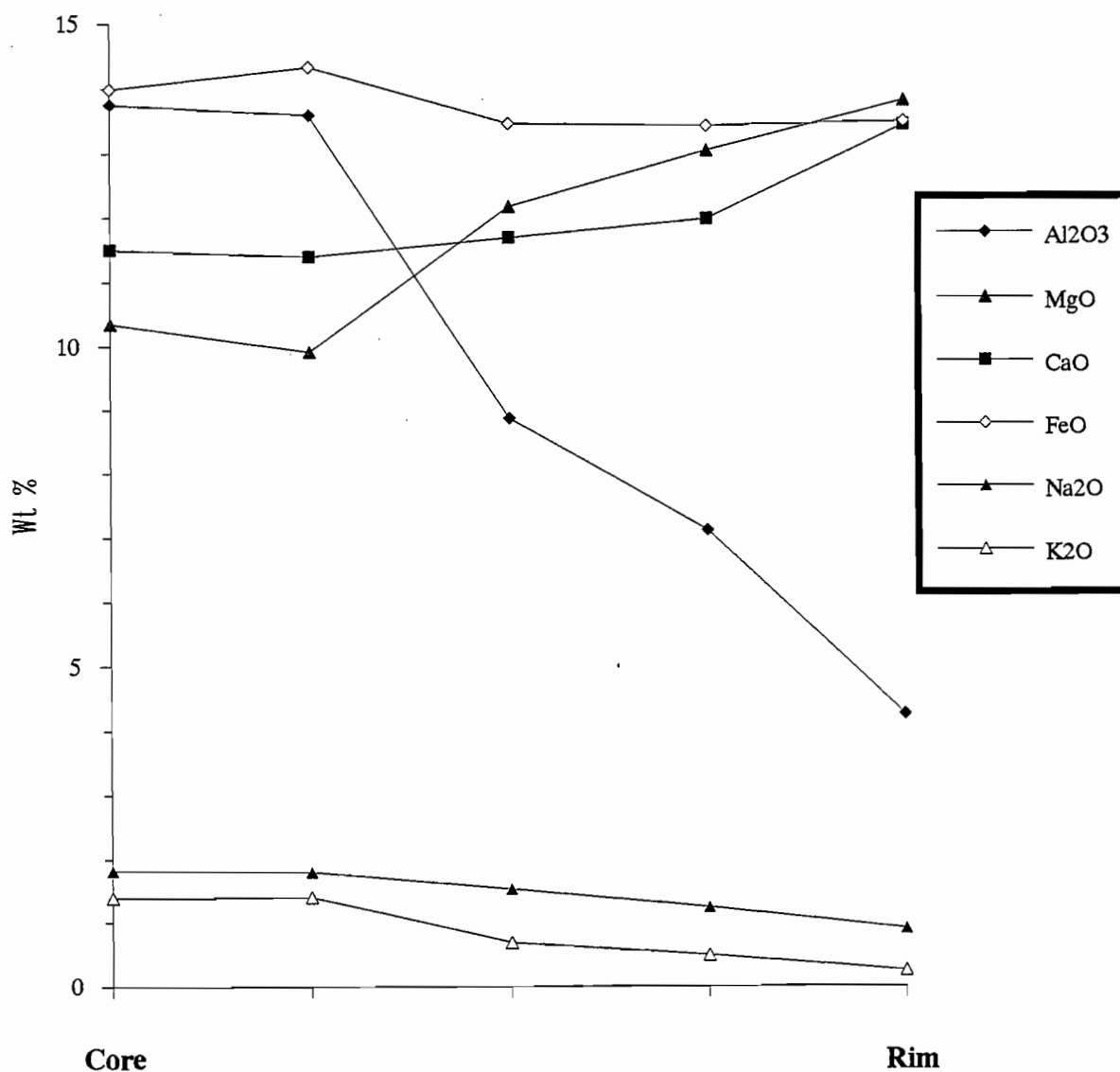


Figure 5.10: Amphibole zonation in 75627.

Sphene is abundant as 0.1mm inclusions in garnet cores (Pl.5.2) and as 0.1-0.3mm matrix grains and rutile is restricted to rare inclusions in garnet rims. Unlike the garnet amphibolites, there is no evidence of sphene directly replacing rutile

5.1.2.3 RETROGRESSIONED AMPHIBOLITES:

Amphibolites from the Claytons Rivulet, contain lenses of coarse undulose dark olive green amphibole and rare strongly altered garnet (75612) in a fine-grained matrix of foliated amphibole, interstitial plagioclase and epidote with minor chlorite, muscovite and disseminated hematite. The mineral chemistry of 75605, which is considered representative of the suite, is presented in table 5.9.

	Plag.		Amp-mtx		Amp-porb		Mus.	Epidote	
	core	rim	core	rim	core	rim		core	rim
SiO ₂	68.76	66.52	45.03	44.76	44.01	44.84	50.07	37.73	37.67
TiO ₂	0.01	0.06	0.60	0.69	0.65	0.69	0.19	0.16	0.16
Al ₂ O ₃	20.33	20.28	12.36	13.06	13.61	13.73	28.73	24.33	25.81
Fe ₂ O ₃	0.13	0.66	-	-	-	-	-	11.82	9.92
MgO	-	0.79	12.03	11.57	11.25	11.07	2.77	0.44	0.10
CaO	0.35	0.44	12.04	11.62	11.85	10.63	0.04	23.61	24.11
MnO	0.01	-	0.09	0.12	0.20	0.15	0.02	0.16	0.14
FeO	-	-	13.34	13.12	13.91	14.10	2.83	-	-
Na ₂ O	11.05	10.66	2.17	2.45	2.35	2.74	1.03	0.12	-
K ₂ O	0.04	0.50	0.33	0.42	0.35	0.50	9.82	-	-
Σ	100.68	99.91	97.99	97.81	98.18	98.45	95.50	98.37	97.91
Cations									
Si	2.98	2.92	6.55	6.52	6.42	6.50	3.32	2.98	2.97
Ti	-	-	0.07	0.08	0.07	0.08	0.01	0.01	0.01
Al	1.04	1.05	2.12	2.24	2.34	2.35	2.25	2.27	2.40
Fe ₃	-	0.02	-	-	-	-	-	0.70	0.59
Mg	-	0.05	2.61	2.51	2.45	2.39	0.27	0.05	0.01
Ca	0.02	0.02	1.88	1.81	1.85	1.65	-	2.00	2.04
Mn	-	-	0.01	0.02	0.03	0.02	-	0.01	0.01
Fe ₂	-	-	1.62	1.62	1.69	1.71	0.15	-	-
Na	0.93	0.91	0.61	0.69	0.67	0.77	0.13	0.02	-
K	-	0.03	0.06	0.08	0.07	0.09	0.83	-	-
Σ	4.97	5.00	15.53	15.57	15.59	15.56	6.96	8.04	8.03
No. O	8	8	23	23	23	23	11	13	13
Mg#	-	-	61.70	60.77	59.18	58.29	64.29	-	-

Table 5.9: Representative mineral analyses of plagioclase, amphibole, epidote and muscovite from 75605.

Epidote is abundant and occurs as equant disseminated 0.1 mm matrix grains and more rarely as optically and chemically zoned 1mm augen grains, with cores of 12% and rims of 10% Fe_2O_3 , which are wrapped around by the fine-grained amphibole foliation. Matrix plagioclase of albite composition ($\text{An}_{2.5}$) is locally segregated into 0.5mm wide granoblastic bands. The albite is intergrown with late muscovite, which appears to be crystallographically controlled. The amphibole of both relict coarse clots and the foliated matrix is aluminous hornblende and differs little from that of unaltered garnet amphibolites. In 75612, the foliation is cross-cut by veins of coarse randomly aligned deep blue-green amphibole and relict garnet porphyroblasts show zonal alteration - with cores of fine-grained epidote + chlorite enclosed within substantially unaltered inclusion-free rims (Pl.5.2).

Apart from the Claytons Rivulet, garnet amphibolites show little evidence of retrogression. At DQ368350, however, a single band of chlorite-actinolite greenschist (75651), interbanded with mica-free and micaceous garnet amphibolites, contains 1.5mm clots of decussate chlorite, probably after garnet, in a weakly foliated matrix of prismatic actinolite, chlorite and minor calcite.

5.1.2.4 MICACEOUS AMPHIBOLITES:

The field setting, geochemistry and structural setting of mica-rich amphibolites from the Forth Valley have been discussed earlier. Petrographically, the rocks contain layers of amphibole and garnet in a matrix of quartz, plagioclase, biotite and muscovite - with locally complex grain textures.

Amphibole is optically and chemically distinct, forming colourless to pale green ragged xenoblastic grains up to 2mm long with strong to moderate undulose extinction, linear inclusion trails of fine-grained ?iron oxides and a weak grain preferred orientation sub-parallel to quartz-amphibole layering (S2). Compositionally, the amphiboles have higher alkali site occupancy - with elevated K - and are more aluminous than those of mica-free assemblages (fig.5.11).

In 75631, the amphibole cleavage is occupied by trails of Si-rich diabantite chlorite (Deer *et al* 1967) and an apparently aluminous amphibole. The latter has poor stoichiometry and may represent a mixed analysis - although the Al_2O_3 content (17%) exceeds that of both the associated chlorite and host amphibole. In terms of the present analysis, it is an almost pure tschermakite-pargasite solution.

	Gar (large)			Gar (small)		Plag.		Zo.	Mus.	Bt.	Amp(mtx)			Amp(porb)		K-fsp	Cht
	core	rim	inc?	core	rim	core	rim				core	rim	?exsol	core	rim		
SiO ₂	38.04	38.20	36.70	37.15	37.96	62.86	63.04	39.12	47.98	38.79	43.28	42.98	40.36	44.26	44.12	63.82	33.36
TiO ₂	0.06	0.08	4.14	0.09	0.05	-	0.02	0.02	0.73	1.31	0.70	0.62	0.34	0.64	0.64	0.88	0.13
Al ₂ O ₃	21.93	21.97	19.21	21.21	21.77	23.39	23.37	32.24	31.21	16.69	15.35	15.54	17.59	15.18	14.97	24.07	16.71
Fe ₂ O ₃	-	-	3.87	-	-	-	-	2.09	-	-	-	-	-	-	-	1.51	-
MgO	3.10	4.25	3.10	3.12	3.75	-	-	0.04	2.50	13.66	11.37	11.16	13.69	11.68	11.99	1.71	18.33
CaO	9.99	10.69	13.06	8.68	9.29	4.58	4.73	24.91	-	0.07	11.18	11.04	6.71	11.05	11.26	0.05	0.95
MnO	5.26	2.15	3.76	1.68	0.40	0.03	-	0.02	0.07	0.04	0.14	0.16	-	0.18	0.10	-	0.13
FeO	23.11	23.00	16.26	27.18	27.03	-	-	-	1.55	14.15	11.23	11.16	12.57	10.97	10.68	-	16.09
Na ₂ O	-	-	-	-	-	8.58	8.58	0.01	0.87	0.12	2.37	2.43	1.44	2.28	2.35	0.69	0.21
K ₂ O	-	-	-	-	-	0.07	0.08	0.01	10.00	8.71	0.80	0.81	0.78	0.70	0.67	7.51	0.37
Σ	101.49	100.34	100.10	99.10	100.25	99.51	99.82	98.46	94.91	93.54	96.42	95.90	93.48	96.94	96.78	100.24	86.28
Cations																	
Si	2.96	2.97	2.87	2.97	2.98	2.79	2.79	2.97	3.20	2.88	6.35	6.34	6.06	6.43	6.42	2.82	3.34
Ti	-	0.01	0.24	0.01	-	-	-	-	0.04	0.07	0.08	0.07	0.04	0.07	0.07	0.03	0.01
Al	2.01	2.02	1.77	2.00	2.01	1.22	1.22	2.89	2.45	1.46	2.66	2.70	3.12	2.60	2.57	1.25	1.97
Fe ₃	-	-	0.23	-	-	-	-	0.12	-	-	-	-	-	-	-	0.05	0.20
Mg	0.36	0.49	0.36	0.37	0.44	-	-	0.01	0.25	1.51	2.49	2.45	3.07	2.53	2.60	0.11	2.74
Ca	0.83	0.89	1.10	0.74	0.78	0.22	0.22	2.03	-	0.01	1.76	1.75	1.08	1.72	1.76	-	0.01
Mn	0.35	0.14	0.25	0.11	0.03	-	-	-	-	-	0.02	0.02	-	0.02	0.01	-	0.10
Fe ₂	1.51	1.50	1.06	1.82	1.77	-	-	-	0.08	0.88	1.38	1.38	1.58	1.33	1.31	-	1.15
Na	-	-	-	-	-	0.74	0.74	-	0.11	0.02	0.67	0.70	0.42	0.64	0.66	0.06	0.04
K	-	-	-	-	-	-	0.01	-	0.85	0.83	0.15	0.15	0.15	0.13	0.12	0.42	0.05
Σ	8.02	8.02	7.88	8.02	8.01	4.97	4.98	8.02	6.98	7.66	15.56	15.56	15.52	15.47	15.52	4.74	9.61
No. O	12	12	12	12	12	8	8	13	11	11	23	23	23	23	23	8	14
Mg#	19.3	24.6	25.4	17.0	19.8	-	-	-	75.8	63.2	64.3	64.0	66.0	65.5	66.5	-	70.4

Table 5.10: Representative mineral analyses of from 75669.

Micas:

Abundant biotite and to a lesser extent muscovite, making up to 20 vol%, is the distinctive mineralogical (and consequently geochemical) feature of these rocks. Biotite occurs as oriented masses, rimming and apparently replacing amphibole (Pl.5.2) or as rare xenoblastic plates and has a consistent Mg# of around 60 - despite significant K-variation (fig.5.2). Muscovite is interleaved with biotite in 75631, but more commonly forms coarse unoriented flakes which transect the amphibole foliation. Grain textures suggest that biotite growth was synchronous with S2 (and earlier than muscovite), although this may reflect mimetic growth on a pre-existing amphibole foliation.

Garnet occurs as two distinct grain-size populations (Pl.5.2). Large (>1mm) sub-idioblastic inclusion-rich porphyroblasts with distinct inclusion-free rims are wrapped around by matrix amphibole. Small (0.2mm) equant matrix grains are concentrated along the margins of quartz layers/veins (Pl.5.2), appear to overgrow the foliation and are in apparent textural equilibrium with late xenoblastic biotite.

The garnets are intermediate between pelitic and amphibolite compositions, but have higher MnO cores (up to 5.26%) and show reverse CaO zoning similar to the garnet clinopyroxene gneisses. Apart from lower Mn, the smaller garnets are of similar composition.

Plagioclase of variable composition (An_{15-22}) occurs as xenoblastic grains in quartz-rich domains and is often intergrown with late muscovite. Calcite is relatively abundant in 75624, where it forms xenoblastic masses corroding garnet and plagioclase. In contrast to mica-free amphibolites zoisite is rare, but where present (75631) occurs as 1-1.5mm prismatic grains aligned sub-parallel to S2. In contrast to the other metabasites, abundant granular rutile is largely unreplaced by sphene.

5.1.2.5 SERPENTINITE:

Apart from the ultramafic schist at 367371, the petrology of the serpentinites has not been studied in detail. Petrographic features of the former have been described in section 4.2.1.3 and representative mineral compositions are given in table 5.11.

All silicate phases are Mg-rich (as is consistent with the bulk geochemistry) and magnetite contains up to 4.5% Cr_2O_3 . Chlorite appears to be the only Al-bearing phase, suggesting relatively low P conditions (< 5 kb, Will *et al* 1990) and the presence of serpentine (probably antigorite) indicates an upper T limit of approximately 550° C (Will *et al* 1990). These constraints are well below syn-S2 peak T conditions inferred for the metabasites (see 5.2-3) and despite the close spatial association between the two units (see 4.2.1.3), 75636 appears to have developed under lower P-T conditions.

Similar P-T conditions are inferred for D3 in the Claytons Valley, but microstructural features of the ultramafic schist are inconsistent with the eastward vergence of this deformation. West vergent shear bands are however, compatible with the Berry & Crawford (1988) ophiolite model and the inferred P-T conditions may have developed in a locally water-saturated shear environment, near the base of a Cambrian ultramafic thrust sheet.

	Serp.		Cht.	Amp.		Mag.	Hem.
	massive	fibrous		core	rim		
SiO₂	42.40	41.34	33.04	58.12	58.64	-	-
TiO₂	0.05	0.06	0.02	0.05	0.13	0.41	-
Al₂O₃	0.30	0.07	14.67	0.45	0.58	-	-
Cr₂O₃	-	-	0.68	0.03	0.10	4.43	0.12
Fe₂O₃	-	-	-	-	-	63.27	98.75
MgO	37.49	38.25	32.55	23.01	24.07	0.41	0.11
CaO	0.08	0.07	0.03	12.80	12.61	-	-
MnO	0.23	0.06	0.02	0.07	0.46	0.16	0.19
FeO	4.06	4.10	4.68	2.47	2.66	30.40	-
Na₂O	-	-	-	0.23	0.24	-	-
K₂O	-	-	-	0.02	0.03	-	-
Σ	84.60	83.95	85.70	97.23	99.52	99.09	99.17
Cations							
Si	2.05	2.02	3.18	7.97	7.89	-	-
Ti	-	-	-	0.01	0.01	0.01	-
Al	0.02	-	1.66	0.07	0.09	-	-
Cr	-	-	0.05	-	0.01	0.14	-
Fe₃	-	-	-	-	-	1.84	1.99
Mg	2.70	2.78	4.66	4.70	4.82	0.02	-
Ca	-	-	-	1.88	1.82	-	-
Mn	0.01	-	-	0.01	0.05	0.01	-
Fe₂	0.16	0.17	0.38	0.29	0.30	0.98	-
Na	-	-	-	0.06	0.06	-	-
K	-	-	-	-	-	-	-
Σ	4.94	4.97	9.94	15.00	15.06	3.00	1.99
No. O	7	7	14	23	23	4	3
Mg#	94.4	94.2	92.5	94.2	94.1	2.4	-

Table 5.11: Representative mineral analyses of serpentine, chlorite, tremolite magnetite and hematite from 75636.

5.2 THERMOBAROMETRY:

5.2.1 INTRODUCTION:

Reactions between end-member components of stable phase assemblages, can be used to estimate equilibrium P-T conditions, according to the general thermodynamic constraint:

$$\Delta G^\circ = \Delta H^\circ + T\Delta S^\circ + (P-1)\Delta V^\circ + RT\ln K_a = 0 \quad (\text{Eq.5.1})$$

where,

G° = Gibbs Free Energy

H° = Enthalpy

S° = Entropy

V° = Volume

K_a is the activity product, describing the thermodynamic 'concentration' of end-members in the balanced chemical reaction.

5.2.2.1 CALIBRATIONS:

In principle, if the energy, volume and compositional parameters in equation 5.1 are known, any reaction can be used to estimate P and T and thus be used as a geologic thermobarometer (Powell 1985a).

In practice, calibration of potential thermobarometers has been restricted to fluid-absent reactions between well characterised end-members and three general methods have been employed. Direct experimental determination of the relationship between $\ln K_a$, P and T is the most reliable, but only practical for low variance assemblages and simple chemical systems (e.g. Ferry & Spear 1978, Koziol & Newton 1988, Ellis & Green 1979).

Reactions which are difficult or impossible to study experimentally may be calibrated by empirical (statistical) methods (Hodges & Crowley 1985). Compositional data (formulated as $\ln K_a$ for the reaction of interest), and independent P-T estimates are fitted to an equation of the form,

$$-RT\ln K_a = A - BT + (P - 1)C \quad (\text{Eq.5.2})$$

where A, B and C are regression parameters (Hodges & Crowley 1985). Unfortunately, the propagation of experimental, analytical and theoretical errors through the regression leads to large

uncertainties of up to ± 5 kb for most barometer calibrations (Hodges & Crowley 1985, Kohn & Spear 1990).

A third alternative is the theoretical calculation of specific equilibrium relationships (eq.5.1) using experimentally constrained thermodynamic data (Newton & Perkins 1982, Mukhopadhyay 1990). Uncertainties result from the propagation of experimental errors and the use of poorly constrained activity models and are commonly in the range of 1-2 kb (Newton & Perkins 1982).

This approach is the foundation of recent dataset systems, pioneered by Berman et al (1986) and Holland & Powell (1990). These authors have derived internally consistent thermodynamic parameters from calorimetric and experimental data using linear regression and mathematical programming respectively. The thermodynamic data may be used in conjunction with software systems (THERMOCALC - Powell & Holland 1988 and GEOCALC - Perkins et al 1986, Brown et al 1987, 1988) to calculate and display simultaneously operating equilibria for a given phase assemblage.

5.2.1.2 ACTIVITY MODELS:

Where natural assemblages deviate from the end-member compositions, activity models are required to characterise mixing of the excess components (Hoish 1990). Non-ideal mixing occurs because elements of dissimilar size (or charge) behave differently in the same structural environment: activity models describe the magnitude and direction of these departures (Indares & Martignole 1985).

In garnets, mixing of Fe, Mg, Ca and Mn on the M1 octahedral site can be modelled as quaternary sub-regular solution (Ganguly & Kennedy 1974), in which mixing is described by constituent binary (Margules) parameters and additional ternary/quaternary interaction terms. Quantification of the quaternary solution has been the subject of much debate and currently available models use different Margules parameters (W), derived from calorimetric (Hodges & Spear 1982) and natural Fe-Mg partitioning data (Ganguly & Saxena 1984). Mixing on the Fe-Ca binary join is probably ideal (Cressey et al 1978) and ideal spessartine solution is a reasonable assumption in the range 400-600°C (Hodges & Spear 1982). Hodges & Spear (1982) suggest that under amphibolite facies conditions, garnet non-ideality is largely a result of mixing on the Mg-Ca join, although Ganguly & Saxena (1984) include additional mixing parameters for the Mn-Fe, Mn-Mg and also the Fe-Mg binary joins. Mixing properties of the almandine-pyrope join are critical for a number of thermobarometer applications, but are at present unresolved (Spear & Peacock 1990).

Binary sub-regular solution models for plagioclase have been developed by Hodges & Royden (1984) and Newton *et al* (1980), and despite uncertainty as to the importance of selective Al-partitioning, the models give generally similar results.

Activity models for more complex multi-site interactions (e.g. micas, amphiboles and pyroxenes) are very poorly constrained (Moecher *et al* 1988, Spear & Peacock 1990), although semi-quantitative models have been suggested by a number of empirical geobarometer calibrations (Kohn & Spear 1989, 1990).

In the following discussion, the choice of activity model is dictated by the assumptions and compositional limits of individual calibrations, and the database modelling in section 5.3 uses models which best approximate experimental or empirical P-T estimates.

5.2.2 THERMOMETRY:

Fluid-absent inter-crystalline Fe-Mg exchange reactions involve very small ΔV and have inspired a number of experimentally and empirically calibrated geothermometers. Where non-ideality is not explicitly included, the effect of additional components on Fe-Mg exchange, can be formulated as follows:

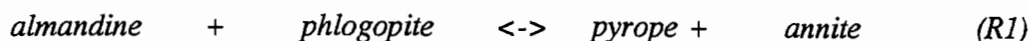
$$\Delta H^\circ - T\Delta S^\circ + (P-1)\Delta V^\circ + RT\ln K_d + RT\ln K_\gamma = 0 \quad (\text{Eq.5.3})$$

where K_d is the (experimentally derived) distribution coefficient $(\text{Fe}^{2+}/\text{Mg})_1/(\text{Fe}^{2+}/\text{Mg})_2$ and K_γ is the ratio of activity coefficients for non-ideal solution (Essene 1982).

Where mineral compositions are determined by electron microprobe analysis (as is the case here), potential Fe^{3+} substitution is unconstrained, and the calculated K_d may differ from its true value (Schumacher 1990). For garnet and clinopyroxene, Fe^{3+} has been calculated on the basis of stoichiometric and charge balance constraints, according to the method of Ryburn *et al* (1976). In biotite, phengite and amphibole however, vacancy substitutions occur on the alkali site and similar charge balance constraints are not possible. In the following, where recalculation is not possible, all Fe has been taken to be Fe^{2+} , and as a result, all calculated temperatures will be maximum. This assumption appears to be validated by the close agreement with garnet-clinopyroxene temperatures, which are not subject to this uncertainty.

5.2.2.1 GARNET-BIOTITE:

The Fe-Mg exchange reaction:



has been experimentally and theoretically calibrated by a number of authors and is widely used as a thermometer in amphibolite facies metapelites.

Ferry and Spear (1978) equilibrated synthetic binary garnet-biotite compositions in the simple AKFM system and generated the following polythermal, polybaric expression for the exchange reaction:

$$12454 - 4.662T(^{\circ}\text{K}) + 0.057P(\text{bars}) + 3RTL\ln K_d = 0 \quad (\text{Eq.5.4})$$

In natural systems, pure Fe-Mg exchange may be modified by excess components and this expression should only be used for compositions approaching binary Fe-Mg solutions (Ferry & Spear 1978). A range of garnet non-ideality corrections have been applied to equation 5.4, based on the following relationships (Hodges & Spear 1982, Ganguly and Saxena 1984, Indares & Martignole 1985, Berman 1990):

$$\ln K_a = \ln K_d + \ln K_{\gamma} \quad (\text{Eq.5.5})$$

$$K_{\gamma} = \gamma_{\text{Fe}^{2+}}^{\text{ga}} / \gamma_{\text{Mg}}^{\text{ga}} \quad (\text{Eq.5.6})$$

In biotites, Fe-Mg solution is essentially ideal, although systematic variation in $\ln K_d$ may result from Al and Ti substitution, particularly in granulite facies metapelites. Indares & Martignole (1985) correct the Ferry & Spear calibration for Al and Ti in biotite, using both the Hodges & Spear (1982) and Ganguly & Saxena (1984) garnet models.

For the metapelites (75637, 75641 - table 5.12), maximum (i.e. all Fe^{2+}) rim temperatures obtained with the Ferry & Spear (1978) calibration vary systematically, depending on the proximity of the two phases, with grains in contact giving temperatures up to 200° C lower than those separated by a non-ferromagnesian phase (e.g. quartz). This is consistent with aspects of garnet-biotite compositional zoning (see above), suggesting localised re-equilibration during cooling.

There is no systematic variation in temperature estimates obtained with garnet non-ideality corrections and some results (e.g. Hodges & Spear 1982) approach albite and muscovite breakdown and are clearly too high. The Indares & Martignole calibration, with Ganguly and Saxena garnet appears to give the most consistent results and suggests peak rim temperatures of about 710° C (+/- 50° C).

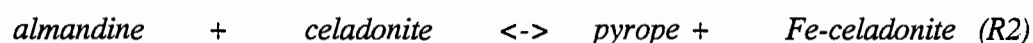
Sample	75637 adj	75637 adj	75637 sep	75641 inc	75641 adj	75641 sep	75632 adj	75632 adj	75631 sep
P (kb)	17.5	17.5	17.5	13.0	13.0	13.0	13.0	13.0	13.0
lnKd	-1.910	-1.694	-1.418	-1.859	-1.716	-1.530	-1.752	-1.952	-1.907
X Ti-bt	0.039	0.032	0.031	0.006	0.019	0.018	0.030	0.029	0.028
X Al6-bt	0.121	0.110	0.105	0.130	0.105	0.167	0.114	0.107	0.109
X Ca-gnt	0.077	0.077	0.077	0.136	0.136	0.163	0.260	0.248	0.267
X Mn-gnt	0.000	0.007	0.003	0.009	0.009	0.010	0.009	0.038	0.016
F&S (1978)	566	639	754	566	614	685	582	519	533
I&M(1985) - GS84	518	605	716	600	638	711	662	606	619
I&M(1985) - HS82	-	-	723	-	-	694	-	-	-
H&S(1982)	-	-	781	-	-	747	-	-	-
G&S(1984) - Sym.	-	-	670	-	-	578	-	-	-
G&S(1984) - Asym.	-	-	640	-	-	549	-	-	-
P&L(1984)	-	-	701	-	-	657	-	-	-
F&S(1978) - B90	-	-	781	-	-	749	-	-	-

Table 5.12: Garnet-biotite thermometry. Results of various calibrations (as discussed in text + Perchuk & Lavrente 1984 and Berman 1990) for adjacent (adj) garnet-biotite pairs and those separated (sep) by a non-ferromagnesian phase.

Temperatures for the micaceous amphibolites are derived from garnet-biotite pairs, which apparently crystallised late in D2, and are 50-100° C lower than independent T estimates for mica-free amphibolites (see 5.2.2.4).

5.2.2.2 GARNET-PHENGITE:

Phengite solution in muscovite enters into Fe-Mg exchange with garnet, according to the reaction:



which has been experimentally calibrated for eclogite facies metabasites (Krogh & Raheim 1978) and extended to pelitic systems by Green & Hellman (1982).

For 75637, the Green & Hellman (1982) expression for low CaO and low Mg# pelitic systems (table 5.12), gives temperatures comparable with the gnt-bt results. Garnet in 75641 has high CaO and temperatures are 30-80° C lower than peak garnet-biotite pairs. Correction for garnet non-ideality,

using equations 5.4 and 5.5 and the Hodges & Spear (1982) model increases the estimate by approximately 60° C, but the revision for 75637 appears to be too high. This exchange is less reliable than the gnt-bt thermometer and suggests temperatures in the range 670-720° C.

Sample	lnKd	P (kb)	T (C)	X Ca-gnt	X Mn-gnt	T - corrected (C)	Average
75637(1)	1.798	17.5	718	0.090	0.007	778	757
75637(2)	1.901	17.5	702	0.077	0.007	755	
75637(3)	1.993	17.5	688	0.077	0.003	739	
75641(1)	2.364	13.0	625	0.133	0.010	688	711
75641(2)	2.024	13.0	672	0.163	0.010	752	
75641(3)	2.041	13.0	670	0.123	0.003	728	
75641(4)	2.406	13.0	620	0.130	0.003	678	
75602(1)	1.958	10.0	665	0.150	0.023	746	730
75602(1)	2.158	10.0	637	0.150	0.023	715	
75602(1)*	2.651	10.0	574	0.150	0.023	647	634
75602(2)*	2.851	10.0	551	0.150	0.023	622	
*Fe3/Fe2 = .5							

Table 5.13: Garnet-phengite thermometry.

Garnet-phengite temperatures for 75602 are inconsistent with petrogenetic constraints on staurolite and chlorite stability (see 5.3) and the presence of abundant matrix hematite may indicate significant Fe³⁺ substitution. An assumed Fe₃/Fe₂ ratio of 0.5 and garnet correction gives temperatures of around 630° C which are more consistent with phase equilibria constraints.

5.2.2.3 GARNET-CLINOPYROXENE:

Garnet-clinopyroxene Fe-Mg exchange has received widespread use as a thermometer for eclogites and mafic granulites, and at least eight formulations of $\ln K_d = f(P,T)$ have been proposed (Essene 1982).

Raheim & Green (1974) calibrated the exchange for natural low-Ca garnet and low-Na clinopyroxene assemblages under mantle P-T conditions and further experimental work by Ellis & Green (1979) quantified the effect of Ca in garnet - extending the thermometer to a wider range of non-binary applications. Powell (1985) modified the Ellis and Green calibration using a robust regression

technique and more recent experimental work by Pattison & Newton (1989) has supported a revised calibration for garnets with $X_{gr} > 0.15$.

Results of these four calibrations for garnet clinopyroxene gneisses and clinopyroxene-bearing amphibolites are given in table 5.14.

Sample		P (kb)	X Ca-gnt	lnKd	T (C)				
						R&G(1974)	E&G(1979)	P(1985)	P&N(1989)
Gneisses									
75662(1)	Core	13	0.331	2.462	591	689	670	568	
75662(1)	Rim	13	0.408	2.616	564	709	692	-	
75662(2)	Rim	13	0.404	2.379	607	760	745	-	
75662(2)	Rim	13	0.407	2.658	556	699	683	528	
75627	Core	13	0.405	2.668	555	696	679	-	
75663	Core	13	0.502	3.052	494	681	666	-	
75619(1)	Rim	13	0.703	3.350	453	746	735	146	
75619(2)	Rim	13	0.644	3.155	480	749	738	194	
75625	Core	13	0.364	2.458	592	713	696	-	
75625	Rim	13	0.493	2.778	536	731	717	-	
Amphibolites									
75622(1)	Core	13	0.405	2.896	518	650	632	-	
75622(2)	Core	13	0.390	2.747	542	669	652	511	
75628(1)	Core	13	0.376	2.613	564	688	670	541	
75628(1)	Rim	13	0.360	2.299	622	748	731	637	
75628(2)	Core	13	0.359	2.764	539	645	626	-	
75628(2)	Rim	13	0.364	2.324	617	744	728	-	

Table 5.14: Garnet-clinopyroxene thermometry.

Low temperatures for the Raheim & Green (1974) reflect the high grossular component of these garnet compositions. For both lithologies, the Ellis & Green (1979) thermometer gives consistently high rim temperatures of 730-740° C and suggests a prograde core -> rim temperature increase of 30-80° C. The Pattison & Newton calibration reduces the temperature estimate by approximately 100° C and in the case of 75619, which interestingly has very high CaO (up to 28%) gives unreasonably low temperatures of <200° C.

5.2.2.4 GARNET-HORNBLLENDE:

A garnet-hornblende geothermometer has been empirically calibrated by Graham & Powell (1984) against the Ellis & Green garnet-cpx thermometer using a dataset of natural garnet-clinopyroxene-hornblende assemblages, and assuming all Fe as Fe²⁺. This assumption has been justified by the low Fe³⁺ content of most medium to high grade amphiboles - particularly in the presence of garnet (Graham & Powell 1984, Blundy & Holland 1990).

Sample		X Ca-gnt	lnKd	T(C)
Garnet Amphibolites				
75622(1)	Core	0.405	2.232	631
75622(1)	Rim	0.388	1.886	690
75628(1)	Core	0.376	1.967	663
75628(1)	Rim	0.360	1.462	772
75628(2)	Core	0.359	2.050	633
75628(2)	Rim	0.364	1.622	733
75622	Core-inc	0.430	1.276	882
Gnt-cpx gneisses				
75662	Rim	0.408	1.930	695
75627(1)	Rim	0.430	1.637	783
75627(2)	Rim	0.340	1.993	631
75627	Core-inc	0.340	0.798	897
Micaceous Amphibolites				
75632(1)	Rim	0.225	2.239	502
75632(2)	Rim	0.256	2.321	510
75631	Rim	0.267	2.016	573
75669	Core	0.272	2.024	575
75669	Rim	0.295	1.693	661

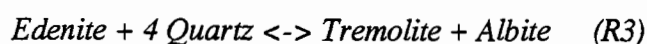
Table 5.15: Garnet-hornblende thermometry.

Rim estimates of 730 - 740° C for garnet amphibolites are in good agreement with garnet-clinopyroxene results. Core temperatures (640° C) are approximately 20-30°C lower than gnt-cpx results suggesting that amphibole may have developed at an intermediate stage. For the garnet

clinopyroxene gneisses, Fe-rich amphibole inclusions give unreasonably high temperatures - possibly due to unaccounted for Fe³⁺ - and texturally late amphibole results are inconsistent with gnt-cpx estimates - suggesting dis-equilibrium.

5.2.2.5 PLAGIOCLASE-HORNBLENDE:

Blundy & Holland (1990) argue that the temperature dependence of systematic Al and Na substitution in natural and experimental amphiboles can be modelled by edenite substitution, (Na_[1])^A(AlSi₁)^{T1} from a hypothetical tremolite end-member. This is illustrated in figure 5.11a as a compositional band parallel to the Tremolite-edenite join, and in fig.5.11b as a steep Al_{iv} vs. Al_{vi} trend. On the basis of this substitution model, the following equilibria:



have been used to quantify a positive correlation between temperature and tetrahedral Al.

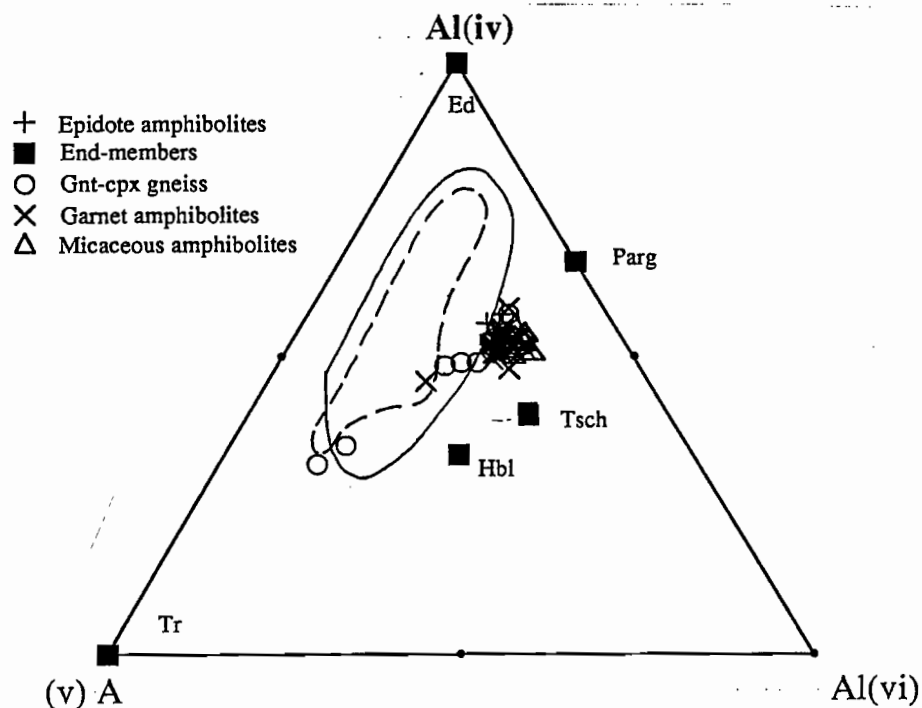
Sample		P (kb)	K	T (C)
Amphibolites				
75622	core	13	1.689	577
75622	rim	13	1.454	600
75628(1)	core	13	1.381	608
75628(1)	rim	13	1.420	604
75628(2)	core	13	1.411	605
75628(2)	rim	13	1.512	594
75617(1)	core	13	1.681	578
75617(1)	rim	13	2.257	536
75617(2)	core	13	2.218	538
75617(2)	rim	13	1.941	557
Mic. Amphibolites				
75632	core	13	1.337	614
75632	rim	13	1.268	622
75631	core	13	1.126	642
75631	rim	13	1.062	653

Table 5.16: Plagioclase-hornblende thermometry.

The results for this thermometer (table 5.16) are on average 70° C lower than gnt-hornblende temperatures estimated using adjacent garnet-amphibole-plagioclase grains and show inconsistent core-rim variation. This discrepancy may reflect unaccounted for Fe³⁺ in the Fe-Mg thermometer or

problems with the feldspar calibration and has been investigated by comparing amphibole substitution trends for the Forth amphibolites, with those of the calibrant dataset.

(a)



(b)

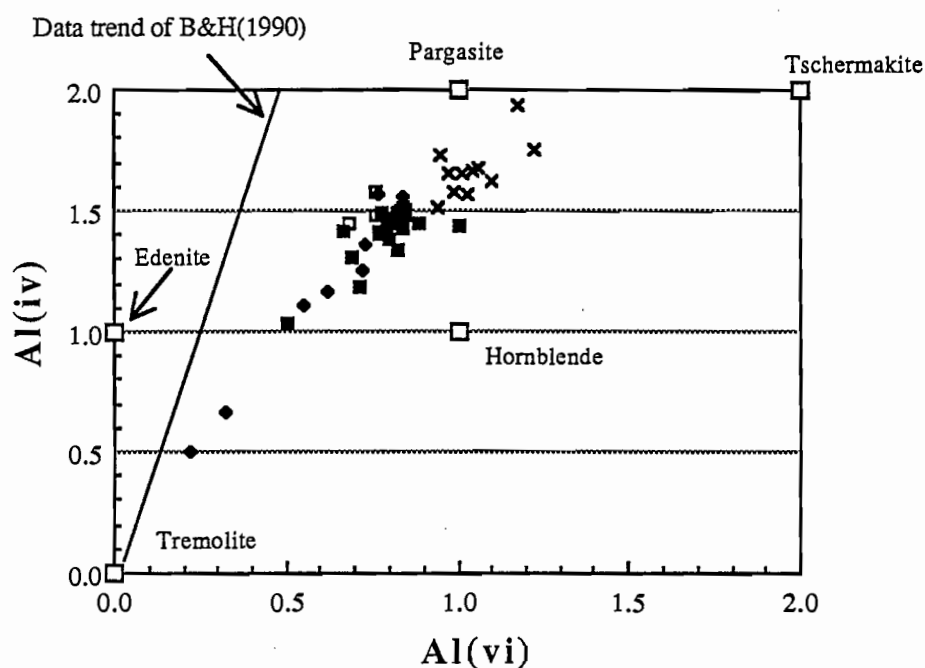


Figure 5.11: (a) (v)A (alkali site vacancy) - Al(iv) (tetrahedral Al) - Al(vi) (octahedral Al) compositional variation of amphiboles in garnet amphibolites, gnt-cpx gneisses and micaceous amphibolites. Compositional fields are experimental (solid) and natural (dashed) dataset of Blundy & Holland (1990). (b) Al_{iv} vs Al_{vi} . End-members from Blundy & Holland (1990).

As illustrated in figure 5.11, amphiboles from the Forth metabasites show a significant component of pargasite-tschermakite substitution, in addition to the steep 'edenite' trend characteristic of the calibrant dataset. This type of variation is described by Deer *et al* 1967 as a common feature of retrogressed eclogites, in which tschermakitic hornblende results from breakdown of aluminous jadeitic clinopyroxenes.

In tschermakite exchange, Al distribution is charge balanced to a significant extent by octahedral Al and cannot be modelled as pure edenite substitution. The resulting dilution of tetrahedral Al (below that expected from coupled Na-Al variation) is expressed through low T estimates for the Blundy & Holland thermometer, and illustrates the hazard of assuming simple uni-directional substitution in complex solutions, such as amphibole.

In the experimental database ($T > 800^\circ \text{C}$), Al_{iv} and Al_{vi} are not well correlated, suggesting that Tschermakite exchange is more important in natural rocks (particularly retrogressed eclogites), at crustal P-T conditions.

5.2.3 BAROMETRY:

5.2.3.1 METAPELITES:

GARNET-ALUMINOSILICATE-PLAGIOCLASE-QUARTZ (GASP):

The continuous reaction,



was first suggested as a potential fluid absent barometer by Ghent (1976) and is the favoured P-constraint of empirical calibrations for potential Al_2SiO_5 -absent assemblages. Early experimental calibrations by Goldsmith (1980) and Gasparik (1984) were carried out at high P and T - and required long extrapolation to crustal conditions. Recent work by Koziol & Newton (1988), has extended the experimental conditions to 900°C and 19kb and, for this reason is considered to be the most reliable calibration (Spear & Peacock 1990).

Newton & Haselton (1981) formulated the barometer as

$$-P_0 \Delta V_0 + RT \ln(a_{\text{gr}}/a_{\text{an}})^3 + P \Delta V_1 = 0 \quad (\text{Eq.5.7})$$

where P_0 and ΔV_0 are the pressure and volume change of the end-member reaction at the T of interest and ΔV_1 is the partial volume change of the measured compositions at 1 bar. Application of

the calibrated P-T curve requires solution models which constrain the activity of grossular and anorthite in natural garnet and plagioclase compositions and an estimate of the partial molar volume of grossular. The assumptions of a number of calibrations are presented in table 5.17.

In the Forth schists, kyanite is in textural equilibrium with the rims of high Ca garnet in rocks which lack plagioclase. The garnet contains staurolite inclusions suggesting that kyanite was not stable during core growth and the GASP barometer can only be used (with a hypothetical unit anorthite activity) to estimate minimum rim pressures. Results presented in table 5.17 suggest pressures of at least 9 kb.

Calibration	Experimental data	Garnet model	T (C)	P (kb)
Newton & Haselton (1981)	Goldsmith (1980)	Newton & Haselton (1981)	700	8.6
Hodges & Spear (1982)	Goldsmith (1980)	Hodges & Spear (1982)	700	6.4
Ganguly & Saxena (1984)	Goldsmith (1980)	Ganguly & Saxena (1984)	700	8.7
Hodges & Crowley (1985)	Goldsmith (1980)	Hodges & Spear (1982)	700	7.8
Koziol (1989)	Koziol & Newton (1988)	Koziol (1989)	700	8.9

Table 5.17: Minimum pressure results of GASP barometer for 75641 and assumptions of various calibrations.

GARNET-PLAGIOCLASE-MUSCOVITE-BIOTITE (GPMB):

Fe and Mg equilibria between co-existing garnet-plagioclase-muscovite-biotite assemblages have been empirically calibrated against the GASP barometer and garnet-biotite thermometer by Ghent & Stout (1981), Hodges & Crowley (1985) and Hoisch (1990). This assemblage is in apparent textural equilibrium in 75637, but in the absence of plagioclase yields minimum pressures only for 75641.

OTHER EMPIRICAL CALIBRATIONS:

Equilibria involving partial combinations of the phases garnet-aluminosilicate-plagioclase-muscovite-biotite-quartz have been empirically calibrated by a number of authors, and these are summarised in table 5.18.

Sample		Barometer	Calibration	T (C)	P (kb)
75641	Rim	GASP	Koziol (1989)	700	8.9*
75641	Rim	GPMB	Hodges & Crowley (1985)	700	8.2*
75641	Rim	GPMB	Hoisch (1990)	700	9.8*
75641	Rim	GPBQ (Fe)	Hoisch (1990)	700	9.1*
75641	Rim	GPBQ (Mg)	Hoisch (1990)	700	8.9*
75641	Rim	GBMA	Hodges & Crowley (1985)	700	13.0
75637	Rim	GPMB (Fe)	Ghent & Stout (1981)	700	16.5
75637	Rim	GPMB (Mg)	Ghent & Stout (1981)	700	16.8
75637	Rim	GPMQ (Fe)	Hodges & Crowley (1985)	700	18.3

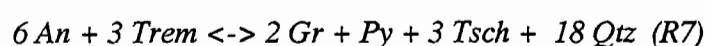
Table 5.18: Pressure estimates from a number of empirically calibrated pelitic barometers.

Garnet-muscovite-biotite-aluminosilicate equilibria constrain an absolute pressure of 13 kb for 75641 and results for 75637 suggest somewhat higher P of 17-18kb, close to the limit of empirical uncertainty.

5.2.3.2 METABASITES:

GARNET-PLAGIOCLASE-HORNBLende-QUARTZ (GPHQ):

Kohn & Spear (1989, 1990) have calibrated the end-member reactions,



(and their Fe-equivalents), using a weighted least squares regression, against the garnet clinopyroxene thermometer and independent pressure estimates derived from the jadeite component in clinopyroxene. The calibration incorporate Hodges & Spear (1982) garnet and Hodges & Royden (1984) plagioclase activity coefficients and two amphibole solution models - ideal mixing on sites and partial local charge balance (for the pargasitic exchange).

Core and rim pressures for two garnet amphibolites are presented in table 5.19 and form an internally consistent cluster at around 12.5kb similar to nearby kyanite-bearing schists. The inferred core -> rim up temperature vector is based on gnt-horn and gnt-cpx thermometry.

The strong pressure dependence of $\ln K_d$ for reaction 5.7, results in very good precision (+/-500 bars), although the accuracy of these barometers is comparable with other empirical calibrations (+/- 5kb).

Sample		Reaction	Amp - model	lnKd	T (C)	P (kb)
75628	Core	Pargasite (Fe)	Individual sites	-6.286	650	10.8
75628	Rim	Pargasite (Fe)	Individual sites	-7.584	700	11.8
75622	Core	Pargasite (Fe)	Individual sites	-7.139	650	11.4
75622	Rim	Pargasite (Fe)	Individual sites	-6.535	700	11.0
75628	Core	Pargasite (Mg)	Individual sites	-2.364	650	10.0
75628	Rim	Pargasite (Mg)	Individual sites	-4.909	700	11.5
75622	Core	Pargasite (Mg)	Individual sites	-3.378	650	10.5
75622	Rim	Pargasite (Mg)	Individual sites	-3.254	700	10.6
75628	Core	Pargasite (Fe)	Local charge	-6.840	650	12.9
75628	Rim	Pargasite (Fe)	Local charge	-8.339	700	14.9
75622	Core	Pargasite (Fe)	Local charge	-8.235	650	14.0
75622	Rim	Pargasite (Fe)	Local charge	-7.325	700	14.1
75628	Core	Pargasite (Mg)	Local charge	-1.821	650	11.6
75628	Rim	Pargasite (Mg)	Local charge	-4.517	700	14.3
75622	Core	Pargasite (Mg)	Local charge	-2.818	650	12.4
75622	Rim	Pargasite (Mg)	Local charge	-2.780	700	12.8
75628	Core	Tschermakite (Fe)	Local charge	8.328	650	12.7
75628	Rim	Tschermakite (Fe)	Local charge	9.826	700	14.2
75622	Core	Tschermakite (Fe)	Local charge	9.892	650	13.7
75622	Rim	Tschermakite (Fe)	Local charge	9.028	700	13.7
75628	Core	Tschermakite (Mg)	Local charge	3.304	650	12.0
75628	Rim	Tschermakite (Mg)	Local charge	5.998	700	14.2
75622	Core	Tschermakite (Mg)	Local charge	4.468	650	12.8
75622	Rim	Tschermakite (Mg)	Local charge	4.478	700	13.1
		Av. P	Range			
75622	core	12.5	10.5 - 14.0			
75622	rim	12.5	10.6 - 14.1			
75628	core	11.7	10.0 - 12.9			
75628	rim	13.5	11.5 - 14.9			

Table 5.19: Garnet-hornblende-plagioclase-quartz barometry.

GARNET-PLAGIOCLASE-CLINOPYROXENE-QUARTZ (GPCQ):

Owing to the high variance of this assemblage, gnt-cpx-plag-qtz barometers - involving either diopside or hedenbergite - have been calibrated exclusively from thermodynamic data using a range of experimental values and activity models (Newton & Perkins 1982, Powell & Holland 1988, Moecher et al 1988).

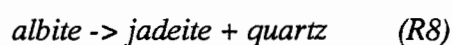
Rim compositions of this assemblage are in possible chemical equilibrium in 75628 and 75622, and the results in table 5.20 suggest pressures of 15-16 kb, which are some 2-3kb higher than gnt-horn-plag estimates.

SAMPLE	REACTION	T (C)	Pressure (kb)		
			M et al (1988)	N & P (1982)	P & H (1988)
75628	Rim / Diopside	700	15.1	15.4	15.1
75622	Rim / Diopside	700	14.0	13.6	13.2
75628	Rim / Hedenbergite	700	17.5	-	18.5
75622	Rim / Hedenbergite	700	16.0	-	17.0
		Av. P			
75628	Rim	16.3			
75622	Rim	14.8			

Table 5.20: Garnet-clinopyroxene-plagioclase-quartz barometry.

JADEITE IN CLINOPYROXENE:

The reaction:



has been developed as a geobarometer based on experimental work by Holland (1980). can be used to estimate minimum pressures for plagioclase-absent garnet clinopyroxene gneisses. For clinopyroxene-bearing amphibolites, absolute core pressure estimates of 11.5 kb (table 5.12) are based on the presence of albite inclusions in garnet and rim pressures of 9-13 kb on possible equilibrium between clinopyroxene rims and matrix plagioclase. These results are comparable with other pressure estimates.

Sample		XJd'	T (C)	P (kb)	
				H (1980)	G&L (1980)
75628	Core(inc.)	0.0427	650	11.5	11.5
75628	Rim(mtx.)	0.0391	700	12.9	13.4
75622	Core	0.0408	650	12.4*	12.4*
75622	Rim(mtx.)	0.0187	700	8.8	9.8
75662	Core	0.007	650	4.4*	5.8*
75662	Rim	0.005	700	3.6*	5.9*
' molecular mixing		* minimum			

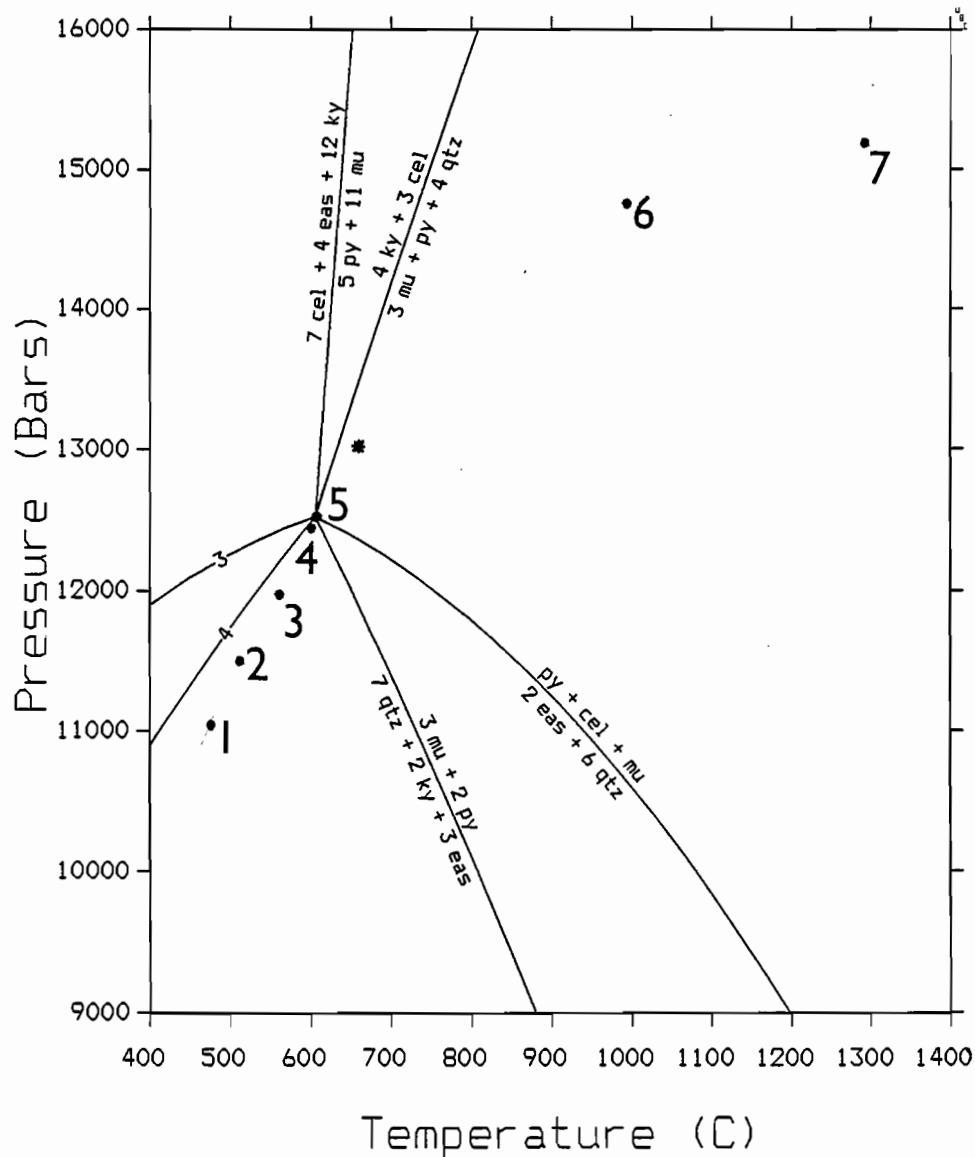
Table 5.21: Jadeite barometry.

5.2.4 DATABASE METHODS:

Independently calibrated P-T estimates have been tested against the internally consistent database method of Berman *et al* (1985, 1986), and Powell & Holland (1988) with generally poor results. Uncertainties are largely due to poorly constrained activity models, as shown in figure 5.12, which illustrates the typical variation in P-T estimates resulting from a range calculated pyrope activities. The Hodges & Spear (1982) garnet model gives results most consistent with independent P-T estimates.

There are similar problems for the metabasites, as none of the currently available models predict pyrope activities high enough to reproduce the experimentally calibrated Ellis & Green (1979) temperatures.

Despite these problems, the database approach offers great flexibility in the investigation of reaction textures and phase relationships, and is employed in a semi-quantitative way below.



REACTION LIST

Assemblages on the left are stable on the:
 high temperature side (for T-X diagrams)
 high pressure side (for P-T and P-X diagrams)

- 1): $7 \text{ cel} + 4 \text{ eas} + 12 \text{ ky} = 5 \text{ py} + 11 \text{ mu}$
- 2): $\text{py} + \text{cel} + \text{mu} = 2 \text{ eas} + 6 \text{ qtz}$
- 3): $2 \text{ ky} + \text{py} + 3 \text{ cel} = 3 \text{ eas} + 11 \text{ qtz}$
- 4): $2 \text{ ky} + 2 \text{ cel} = \text{mu} + \text{eas} + 5 \text{ qtz}$
- 5): $3 \text{ mu} + 2 \text{ py} = 7 \text{ qtz} + 2 \text{ ky} + 3 \text{ eas}$
- 6): $4 \text{ ky} + 3 \text{ cel} = 3 \text{ mu} + \text{py} + 4 \text{ qtz}$

Figure 5.12: Variation in GEOCALC P-T estimates with pyrope activity model for 75641. 1 = Perkins & Chipera (1985), 2 = Newton & Perkins (1982), 3 = Newton & Haselton (1981), 4 = Ganguly & Saxena (1984), 5 = Hodges & Spear (1982), 6 = Moecher *et al* (1988), 7 = Bohlen *et al* (1983a). * is independent thermobarometry estimate.

5.3 PETROGENESIS:

5.3.1 METAPELITES:

The mineral chronology of the Forth schists is complicated by a marked spatial variation in both the style of the early deformation and a significant west to east zonation of pelitic assemblages.

METAPELITES	S1		S2		S3	
	SYN	POST	SYN	POST	SYN	POST
Quartz	—	---	—	---	—	
Muscovite	—	---	—	---	—	
Garnet		—	—			
Kyanite			—			
Plagioclase			—	---		
Biotite	—	---	—			
Chloritoid	—	---	—			
Paragonite		—				
Staurolite			—			
Rutile	—	---	—			
Chlorite			—	---	—	

Table 5.22: Mineral chronology - Forth schists.

The sequence in table 5.22 is a compilation based on reaction textures in isolated units, and does not reflect the chronology of equilibrium assemblages. Thus, although chloritoid and kyanite may have developed at a similar structural stage they are spatially restricted and do not occur together. The present lithological distribution defines the following west to east zonation:

Buttons creek: fine- to medium-grained garnet + biotite + muscovite + plagioclase.

Claytons Rivulet - west bank: medium-grained garnet + chlorite + muscovite + chloritoid + paragonite + incipient granular staurolite.

Claytons Rivulet - east bank: coarse-grained garnet (high Ca) + chlorite + muscovite + chloritoid + paragonite + staurolite.

Forth Valley - west: coarse-grained garnet (high Ca) + kyanite + biotite + muscovite + staurolite as inclusions in garnet

Forth Valley - east: medium-grained garnet (high Ca) + albite + muscovite + biotite

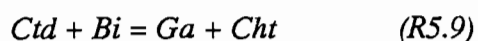
The western margin of the metamorphics is marked by the transition from lower greenschist facies chlorite-muscovite-quartz phyllites of the Ulverstone Metamorphics to fine-grained garnet-bearing schists. The P-T conditions of these rocks have not been determined, owing to poor preservation, but the absence of staurolite suggests peak conditions below about 500° C (Spear & Cheney 1989).

Chloritoid parageneses.

Garnet-phengite temperature estimates for chloritoid-bearing lithologies are complicated by the presence of abundant hematite and give ambiguous results. Owing to the absence of alternative thermobarometers, semi-quantitative P-T estimates have been investigated using published petrogenetic grids.

Chloritoid parageneses are generally restricted to aluminous lithologies with a relatively high Fe/(Fe+Mg+Mn) ratio, and have been the subject of much debate (Spear & Cheney 1989). In favourable bulk compositions, chloritoid is stable under a wide range of P-T conditions and has been reported from low grade Barrovian sequences (Atherton 1977) and from high P-low T metamorphic terranes such as eastern New Caledonia (Ghent *et al* 1982) and the Saih-Hatat window of north-eastern Oman (El-Shazley & Liou 1991). Mg-rich chloritoid, in association with the rare mineral Mg-carpholite and talc is diagnostic of extreme high pressure ($P > 18\text{kb}$, Chopin 1983) 'whiteschist' terranes where more Mg-rich compositions produce talc + kyanite assemblages (Yardley), such as those reported from the Collingwood River area (Kamperman 1983).

75596 and 75602 have the syn-S2 assemblage garnet-chlorite-chloritoid-staurolite-muscovite-quartz (*no biotite*) with staurolite and late chlorite apparently developing at the expense of chloritoid (Pl.5.1). Petrogenetic grids in KFMASH (Spear & Cheney 1989, Wang & Cheney 1991) restrict these biotite-absent assemblages to a narrow sub-vertical P-T window bounded by the continuous reactions:



and enclosing the univariant equilibrium:

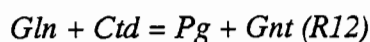


Petrographic evidence for this reaction is well-preserved and according to figure 5.13a indicates temperatures of 540-580 °C at pressures from 6-15 kb. The stability of this assemblage is expanded to higher P-T conditions in the KFMASHMn (and Ca) systems owing to a reduction in almandine and pyrope activity (fig.5.13b), although the position of reaction 5.11 is substantially unchanged.

The evolution of the gnt-ctd-cht-st assemblage is also demonstrated in figure 5.14, which shows the progressive core-rim decrease in chloritoid Mg# and the four phase univariant intersection of rim compositions.

Paragonite parageneses:

Gnt-ctd-cht-paragonite assemblages have been described from the Saih-Hatat window in NE Oman, where paragonite also occurs as rims between chloritoid and garnet (El-Shazley & Liou 1991) and the presence of rare glaucophane suggests the prograde reaction:



El-Shazley & Liou (1991) have modelled phase relationships in NaFASH using the GEOCALC PTX system and predict an upper T limit of approximately 500° C (13 kb) for this assemblage - marginally lower than inferred peak conditions in associated metabasites.

Textural relationships and the mineral chemistry of 75602 are consistent with this reaction, although the higher T conditions indicated by staurolite stability have removed all evidence of possible early glaucophane. An interesting similarity between both 75602 and the Oman assemblages is the presence of titaniferous hematite (11.5% TiO₂), although the significance of this has not been investigated.

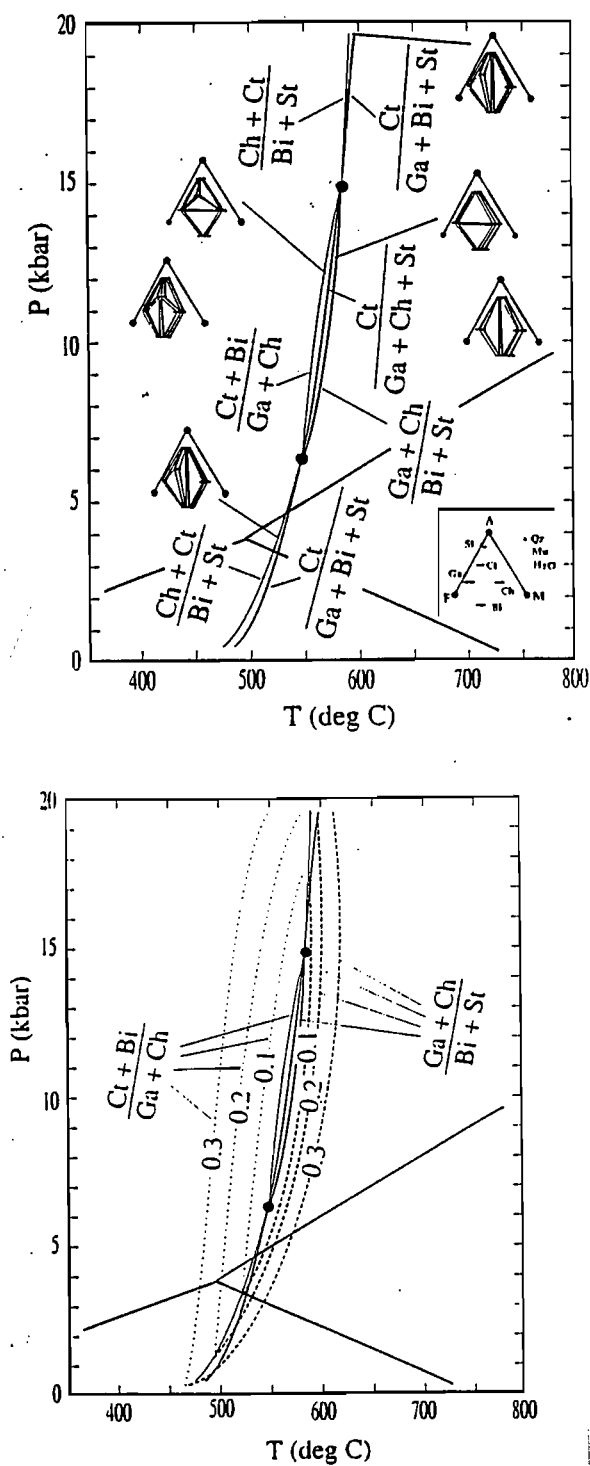


Figure 5.13: (a) KFMASH invariant points and divariant curves for assemblages with garnet (Ga), chloritoid (Ct), chlorite (Ch), biotite (Bi), staurolite (St), muscovite (Mu), quartz (Qz) and H₂O. (b) Effect of Mn (+ Ca) in garnet on the stability of biotite-absent garnet + chlorite + chloritoid + staurolite assemblages.

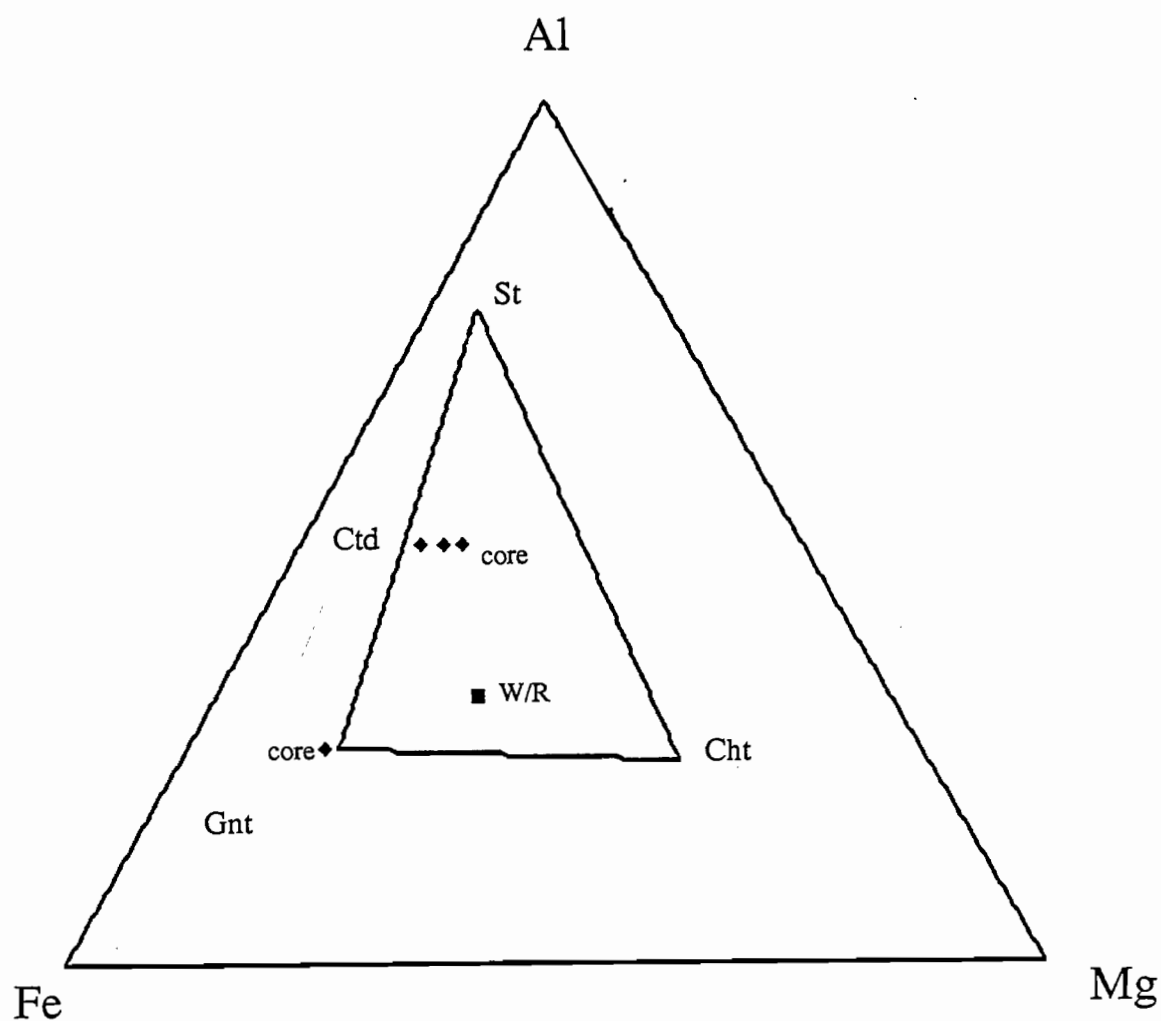
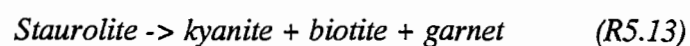


Figure 5.14: Thompson AFM muscovite projection of 75602. Three phase triangle is for garnet-staurolite and chlorite rim compositions. Diamond show core and intermediate chloritoid and garnet compositions and square is whole-rock analysis.

Kyanite parageneses:

Aluminous kyanite-bearing assemblages are preserved in the Forth Valley, where peak conditions reached 700 °C and 13 kb during D2. Kyanite probably developed during the continuous reaction:



which occurs at about 680 °C (12 kb) (Spear & Cheney 1989), based on phase relationships in KFMASH (fig.5.16) and the presence of staurolite inclusions in garnet (Pl.5.1).

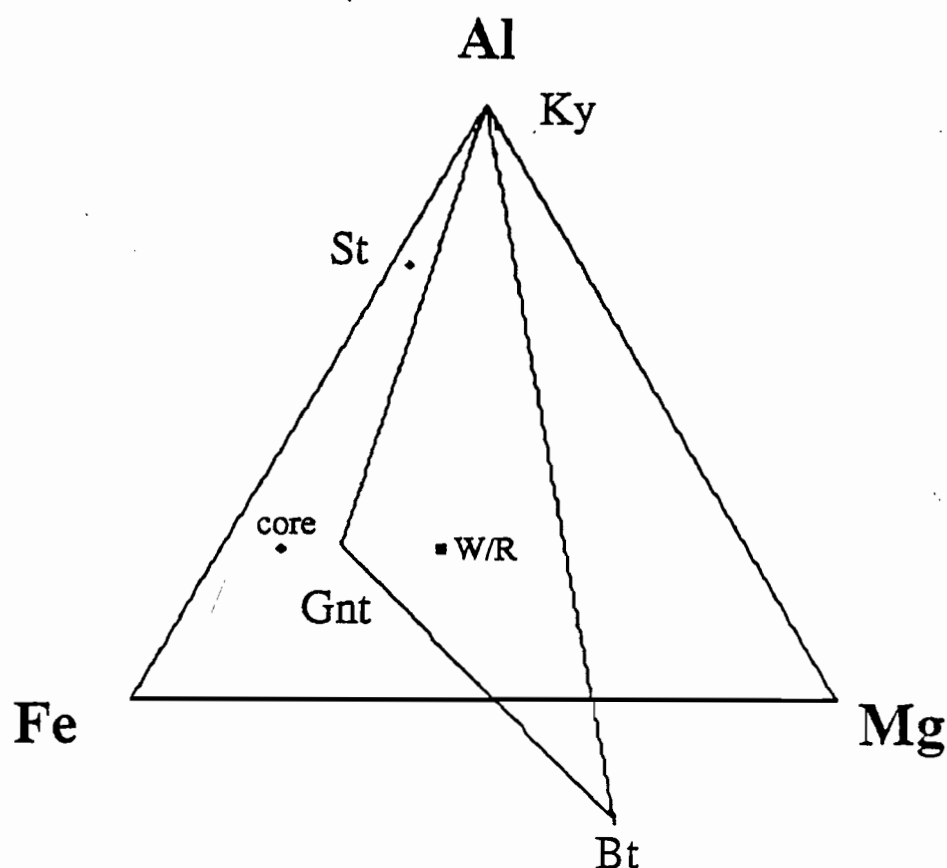


Figure 5.15: Thompson AFM muscovite projection for 75641.

Albite parageneses:

Albite porphyroblasts occur in garnet-free schist bands east of the Forth River, but owing to their poor preservation and the largely unresolved question of albite parageneses, have not been studied in detail.

The textural evolution of albite-rich schists from the Fleur de Lys Supergroup (Western Newfoundland) has been described by Jamieson & O'Bierne-Ryan (1991) who use inclusion suites and independent P-T constraints to model decompression albite growth - based on P-T dependant changes in the $a(K^+/H^+)$ - $a(Na^+/H^+)$ stability of albite and paragonite (fig.5.16).

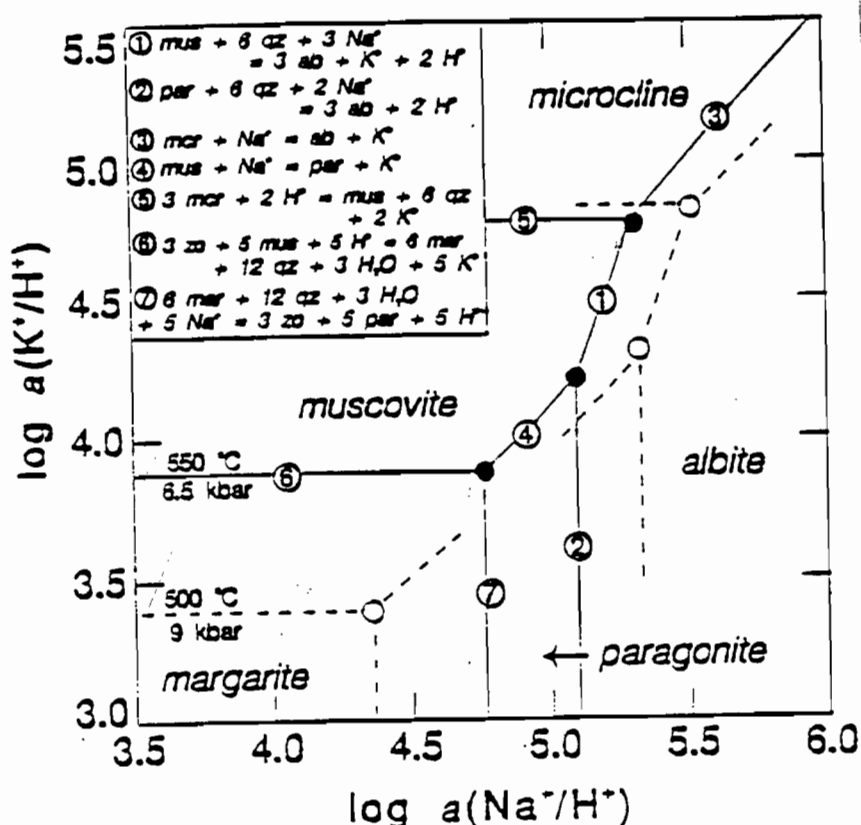
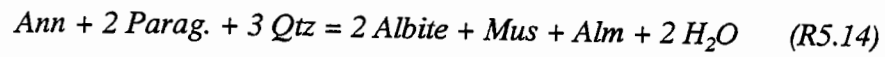


Figure 5.16: Relationship between fluid composition and mineral equilibria at different P-T conditions, showing the expansion of albite stability relative to microcline, muscovite and paragonite during decompression (modified from Jamieson & O'Beirne-Ryan 1991).

In the Forth Metamorphics, local mylonite zones and the preservation of substantially unaltered peak assemblages suggest relatively rapid syn- to late-S2 uplift and cooling (see below) and albitic schist bands may have developed during late S2 decompression, as modelled above. Texturally late granular plagioclase is present in low grade garnet-biotite-muscovite assemblages from the Claytons Rivulet, and the close spatial association with paragonite-bearing units may indicate a similar paragenesis. Fresh samples and detailed microprobe work are needed to evaluate this possibility.

Pressure estimates for rare albite garnet assemblages in the Forth Valley are 3-5 kb higher than estimates for kyanite-bearing metapelites and garnet amphibolites and are apparently supported by the Berman *et al* (1985) database (fig.5.16). The presence of biotite as relatively rare and somewhat corroded grains may indicate the continuous prograde reaction:



The phase equilibria shown in figure 5.17 are consistent with the absence of kyanite, despite the relatively high P conditions.

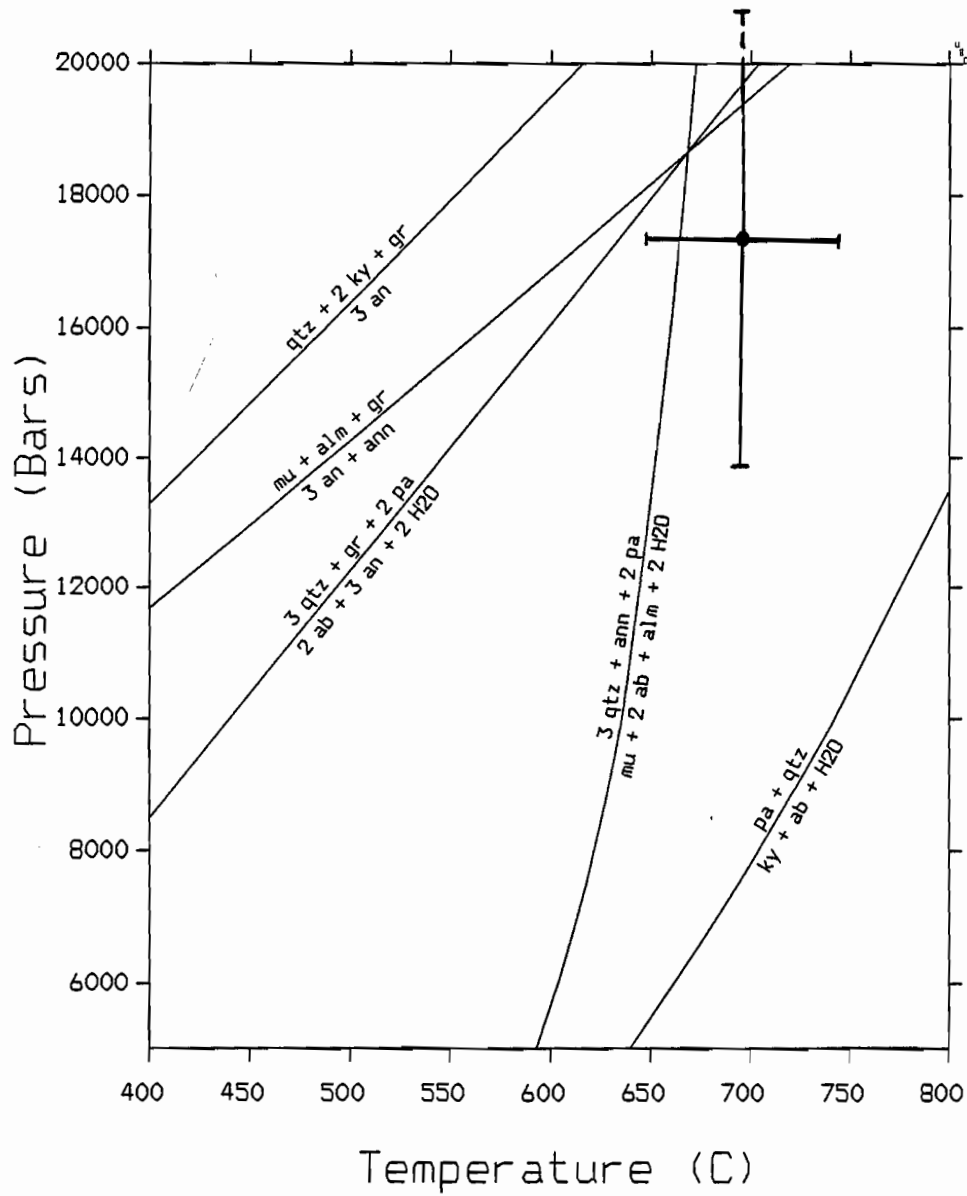


Figure 5.17: GEOCALC results - 75637.

Retrogression:

All samples show chemical re-equilibration of adjacent garnet-biotite compositions and some evidence of post-S2 chlorite and muscovite growth, either as undeformed neoblasts or syntaxial overgrowths on garnet, biotite and kyanite. The general lack of retrogression and preservation of high P-T assemblages suggests a relatively rapid cooling history which is discussed in Chapter 6.

Lower greenschist facies conditions during D3 are indicated by quartz sub-grain textures and apparent syn-S3 chlorite in 75600, although this P-T event appears to be at least post-Middle Cambrian and unrelated to the early metamorphism.

5.3.2 METABASITES:

Owing to the poor record of D1-2 interactions, the sequence of mineral growth in the Forth amphibolites, gneisses and micaceous amphibolites (table 5.23), is inferred largely from inclusions and reaction textures.

METABASITES	S1		S2		S3	
	SYN	POST	SYN	POST	SYN	POST
Garnet	—	---	—	---		
Amphibole			—	---	---	
Clinopyroxene	---	---				
Zoisite	---	---	---	---		
Epidote			---	---	---	
Plagioclase (>An15)			---	---		
Rutile	---	---	---	---		
Quartz	---	---	---	---		
Sphene		---	---	---		
Albite	---				---	
Muscovite			---	---	---	
Biotite			---	---		
Chlorite				---	---	---

Table 5.23: Chronology of mineral growth - Forth Metabasites.

5.3.2.1 AMPHIBOLITES:

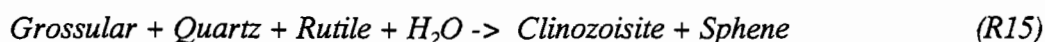
P-T estimates for equilibrium garnet-hornblende-plagioclase assemblages are reasonably well-constrained by traditional thermobarometric methods, indicating average rim conditions of 740° C and 13-15 kb - similar to kyanite-bearing pelitic assemblages in the Forth Valley.

The interpretation of pre-peak conditions is complicated by the presence of relict clinopyroxene with ambiguous textural relationships. Core-rim temperature estimates for garnet-cpx pairs are comparable with those for garnet clinopyroxene gneisses and suggest prograde heating from 660 -> 740° C and jadeite barometry constrains maximum core pressures to 11.5 kb.

Average garnet-amphibole core temperatures of 640° C are lower than the gnt-cpx results and amphibole probably developed at an intermediate stage. Garnet-cpx-plag-horn rim pressures (15kb) exceed those of the cpx-absent assemblage (13 kb) and also cpx-matrix plagioclase (9-13 kb) but are within the uncertainty of these calibrations.

These considerations suggest that the garnet-plag-cpx-horn assemblage was stable at peak conditions of 740° C, 13 - 15 kb during prograde metamorphism of an original garnet-cpx-albite assemblage, stable at 660° C and 11.5 kb.

In the amphibolites, a late increase in calcium activity is implied by the apparent replacement of rutile by sphene. This reaction texture and the evidence for late clinozoisite overgrowths on zoisite have been modelled, in GEOCALC by the fluid-dependant down-pressure reaction:



The calculated equilibrium runs at about 700° C - 10 kb, and is consistent with decompression growth of sphene and late zoisite/clinozoisite during cooling. The apparent stability of calcic plagioclase (rather than albite) during rim growth may also reflect increased calcium activity due to grossular breakdown and raises the possibility of higher P conditions prior to the thermal maximum.

Retrogression:

Apart from very minor late chlorite, the majority of metabasites show no evidence of retrogression. Textural and mineralogical features of epidote amphibolites from the Claytons Rivulet, indicate at least local epidote-albite 'greenschist' facies retrogression of original garnet amphibolite assemblages, during D3 thrusting. In the Forth Valley, local chlorite-actinolite amphibolite bands along strike from a smaller fault-bounded serpentinite body may also be a result of late deformation.

5.3.2.2. GARNET-CLINOPYROXENE GNEISSES:

Garnet-cpx thermometry results for the garnet clinopyroxene gneisses indicate peak rim temperatures of 730° C, and a core to rim up temperature vector of about 60° C. The low jadeite content in clinopyroxene gives very low minimum pressures of < 5kb and no absolute pressure estimates are available.

Textural evidence indicates two phases of garnet growth - an early porphyroblast phase forming coarse granoblastic domains and a late phase of small high CaO matrix grains and high CaO rim overgrowths on earlier garnet. Textures in 75619 suggest that the late garnet may have formed during breakdown of zoisite, in a shear environment. Rutile is very rare and, where present confined within rim overgrowths on garnet.

These reaction textures and phase relationships have been investigated using the Powell & Holland (1988) database, in conjunction with the GEOCALC software system of Brown *et al* (1988) (for which hedenbergite data is unavailable). Owing to large uncertainties in pyrope activity, modelling has been restricted to Fe-assemblages, using the Hodges and Spear (1982) garnet and Moecher *et al* (1988) clinopyroxene models.

High bulk-rock CaO was probably due to localised calcite veining (Chapter 3), and prograde metamorphism may have been accompanied by a mixed H₂O-CO₂ fluid. The absence of carbonate, as either inclusions or a matrix phase allows calcite-absent assemblages and reactions to be used as a semi-quantitative constraint on X_{H₂O}. In the Fe-system, the calcite-absent core assemblage in 75662, suggests an upper limit for X_{H₂O} of approximately 0.3. Rim X_{H₂O} is more tightly constrained at around 0.2 (fig.5.18).

These constraints have been used to model core-rim P-T conditions and reactions between Fe and Ti end-members in sample 75662 and the results, shown in figure 5.19, support the following (semi-quantitative) petrogenetic model:

1) Garnet-cpx-zoisite assemblage developed at 670-700° C and 8-11 kb in the presence of a mixed H₂O-CO₂ fluid, with sphene + CO₂, rather than rutile + calcite as the stable Ca-Ti-C assemblage, according to the equilibrium:



2) Prograde heating and compression to rim conditions of 730-740° C and 13-15kb with late high-Ca garnet developed as neoblasts and rim overgrowths during continuous breakdown of zoisite:



At peak conditions rutile + calcite may have been stable, as suggested by the presence of rare rutile inclusions in rim overgrowths.

3) Sphene re-stabilised through decompression below about 12kb. Low X_{H_2O} conditions during cooling preserved peak garnet-cpx assemblage with only minor amphibolitisation continuing into actinolite, rather than hornblende stability.

The accuracy of reaction R.17 has been checked using rim compositions of garnet clinopyroxene and zoisite from 75619 - which differ significantly from those of 75622 (cf. table 5.7 and 5.8). The reaction is reproduced to within 1 kb, despite the marked compositional variation and suggests that the model assumptions are reasonable.

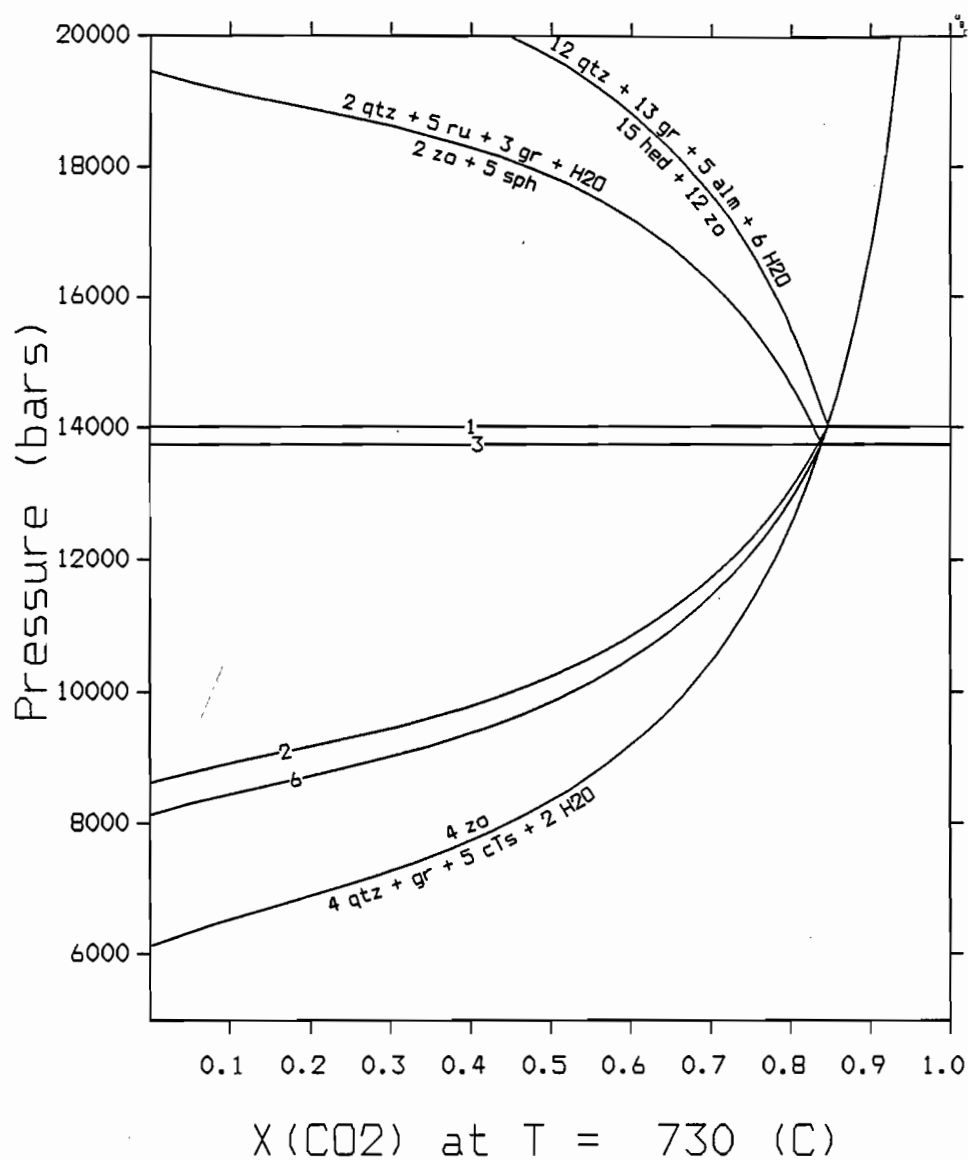
Although only semi-quantitative (at best), this model is consistent with garnet zoning/growth textures, the restricted occurrence of rutile and absence of calcite. The preservation of relatively fresh garnet-clinopyroxene assemblage is largely due to local H_2O dilution resulting from an early carbonate alteration event.

More widespread garnet amphibolites were stabilised in an H_2O -saturated environment, during prograde metamorphism of an early garnet-cpx-albite-rutile-zoisite assemblage and under these conditions zoisite breakdown was inhibited by high X_{H_2O} . Plagioclase-free 'eclogitic' assemblages may have developed prior to peak T, although amphibole rather than clinopyroxene appears to have been the preferred Na-bearing phase.

5.3.2.3 MICACEOUS AMPHIBOLITES:

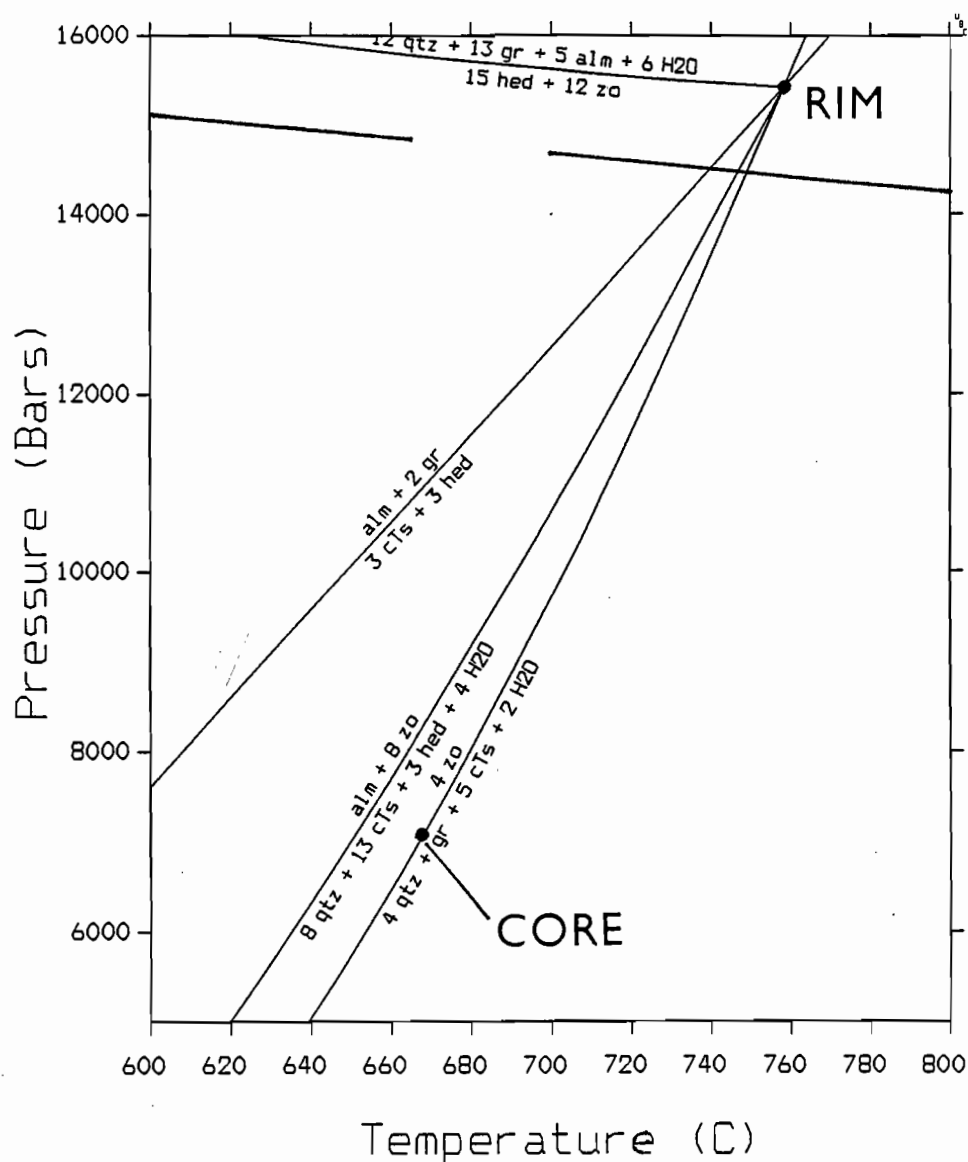
Corrected garnet-biotite temperatures for the micaceous amphibolites, based on apparent textural equilibrium between late biotite and granular garnet range from 610-660° C, and although well below peak estimates for interbanded mica-free assemblages, are consistent with textural and geochemical evidence for late retrogression/metasomatism. Garnet-hornblende and plagioclase-hornblende rim temperatures are also low (500 to 660° C) and probably due to fluid-enhanced re-equilibration of peak compositions. The preservation of rutile, rather than sphene as the dominant Ti-phase, suggests that the down pressure increase in Ca-activity indicated for the other metabasites, may have been diluted by the metasomatising fluids.

This retrogressive mica-garnet-quartz alteration is confined to a restricted high strain zone and may have developed during late D2 decompression thrusting of garnet amphibolite against adjacent pelitic lithologies.



REACTION LIST	
Assemblages on the left are stable on the:	
high temperature side (for T-X diagrams)	
high pressure side (for P-T and P-X diagrams)	
1):	alm + 2 gr = 3 cTs + 3 hed
2):	8 zo + alm = 3 hed + 13 cTs + 8 qtz + 4 H ₂ O
3):	gr + 2 ru = 2 sph + cTs
4):	4 zo = 4 qtz + gr + 5 cTs + 2 H ₂ O
5):	12 qtz + 13 gr + 5 alm + 6 H ₂ O = 15 hed + 12 zo
6):	2 zo + ru = 2 qtz + sph + 3 cTs + H ₂ O
7):	2 qtz + 5 ru + 3 gr + H ₂ O = 2 zo + 5 sph

Figure 5.18: GEOCALC P-X_{CO₂} results - 75662 rim. Compositions from table 5.7 and activity models as indicated in text.



REACTION LIST

Assemblages on the left are stable on the:
 high temperature side (for T-X diagrams)
 high pressure side (for P-T and P-X diagrams)

- 1): $\text{alm} + 2 \text{ gr} = 3 \text{ cTs} + 3 \text{ hed}$
- 2): $\text{alm} + 8 \text{ zo} = 8 \text{ qtz} + 13 \text{ cTs} + 3 \text{ hed} + 4 \text{ H}_2\text{O}$
- 3): $4 \text{ zo} = 4 \text{ qtz} + \text{gr} + 5 \text{ cTs} + 2 \text{ H}_2\text{O}$
- 4): $12 \text{ qtz} + 13 \text{ gr} + 5 \text{ alm} + 6 \text{ H}_2\text{O} = 15 \text{ hed} + 12 \text{ zo}$

Figure 5.19: GEOCALC P-T results for 75622. Core and rim compositions from table 5.7 and $X_{\text{H}_2\text{O}} = 0.2$ from fig. 5.18. Zoisite breakdown reaction for 75619 also shown for comparison (see text).

CHAPTER 6

CONCLUSIONS

The lithological characteristics of the Forth Metamorphics indicate derivation from a largely clastic sequence with potassic continental sedimentary affinities. Interlayered garnet amphibolites have tholeiitic MORB-type affinity and the sequence was probably deposited/erupted on a passive continental margin.

6.1 P-T SUMMARY:

Peak metamorphic conditions of 700 \pm 50° C and 13 \pm 2 kb are recorded by kyanite-garnet-biotite schists in the Forth Valley which developed during breakdown of early staurolite. Garnet amphibole plagioclase assemblages indicate similar pressures of 13-15 kb and slightly higher peak temperatures of 740° C but within the uncertainty of these estimates. In the metabasites ?amphibole-free garnet-clinopyroxene-albite assemblages constrain core conditions of 660° C and 11 kb during core growth. These results are supported by semi-quantitative P-T modelling of local calcite-altered garnet clinopyroxene interbands, which formed in a locally H₂O-poor environment during compression/heating from 675° C 9-11 kb to peak conditions of 740° C and 13-15 kb.

Peak temperatures some 100° C lower are inferred for staurolite-bearing assemblages 4 km west in the Claytons Rivulet, and staurolite/chloritoid-free garnet-biotite-muscovite assemblages along the western margin probably formed at less than 500° C. There is no direct pressure constraint for these lower grade units, although the high-Ca garnet/paragonite association and absence of syn-S2 plagioclase suggest moderately high pressures.

Peak assemblages are in textural equilibrium with the S2 foliation but there is little constraint on P-T conditions during early D1 isoclinal folding. Chloritoid west of the Claytons Rivulet appears to be syn-S1 and paragonite textures are consistent with early glaucophane breakdown. In this context, S1 may have developed under high P - low T conditions during early rapid burial.

Apart from minor chloritisation, late sphene and possible decompression albite growth, the high grade units preserve little evidence of their cooling history. Mylonitic quartzite and albitic schists formed under high T, relatively low strain conditions during D2 and shear indicators record west-directed transport at this time. Relatively rapid uplift is implied by these observations, and the present

east to west zonation of local pelitic assemblages (and regional tectono-metamorphic units) may have developed during west directed decompression thrusting. Late garnet-biotite temperatures of around 600° C suggest that local K-metasomatism of garnet amphibolite occurred at this time, along the high strain margin between pelitic and metabasic units.

6.2 TECTONIC IMPLICATIONS:

PRECAMBRIAN:

The age and tectonic evolution of the Tasmanian crystalline basement is very poorly constrained, despite its uniqueness in the Tasman Fold Belt (Turner 1989). Model ages suggest that the largely sedimentary sequences were deposited from about 1100 Ma to latest Precambrian time (Raheim & Compston 1977) and syn-metamorphic age determinations, based on a variety of decay systems, range from 800-500 Ma.

Most workers have assumed a late Precambrian tectono-metamorphic age, on the basis of these constraints and local unconformable relationships with Lower Cambrian sediments (Turner 1989). The contrast between regionally metamorphosed units of the Tyennan/Forth Regions and relatively unmetamorphosed turbidites of the Rocky Cape Group has been used to support a two-stage orogenic model (Spry 1962) but recent workers, have favoured a single stage tectono-metamorphic cycle - the Penguin Orogeny - with peak conditions at about 700Ma (Turner 1989). The present juxtaposition of regionally metamorphosed and relatively unmetamorphosed units is attributed to

The P-T conditions of this event are not well constrained, but petrological work where available indicates predominantly medium pressure Barrovian type metamorphism (McNeill 1985). High P-T conditions of 720° C and 16 kb have been documented for eclogites and kyanite-bearing metapelites from the centre of the Tyennan Region and Kamperman (1984) suggested a tentative subduction model to account for the metamorphism in that area. P-T conditions reported in this study - indicating burial to approximately 40- 50km - and indirect evidence for early high P-low T chloritoid-paragonite-?glaucophane assemblages support a similar conclusion, although correlation between these areas is complicated by the apparently conflicting sense of D2 vergence.

The possibility of a high pressure N-S trending subduction-related zone and evidence for high T low P metamorphism on King Island may indicate paired metamorphism, as defined by Myashiro (1973), but further work is required to clarify this.

CAMBRIAN:

Cambrian tectonism under lower P-T conditions is indicated by the presence of ultramafic bodies and minor post-S2 thrust structures in the metamorphics. Shear indicators are consistent with current tectonic models suggesting emplacement of the ultramafics from the east (Berry & Crawford 1988).

Chloritoid-bearing units in the Forth Metamorphics bear petrological similarities to high P-T metamorphics in NE Oman (Saih-Hatat Window), which formed during Late Cretaceous A-type subduction of the NE Arabian continental margin - prior to emplacement of the Semail ophiolite (El-Shazley & Liou 1990). The tectonic similarities between this area and the Cambrian evolution of Tasmania have been emphasised by Berry & Crawford (1988) and the apparent coincidence of D2 and Cambrian thrust vergence raises an alternative but highly speculative possibility that metamorphism in the Forth Region is due to Cambrian, rather than Precambrian subduction. This model would imply significant westward transport of the entire Forth Region, as recently suggested by Woodward *et al* (*in press*) and is supported by available radiometric age determinations (500Ma - Turner 1989). This is an interesting possibility, but remains to be tested.

DEVONIAN:

Significant E-W crustal shortening in the Devonian, further modified and enhanced the zonation of tectono-metamorphic units under an east-directed thrust regime, which extended from the Dial Range Trough at least as far as the Forth Valley. The metamorphics overthrust serpentinite bodies in the Claytons Rivulet at this time and were displaced along conjugate wrench faults. Zones of sheared albite-epidote amphibolites and microstructural features of the S3 cleavage suggest lower greenschist facies conditions (300-350° C), locally developed in the vicinity of major thrust zones. The inferred temperature conditions are not well constrained but imply considerable structural depth and as the metamorphics were probably overlain by a significant pile of Lower Paleozoic sediments at this time, this is not an unreasonable conclusion.

The polyphase compressional tectonic evolution of the Forth Metamorphics ended in the Devonian but localised normal faulting under an extensional regime continued, probably into the Tertiary and down-faulted Permian sediments against the eastern margin of the metamorphics.

APPENDIX A

WHOLEROCK ANALYSES

75622

	Gnt-cpx gneisses				Amphibolites				Wet (Spry, 1962)		
	75662	75663	75664	75619	75617	75618	75662	75660	75661	1	2
SiO₂	45.53	49.11	46.59	49.76	48.85	46.58	52.38	45.99	46.96	48.48	41.16
TiO₂	1.71	1.44	1.57	1.37	1.03	0.58	1.00	0.84	1.38	0.8	2
Al₂O₃	12.26	11.86	12.06	11.98	14.75	14.15	14.66	13.79	14.23	15.68	15.94
Fe₂O₃	12.36	10.52	11.71	10.40	11.09	11.68	10.67	11.17	11.61	3.92	2.57
FeO	-	-	-	-	-	-	-	-	-	10.98	18.35
MnO	0.18	0.13	0.15	0.16	0.14	0.16	0.17	0.19	0.18	0.21	0.32
MgO	6.00	5.00	5.65	3.08	7.06	8.54	6.20	12.04	9.62	5.72	4.21
CaO	19.83	19.07	20.17	20.55	11.43	12.79	11.15	10.38	10.02	8.37	12.12
Na₂O	0.73	0.98	0.65	1.64	3.50	3.27	2.27	2.84	2.71	2.47	1.17
K₂O	0.08	0.06	0.06	0.09	0.30	0.26	0.25	0.47	0.75	1.17	0.21
P₂O₅	0.17	0.25	0.20	0.34	0.07	0.03	0.10	0.10	0.14	-	0.18
LOI	0.99	1.56	1.61	0.49	1.42	2.09	1.42	1.60	1.84	1.52	2.35
TOTAL	99.84	99.98	100.42	99.86	99.66	100.13	100.27	99.41	99.44	99.32	100.58
Nb	20	20	18	18	7	4	4	8	18	-	-
Zr	166	175	161	160	53	26	53	50	103	-	-
Y	34	36	32	37	19	13	25	18	24	-	-
Sr	524	512	503	696	184	152	103	97	165	-	-
Rb	1	0	3	3	5	4	3	7	16	-	-
Ni	120	100	128	74	160	475	105	391	232	-	-
Cr	252	254	264	145	296	1036	401	730	570	-	-
V	257	216	244	188	298	241	325	228	301	-	-
Zn	101	103	104	158	80	66	92	89	99	-	-
Cu	85	88	91	1	50	89	74	23	60	-	-

	Epidote amphibolites			Micaceous amphibolites			Pelitic schists	
	75606	75608	75612	75673	75632	75670	75602	75641
SiO₂	51.36	45.94	41.47	65.07	54.31	61.12	58.96	64.87
TiO₂	0.88	0.46	0.98	0.95	2.15	1.51	0.91	0.80
Al₂O₃	15.09	16.46	16.96	15.43	13.77	13.64	20.25	17.21
Fe₂O₃	10.79	11.20	12.35	5.63	12.67	10.00	7.42	6.76
FeO	-	-	-	-	-	-	-	-
MnO	0.14	0.12	0.19	0.02	0.16	0.12	0.00	0.03
MgO	6.12	9.42	6.97	2.33	5.03	4.07	2.12	2.48
CaO	8.22	10.01	17.24	0.59	5.70	1.63	0.02	0.83
Na₂O	4.95	4.57	1.47	1.42	2.12	2.68	0.99	0.53
K₂O	0.60	0.32	0.14	3.98	1.30	2.38	4.27	3.63
P₂O₅	0.09	0.04	0.09	0.11	0.29	0.22	0.05	0.14
LOI	1.52	1.51	1.91	3.68	1.81	2.12	4.62	2.55
TOTAL	99.76	100.05	99.77	99.21	99.31	99.49	99.61	99.83
Nb	8	1	7	19	33	41	-	-
Zr	56	16	60	192	295	365	-	-
Y	21	16	26	27	52	59	-	-
Sr	120	238	323	131	215	142	-	-
Rb	14	6	0	162	41	85	-	-
Ni	181	357	138	62	110	88	-	-
Cr	678	625	222	78	234	143	-	-
V	276	208	322	142	260	154	-	-
Zn	88	73	88	105	152	127	-	-
Cu	57	8	49	65	78	57	-	-

Hornblende mylonites

	71277	71279	71281	71282	71293	71295	71298	71303	71307	71320	75636
SiO₂	44.52	46.14	46.71	45.24	46.93	46.18	47.17	44.85	44.39	45.29	36.63
TiO₂	0.58	0.53	0.10	0.50	1.57	1.04	1.03	0.30	0.38	0.12	0.22
Al₂O₃	11.59	13.97	10.06	12.33	15.13	15.27	14.18	11.19	12.23	9.09	4.55
Fe₂O₃	10.34	10.45	9.50	10.73	13.06	13.04	13.95	10.16	10.63	8.83	12.28
FeO	-	-	-	-	-	-	-	-	-	-	-
MnO	0.15	0.17	0.15	0.18	0.21	0.16	0.22	0.28	0.20	0.12	0.16
MgO	18.82	10.83	21.64	16.21	5.60	8.09	7.60	17.98	17.36	21.44	31.61
CaO	9.02	12.43	8.12	10.39	10.16	10.68	10.60	9.48	9.56	9.31	2.84
Na₂O	1.44	2.16	1.30	1.37	4.01	2.64	2.75	1.72	2.12	1.87	1.04
K₂O	0.06	0.30	0.05	0.21	0.78	0.92	1.10	0.11	0.13	0.15	0.06
P₂O₅	0.03	0.03	0.02	0.05	0.16	0.05	0.11	0.02	0.02	0.02	0.02
LOI	3.76	2.73	2.89	2.84	2.04	1.58	1.62	3.49	3.12	4.35	10.66
TOTAL	100.31	99.74	100.54	100.05	99.65	99.65	100.33	99.58	100.14	100.59	100.07
Nb	2	2	1	6	3	2	3	2	1	0	2
Zr	23	16	4	43	86	42	51	15	19	8	10
Y	15	22	8	18	31	31	35	12	15	8	8
Sr	27	112	18	76	259	233	197	25	27	19	13
Rb	0	8	2	4	23	20	27	1	2	2	0
Ni	946	238	912	604	41	122	76	799	738	993	1794
Cr	2309	632	2580	1647	116	248	321	2179	2015	2582	3001
V	216	277	166	218	408	394	388	200	207	150	65
Zn	54	67	54	75	106	84	92	97	81	50	51
Cu	53	207	52	36	165	39	280	76	89	6	16

APPENDIX B

ROCK CATALOGUE

The following specimens are housed in the University of Tasmania, Geology Department collection.

Abbreviations are:

R	Rock sample
T	Thin section
P	Polished thin-section
PPP	Pressed powder pellet
FD	Fusion disk

Number	Description	Grid ref.	Preparation
75595	Quartz mica schist	DQ316397	R
75596	Gnt-ctd-st-parag. schist	DQ341379	R
75597	Chloritic schist	DQ319386	R
75598	Garnet mica schist	DQ315385	R
75599	Quartz mica schist	DQ314384	R
75600	Quartz mica schist	DQ325413	R,T
75601	Banded quartzmica schist	DQ314379	R
75602	Gnt-ctd-st-parag. schist	DQ330364	R,P,PPP,FD —
75603	Albitic schist	DQ332405	R
75604	Quartzite	DQ337391	R,T
75605	Epidote amphibolite	DQ331405	R,P
75606	Epidote amphibolite	DQ331405	
75607	Epidote amphibolite	DQ328401	R,T
75608	Epidote amphibolite	DQ327402	R,P,PPP,FD —
75609	Epidote amphibolite	DQ327402	R
75610	Serpentine	DQ327402	R
75611	Serpentine	DQ329404	R
75612	Gnt epidote amphibolite	DQ328401	R,P,PPP,FD —
75613	Garnet mica schist	DQ333393	R
75614	Quartz mica schist	DQ331394	R
75615	Serpentine	DQ364385	R
75616	Amphibolite	DQ357401	R
75617	Amphibolite	DQ357401	R,P,PPP,FD —
75618	Garnet amphibolite	DQ357401	R,PPP,FD —
75619	Gnt cpx zoisite gneiss	DQ359369	R,P
75620	Garnet amphibolite	DQ357367	R
75621	Garnet amphibolite	DQ357367	R
75622	Garnet amphibolite	DQ363386	R,P,PPP,FD —
75623	Garnet amphibolite	DQ358383	R
75624	Garnet amphibolite	DQ358383	R,T
75625	Gnt cpx gneiss	DQ361382	R,P
75626	Gnt cpx gneiss	DQ361382	R,P
75627	Gneiss-amphibolite	DQ361382	R,P
75628	Garnet amphibolite	DQ363383	R,P
75629	Garnet mica schist	DQ360375	R,T
75630	Micaceous amphibolite	DQ361375	R,T
75631	Micaceous amphibolite	DQ362376	R,P
75632	Micaceous amphibolite	DQ362376	R,P,PPP,FD —

Number	Description	Grid ref.	Preparation
75633	Garnet amphibolite	DQ362376	R
75634	Garnet amphibolite	DQ367372	R
75635	Garnet amphibolite	DQ367372	R
75636	Serp cht tremolite schist	DQ367371	R,P,PPP,FD —
75637	Garnet mica schist	DQ372366	R,P
75638	Micaceous quartzite	DQ370360	R
75639	Micaceous quartzite	DQ369360	R
75640	Micaceous quartzite	DQ368361	R,P
75641	Kyanite garnet schist	DQ368361	R,P,PPP,FD —
75642	Micaceous quartzite	DQ382364	R
75643	Quartzite	DQ386365	R
75644	Quartz mica schist	DQ366349	R,T
75645	Garnet amphibolite	DQ367349	R
75646	Garnet amphibolite	DQ367349	R
75647	Garnet amphibolite	DQ368350	R
75648	Garnet amphibolite	DQ372353	R
75649	Garnet amphibolite	DQ372353	R
75650	Garnet amphibolite	DQ368350	R
75651	Micaceous amphibolite	DQ368350	R,T
75652	Quartzite	DQ365380	R
75653	Albite muscovite mylonite	DQ407386	R,P
75654	Quartz mica schist	DQ407384	R
75655	Albitic schist	DQ407384	R,T
75656	Albitic schist	DQ407384	R,T
75657	Quartzite	DQ409373	R,P
75658	Quartz mica schist	DQ409373	R,T
75659	Serpentinite	DQ365380	R
75660	Garnet amphibolite	DQ357401	R,PPP,FD —
75661	Hornblendite	DQ357401	R,PPP,FD —
75662	Gnt cpx zoisite gneiss	DQ361382	R,P,PPP,FD —
75663	Gnt cpx gneiss	DQ361382	R,P,PPP,FD —
75664	Gnt cpx gneiss	DQ361382	R,PPP,FD —
75665	Phengitic quartzite	DQ393352	R,P

REFERENCES CITED:

- ATHERTON, M.P., 1977.** The metamorphism of the Dalradian rocks of Scotland. *Scott. J. Geol.*, **13**(4): 331-370.
- AVE'LALLEMENT, H.G. & CARTER, N.L., 1971.** Pressure dependance of quartz deformation lamellae orientations. *Amer. J. Science*, **270**: 218-235.
- BELL, T.D., RUBENACH, M.J. & FLEMING, P.D., 1986.** Porphyroblast nucleation, growth and dissolution in regional metamorphic rocks as a function of deformation partitioning during foliation development. *J. Metamorphic Geol.*, **4**: 37-67.
- BERMAN, R.G., 1988.** Internally consistent thermodynamic data for minerals in the system Na₂O-K₂O-CaO-MgO-FeO-Fe₂O₃-Al₂O₃-SiO₂-TiO₂-H₂O-CO₂. *Journal of Petrology*, **29**: 445-522.
- BERMAN, R.G. & BROWN, T.H., 1985.** Heat capacities of minerals in the system Na₂O-K₂O-CaO-MgO-FeO-Fe₂O₃-Al₂O₃-SiO₂-TiO₂-H₂O-CO₂: representation, estimation and high temperature extrapolation. *Contrib. Mineral. Petrol.*, **89**: 168-183.
- BERMAN, R.G., BROWN, T.H. & GREENWOOD, H.J., 1985.** An internally consistent thermodynamic data base for minerals in the system Na₂O-K₂O-CaO-MgO-FeO-Fe₂O₃-Al₂O₃-SiO₂-TiO₂-H₂O-CO₂. *Atomic Energy of Canada Ltd. Technical Report 377*, 62p.
- BERMAN, R.G., ENGI, M., GREENWOOD, H.J. & BROWN, T.H., 1986.** Derivation of internally consistent thermodynamic data by the technique of mathematical programming: a review with application to the system MgO-SiO₂-H₂O. *Journal of Petrology*, **27**(6): 1331-1364.
- BERRY, R.F., 1988.** The tectonic significance of mylonites on the margins of Cambrian mafic-ultramafic complexes in Tasmania. In Turner, N.J. (ed) *The geology and evolution of the latest Precambrian to Cambrian rocks in the Western Tasmania Terrane*. Abstracts Volume. Geol. Soc. Aust. (Tasm. Div.): 12-14.
- BERRY, R.F. & CRAWFORD, A.J., 1988.** The tectonic significance of the Cambrian allochthonous mafic-ultramafic complexes in Tasmania. *Australian Journal of Earth Sciences*, **35**: 161-171.
- BERRY, R.F., ELLIOTT, C.G. & GRAY, D.R., 1990.** Structure and Tectonics of western and northern Tasmania. *10th Australian Geological Convention Excursion Guide E3*, 53p.
- BIDEAU, D., HEIBERT, R., HEKINIAN, R. & CANNAT, M., 1991.** Metamorphism of deep-seated rocks from the Garrett Ultrafast Transform (East Pacific Rise near 13°25'S). *J. Geophys. Res.*, **96**(B6): 10079-10099.

- BLAKE, F., 1928c.** Rutile and sand in the Clayton River district, Ulverstone. *Rep. Dep. Min. Tas.* (Unpublished).
- BLUNDY, J.D. & HOLLAND, T.J.B., 1990.** Calcic amphibole equilibria and a new amphibole-plagioclase geothermometer. *Contrib. Mineral. Petrol.* **104**: 208-224.
- BOHLEN, S.R., WALL, V.J. & BOETTCHER, A.L., 1983a.** Experimental investigation and application of garnet granulite equilibria. *Contrib. Mineral. Petrol.*, **83**:52-61.
- BOULTER, C.A., 1978.** The structural and metamorphic history of the Wilmot and Frankland Ranges, south-west Tasmania. Ph.D. thesis, Univ. Tasm. (unpubl.).
- BROWN, T.H., BERMAN, R.G. & PERKINS, E.H., 1987.** GEO-CALC: A software package for rapid calculation of stable pressure-temperature-activity phase diagrams. *Geol. Soc. Amer.* 1987 Annual meeting (Abs), **19** (7): 603.
- BROWN, T.H., BERMAN, R.G. & PERKINS, E.H., 1988.** GEO-CALC: Software package for calculation and display of pressure-temperature-composition phase diagrams using an IBM or compatible personal computer. *Computers & Geosciences*, **14**(3): 279-289.
- BURNS, K.L., 1963a.** *Devonport Tasmania*. Tasm. Dep. Mines Geol. Atlas 1 Mile Series, K/55-6-29.
- BURNS, K.L., 1963b.** The tectonic history of the Dial Range area, Tasmania. Ph.D. thesis, Univ. Tasm. (unpubl.).
- BURNS, K.L., 1964.** *Devonport Tasmania*. Tasm. Dep. Mines Geol. Atlas 1:63,360 Series Expl. Rep., Sheet 29(8115N), 1-266.
- BURNS, K.L., 1965.** *Devonport Tasmania*. Tasm. Dep. Mines Geol. Atlas 1 Mile Series Expl. Rep., Sheet K/55-6-29.
- BURRETT, C.F. & MARTIN, E.L. (eds.), 1989.** Geology and Mineral Resources of Tasmania. *Geological Society of Tasmania Special Publication* **15**, 574p.
- CAREY, S.W., 1953.** Geological structure of Tasmania in relation to mineralisation. *5th Empire Min. Metall. Congr.* **1**: 1108-1128.
- CHOPIN, C., 1983.** Magnesiochloritoid, a key mineral for the petrogenesis of high-grade pelitic blueschists. *Bull. Mineral.* **106**:715-717.
- CHRISTIE, J.M. & ARDELL, A.J., 1974.** Sub-structure of deformation lamellae in quartz. *Geology* (Aug.): 105-408.

- CRAWFORD, A.J. & BERRY, R.F., 1991 (In Review).** Tectonic implications of Late Proterozoic igneous rock associations in Western Tasmania. *Tectonophysics*.
- CORBETT, K.D. & TURNER, N.J., 1989.** Early Paleozoic deformation and tectonics, in (Burrett & Martin - eds). *Geology and Mineral Resources of Tasmania*. Geol. Soc. Aust. Spec. Pub. 15: 154-181.
- DEER, W.A., HOWIE, R.A. & ZUSSMAN, J., 1967.** *An introduction to the rock-forming minerals*. Longman, Hong Kong.
- DICKENSON, M.P. & HEWITT, D., 1986.** A garnet-chlorite geothermometer. *Geological Society of America Abstracts with Programs*, 18: 584.
- EL SHAZLEY, A.K. & LIOU, J.G., 1991.** Glaucophane chloritoid-bearing assemblages from NE Oman: petrological significance and a petrogenetic grid for high P metapelites. *Contrib. Mineral. Petrol*, 107: 180-201.
- ELLIOTT, C.G., WOODWARD, N.B. & GRAY, D.R., 1991 (In Review).** Palaeozoic thrusting and strike-slip faulting in the Badger Head region, northern Tasmania. *Australian Journal of Earth Sciences*.
- ELLIS, D.J. & GREEN, D.H., 1979.** An experimental study of the effect of Ca upon garnet-clinopyroxene Fe-Mg exchange equilibria. *Contrib. Mineral. Petrol.* 71: 13-22.
- ESSENE, E.J., 1982.** Geologic thermometry and barometry. In: Ferry, J.M. (ed.) *Characterisation of Metamorphism Through Mineral Equilibria, Review in Mineralogy*, 10, pp. 153-206, Mineralogical Society of America.
- ESSENE, E.J., 1989.** The current status of thermobarometry in metamorphic rocks. In: Daly, J.S., Cliff, R.A. & Yardley, B.W.D (eds.), *Evolution of Metamorphic Belts*. Geological Society Special Publication No. 43: 1 - 44.
- ETCHECOPAR, A., VASSEUR, G. & DAIGNIERES, M., 1981.** An inverse problem in microtectonics for the determination of stress tensors from fault striation analysis. *J. Struct. Geol.*, 3(1): 51-66.
- FERRY, J.M. & SPEAR, F.S., 1978.** Experimental calibration of the partitioning of Fe and Mg between biotite and garnet. *Contrib. Mineral. Petrol.* 66: 113-117.
- FLOYD, P.A. & WINCHESTER, 1975.** Magma type and tectonic setting discrimination using immobile elements. *E.P.S.L.*, 27: 211-218.
- GANGULY, J. & SAXENA, S.K., 1984.** Mixing properties of aluminosilicate garnets: constraints from natural and experimental data, and applications to geothermo-barometry. *American Mineralogist*, 69: 88-97.

- GARBUTT, J.M. & TESSIER, C., 1991.** Prism <c> slip in the quartzites of the Oakhurst Mylonite Belt, California. *J. Struct. Geol.*, **13**(6): 657-666.
- GEE, R.D., 1963.** Structure and petrology of the Raglan Range. *Bull. Geol. Surv. Tasm.* **47**.
- GEE, R.D., 1967b.** The tectonic evolution of the Rocky Cape Geanticline in northwest Tasmania. Ph.D. thesis, Univ. Tasm. (unpubl.).
- GEE, R.D., MARSHALL, B. & BURNS, K.L., 1970.** The metamorphic and structural sequence in the Precambrian of the Cradle Mountain area, Tasmania. *Rep. Geol. Surv. Tasm.* **11**.
- GHENT, E.D., 1976.** Plagioclase-garnet- Al_2SiO_5 -quartz: a potential geobarometer-geothermometer. *American Mineralogist*, **61**: 710-714.
- GHENT, E.D. & STOUT, M.Z., 1981.** Geobarometry and geothermometry of Plagioclase-Biotite-Garnet-Muscovite assemblages. *Contrib. Mineral. Petrol.* **76**: 92-97.
- GHENT, E.D., KNITTER, C.C., RAESIDE, R.P. & STOUT, M.Z., 1982.** Geothermometry and geobarometry of pelitic rocks, upper kyanite and sillimanite zones, Mica Creek area, British Columbia. *Canadian Mineralogist*, **20**: 295-305.
- GHENT, E.D., STOUT, M.Z., BLACK, P.M. & BROTHERS, R.N., 1987.** Chloritoid-bearing rocks associated with blueschists and eclogites, northern New Caledonia. *J. Metamorphic Geol.*, **5**: 239-254.
- GOLDSMITH, J.R., 1980.** Melting and breakdown reactions of anorthite at high pressures and temperatures. *American Mineralogist*, **65**: 272-284.
- GOULD, C., 1867.** River Forth and North Coast: geological report. *Tas. House of Assembly Pap.* **74** (for 1867).
- GRAHAM, C.M. & POWELL, R., 1984.** A garnet-hornblende geothermometer: calibration, testing and application to the Pelona Schist, Southern California. *J. Metamorphic Geol.*, **2**: 13-31.
- GREEN, N.L. & UDANSKY, S.I., 1986a.** Towards a practical plagioclase-muscovite thermometer. *American Mineralogist*, **71**: 1109-1117.
- GREEN, N.L. & UDANSKY, S.I., 1986b.** Ternary feldspar mixing relations and thermobarometry. *American Mineralogist*, **71**: 1100-1108.
- GREEN, T.H. & HELLMAN, P.L., 1982.** Fe-Mg partitioning between co-existing garnet and phengite at high pressure, and comments on a garnet-phengite geothermometer. *Lithos*, **15**: 253-266.

HALL, A.W., 1987. *Igneous Petrology*. Wiley & Sons, New York.

HARDIE, L.A., 1983. Origin of CaCl_2 brines by basalt-seawater interaction: insights provided by some simple mass balance constraints. *Contrib. Mineral. Petrol.*, **82**: 205-213.

HEGELSON, H.C., KIRKHAM, D.H. & FLOWERS, G.C., 1981. Theoretical prediction of the thermodynamic behaviour of aqueous electrolytes at high pressures and temperatures: IV. Calculation of activity coefficients, osmotic coefficients, and apparent molal and standard and relative partial molal properties to 600 C and 5kb. *Amer. J. Sci.*, **281**: 1249-1516.

HODGES, K.V. & CROWLEY, P.D., 1985. Error estimation and empirical geothermobarometry for pelitic systems. *American Mineralogist*, **70**: 702-709.

HODGES, K.V. & ROYDEN, L., 1984. Geologic thermobarometry of retrograded metamorphic rocks: an indication of the uplift trajectory of a portion of the Northern Scandinavian Caledonides. *J. Geophys. Res.*, **89(B8)**: 7077-7090.

HODGES, K.V. & SPEAR, F.S., 1982. Geothermometry, geobarometry and the Al_2SiO_5 triple point at Mt. Moosilauke, New Hampshire. *American Mineralogist*, **67**: 1118-1134.

HOISCH, T.D., 1990. Empirical calibration of six geobarometers for the mineral assemblage quartz + muscovite + biotite + plagioclase + garnet. *Contrib. Mineral. Petrol.* **104**: 225-234.

HOLDAWAY, M.J., 1971. Stability of andalusite and the aluminum silicate phase diagram. *American Journal of Science*, **271**: 97-131.

HOLLAND, T.J.B., 1980. The reaction albite = jadeite + quartz determined experimentally in the range 600-1200 °C. *American Mineralogist*, **65**: 129-134.

HOLLAND, T.J.B. & POWELL, R., 1985. An internally consistent thermodynamic dataset with uncertainties and correlations: 2. Data and results. *Journal of Metamorphic Geology*, **3**: 343-370.

HOLLAND, T.J.B. & POWELL, R., 1990. An enlarged and updated internally consistent thermodynamic dataset with uncertainties and correlations: the system $\text{K}_2\text{O}-\text{Na}_2\text{O}-\text{CaO}-\text{MgO}-\text{MnO}-\text{FeO}-\text{Fe}_2\text{O}_3-\text{Al}_2\text{O}_3-\text{TiO}_2-\text{SiO}_2-\text{C}-\text{H}_2-\text{O}_2$. *Journal of Metamorphic Geology*, **8**: 89-124.

HONNOREZ, J. & KIRST, P., 1975. Petrology of rodingites from the equatorial Mid-Atlantic fracture zones and their geotectonic significance. *Contrib. Mineral. Petrol.*, **49**: 233-257.

INDARES, A. & MARTIGNOLE, J., 1985. Biotite-garnet geothermometry in the granulite facies: the influence of Ti and Al in biotite. *American Mineralogist*, **70**: 272-278.

- ITO, E. & ANDERSON, A.T. (jr.), 1983.** Submarine metamorphism of gabbros from the Mid-Cayman Rise: petrologic and mineralogic constraints on hydrothermal processes at slow spreading ridges. *Contrib. Mineral. Petrol.*, **82**: 371-388.
- JAMIESON, R.A. & O'BEIRNE-RYAN, A.M., 1991.** Decompression-induced growth of albite porphyroblasts, Fleur de Lys Supergroup, western Newfoundland. *J. Metamorphic Geol.*, **9**: 433-439.
- KAMPERMAN, M., 1984.** *The Precambrian metamorphic geology of the Lyell Highway-Collingwood River area.* B.Sc.(Hons) Thesis, University of Tasmania: Hobart.
- KIENAST, J.R. & POGNANTE, U., 1988.** Chloritoid-bearing assemblages in eclogitised metagabbros of the Lanzo peridotite body (western Italian Alps). *Lithos*, **21**: 1-11.
- KOHN, M.J. & SPEAR, F.S., 1989.** Empirical calibration of geobarometers for the assemblage garnet + hornblende + plagioclase + quartz. *American Mineralogist*, **74**: 77-84.
- KOHN, M.J. & SPEAR, F.S., 1990.** Two new geobarometers for garnet amphibolites, with applications to south-eastern Vermont. *American Mineralogist*, **75**: 89-96.
- KOHN, M.J. & SPEAR, F.S., 1991.** Error propagation for barometers: 1. Accuracy and precision of experimentally located end-member reactions. *American Mineralogist*, **76**: 128-137.
- KOHN, M.J. & SPEAR, F.S., 1991.** Error propagation for barometers: 2. Application to rocks. *American Mineralogist*, **76**: 138-147.
- KOZIOL, A.M., 1989.** Recalibration of the garnet-plagioclase-Al₂SiO₅-quartz (GASP) geobarometer and applications to natural parageneses. *EOS*, **70**: 89-96.
- KOZIOL, A.M. & NEWTON, R.C., 1988.** Redetermination of the anorthite breakdown reaction and improvement of the plagioclase-garnet-Al₂SiO₅-quartz geobarometer. *American Mineralogist*, **73**: 216-223.
- KROGH, E.J. & RAHEIM, A., 1978.** Temperature and pressure dependence of Fe-Mg partitioning between garnet and phengite, with particular reference to eclogites. *Contrib. Mineral. Petrol.* **66**: 75-80.
- LAIRD, J., 1989.** Chlorites: Metamorphic petrology. In Hydrous silicates (exclusive of micas), *MSA reviews in mineralogy*, **19**: 405-453.
- LEAKE, B.E., 1964.** The chemical distinction between ortho- and para-amphibolites. *J. Petrology*, **5**(2): 238-254.
- LEAMAN, D.E., 1989.** Geophysics, in (Burrett & Martin - eds). *Geology and Mineral Resources of Tasmania*. Geol. Soc. Aust. Spec. Pub. **15**: 450-467.

- MCNEILL, A.W., 1985.** *The structure and petrology of the Nye Bay area, South-West Tasmania.* B.Sc.(Hons) Thesis, University of Tasmania: Hobart.
- MOECHER, D.P., ESSENE, E.J. & ANOVITZ, L.M., 1988.** Calculation and application of clinopyroxene-garnet-plagioclase-quartz geobarometers. *Contrib. Mineral. Petrol.* **100**: 92-106.
- MUKHOPADHYAY, B., 1990.** Garnet-clinopyroxene geobarometry: The problems, a prospect, and an approximate solution with some applications. *Amer. Mineral.*, **76**: 512-529.
- MYASHIRO, A., 1973.** *Metamorphism and Metamorphic belts (1st. ed).* George, Allen & Unwin, 492 pp.
- NEWTON, R.C. & HASELTON, H.T., 1981.** Thermodynamics of the plagioclase-garnet- Al_2SiO_5 -quartz geobarometer. In R.C. Newton et al (eds.), *Thermodynamics of minerals and melts*, pp. 131-147, Springer-Verlag, New York.
- NEWTON, R.C. & PERKINS, D.III, 1982.** Thermodynamic calibration of geobarometers based on the assemblages garnet-plagioclase-orthopyroxene (clinopyroxene) quartz. *American Mineralogist*, **67**: 203-222.
- NICOLAS, A. & POIRIER, J.P., 1976.** *Crystalline plasticity and solid state flow in metamorphic rocks.* Wiley & Sons, London.
- PATTISON, D.R.M. & NEWTON, R.C., 1989.** Reversed experimental calibration of the garnet-clinopyroxene Fe-Mg exchange thermometer. *Contrib. Mineral. Petrol.* **101**: 87-103.
- PEARCE, J.A. & CANN, J.R., 1973.** Tectonic setting of basic volcanic rocks determined using trace element analyses. *E.P.S.L.*, **19**: 290-300.
- PERKINS, D.III & CHIPERA, S.J., 1985.** Garnet-orthopyroxene-plagioclase-quartz barometry: refinement and application to the English River subprovince and the Minnesota River Valley. *Contrib. Mineral. Petrol.*, **89**: 69-80.
- PERKINS, E.H., BROWN, T.H. & BERMAN, R.G., 1986.** PT-system, TX-system, PX-system: three programs which calculate pressure-temperature-composition phase diagrams. *Computers & Geosciences*, **12(6)**: 749-755.
- PETTERD, W.F., 1893.** Catalogue of the minerals of Tasmania. *Govt. Printer, Hobart.*
- PETTERD, W.F., 1896.** Catalogue of the minerals of Tasmania. *Examiner Press, Launceston.*
- PETTERD, W.F., 1910.** Catalogue of the minerals of Tasmania. *Dep. Min. Tas.*

- PLATT, J.P. & VISSERS, R.L., 1980.** Extensional structures in anisotropic rocks. *J. Struct. Geol.*, **2**: 397-410.
- POWELL, R., 1978.** *Equilibrium thermodynamics in petrology, an introduction*. 284pp. Harper & Row, .
- POWELL, R., 1985(a).** Regression diagnostics and robust regression in geothermometer/geobarometer calibration: the garnet-clinopyroxene geothermometer revisited. *Journal of Metamorphic Geology*, **3**: 231-243.
- POWELL, R., 1985(b).** Geothermometry and geobarometry: a discussion. *J. geol. Soc. Lond.*, **142**: 29-38.
- POWELL, R. & HOLLAND, T.J.B., 1985.** An internally consistent thermodynamic dataset with uncertainties and correlations: 1. Methods and a worked example. *Journal of Metamorphic Geology*, **3**: 327-342.
- POWELL, R. & HOLLAND, T.J.B., 1988.** An internally consistent thermodynamic dataset with uncertainties and correlations: 3. Applications to beobarometry, worked examples and a computer program. *Journal of Metamorphic Geology*, **6**: 173-204.
- RAMSEY, J.G., 1967.** *Folding and fracturing of rocks*. McGraw-Hill, New York.
- RAHEIM, A. & COMPSTON, W., 1977.** Correlations between metamorphic events and Rb-Sr ages in metasediments and eclogite from Western Tasmania. *Lithos*, **10**: 271-289.
- RYBURN, R.J., RAHEIM, A. & GREEN, D.H., 1976.** Determination of the P-T path of natural eclogites during metamorphism - record of subduction. *Lithos*, **9**: 161-164.
- SCHUMACHER, J.C., 1991.** Empirical ferric iron corrections: necessity, assumptions, and effects on selected geothermobarometers. *Mineralogical Magazine*, **55**: 3-18.
- SIMPSON, C., 1986.** Determination of movement sense in mylonites. *Journal of Geological Education*, **34**: 246-261.
- SPEAR, F.S. & PEACOCK, S.M., 1990.** Metamorphic P-T-t paths: program manual and computer exercises for the calculation of metamorphic phase equilibria, pressure-temperature-time paths and thermal evolution of orogenic belts.
- SPRY, A.H., 1969.** *Metamorphic textures*. Pergamon Press Ltd.
- TAYLOR, B.L., 1955.** Asbestos in Tasmania. *Miner. Resour. Geol. Surv. Tas.*, **9**.

- TRACY, R.S., 1982.** Compositional zoning and inclusions in metamorphic minerals. In Ferry, J.M. (ed.), Characterisation of metamorphism through mineral equilibria. *Rev. In Mineral.*, **10**: 355-397.
- TURNER, N.J., 1989.** Precambrian, in (Burrett & Martin - eds). *Geology and Mineral Resources of Tasmania*. Geol. Soc. Aust. Spec. Pub. **15**: 5-46.
- TWELVETREES, W.H., 1906b.** Report on North West Coast mineral deposits. *Ann. Rep. Soc.Min. Tas. for 1905*, 9-59.
- TWELVETREES, W.H., 1909b.** Gunns Plains, Alma and other mining fields, *North West Coast*. *Bull. Geol. Surv. Tas.*, **5**.
- VERNON, R.H., 1976.** *Metamorphic Processes: reactions and microstructure development*. Allen & Unwin, London.
- WILL, T.M., POWELL, R. & HOLLAND, T.J.B., 1990.** A calculated petrogenetic grid for ultramafic rocks in the system $\text{CaO-FeO-MgO-Al}_2\text{O}_3\text{-SiO}_2\text{-CO}_2\text{-H}_2\text{O}$ at low pressures. *Contrib. Mineral. Petrol.*, **105**: 347-358.
- WILLIAMS, E., McCLENAGHAN, M.P. & COLLINS, P.L.F., 1989.** Mid-Paleozoic deformation, granitoids and ore deposits, in (Burrett & Martin - eds). *Geology and Mineral Resources of Tasmania*. Geol. Soc. Aust. Spec. Pub. **15**: 238-292.
- WILSON, C.J.L., 1973.** The prograde microfabric in a deformed quartzite sequence, Mt. Isa, Australia. *Tectonophysics*, **19**: 39-81.
- WINCHESTER, J.A. & FLOYD, P.A., 1976.** Geochemical magma type discrimination: application to altered and metamorphosed basic igneous rocks. *E.P.S.L.*, **28**: 459-469.
- WOODWARD, N.B., GRAY, D.R., & ELLIOTT, C.G., 1991 (In Review).** Repeated Palaeozoic thrusting and allochthoneity of Precambrian Basement, Northern Tasmania. *Australian Journal of Earth Sciences*.
- YARDLEY, B.W.D., 1989.** *Metamorphic petrology*. John Wiley and Sons, New York.

